Nagarjun Malagol
Institut für Rebenzüchtung

Mapping and characterization of resistance to downy mildew in an East Asian grapevine genetic resources

Dissertationen aus dem Julius Kühn-Institut

Julius Kühn-Institut
Bundesforschungsinstitut für Kulturpflanzen

Kontakt | Contact

Nagarjun Malagol
Julius Kühn-Institut (JKI)
Institut für Rebenzüchtung
Geilweilerhof
76833 Siebeldingen
Germany

E-Mail: nagarjun.malagol@julius-kuehn.de

Die Schriftenreihe „Dissertationen aus dem Julius Kühn-Institut" veröffentlicht Doktorarbeiten, die in enger Zusammenarbeit mit Universitäten an Instituten des Julius Kühn-Instituts entstanden sind.

The publication series „Dissertationen aus dem Julius Kühn-Institut" publishes doctoral dissertations originating from research doctorates and completed at the Julius Kühn-Institut (JKI) either in close collaboration with universities or as an outstanding independent work in the JKI research fields.

Der Vertrieb dieser Schriftenreihe erfolgt über den Buchhandel (Nachweis im Verzeichnis lieferbarer Bücher - VLB). Einige der Dissertationen erscheinen außerdem online open access und werden unter einer Creative Commons Namensnennung 4.0 Lizenz (CC-BY 4.0) zur Verfügung gestellt (https://creativecommons.org/licenses/by/4.0/deed.de). Die Schriftenreihe ist nachgewiesen in unserem Repositorium OpenAgrar: https://www.openagrar.de/receive/openagrar_mods_00005667.

The publication series is distributed through the book trade (listed in German Books in Print - VLB). Some of the dissertations are published online open access under the terms of the Creative Commons Attribution 4.0 International License (https://creativecommons.org/licenses/by/4.0/deed.en). The publication series is documented within our repository OpenAgrar: https://www.openagrar.de/receive/openagrar_mods_00005667.

Bibliografische Information der Deutschen Nationalbibliothek
Die Deutsche Nationalbibliothek verzeichnet diese Publikation in der Deutschen Nationalbibliografie: detaillierte bibliografische Daten sind im Internet über http://dnb.d-nb.de abrufbar.

Bibliographic information published by the Deutsche Nationalbibliothek
(German National Library)
The Deutsche Nationalbibliothek lists this publication in the Deutsche Nationalbibliografie; detailed bibliographic data are available in the Internet at http://dnb.dnb.de.

ISBN 978-3-95547-137-8
ISSN (elektronisch) 2510-0602
ISSN (Druck) 2510-0599
DOI 10.5073/20231127-153724-0

Herausgeber l Editor
Julius Kühn-Institut, Bundesforschungsinstitut für Kulturpflanzen, Quedlinburg, Deutschland
Julius Kühn-Institut, Federal Research Centre for Cultivated Plants, Quedlinburg, Germany

From the Institute for Agronomy and Plant Breeding I,
Department of Plant Breeding
of the Justus Liebig University of Giessen
&
From the Julius Kühn-Institute, Federal Research Centre for Cultivated Plants,
Institute for Grapevine Breeding and Genetic Resources, Geilweilerhof

MAPPING AND CHARACTERIZATION OF RESISTANCE TO DOWNY MILDEW IN AN EAST ASIAN GRAPEVINE GENETIC RESOURCES

DISSERTATION

for the award of the doctoral degree (Dr. agr.)

in the Faculty of Agricultural Sciences, Nutritional Sciences and Environmental Management at the Justus Liebig University of Giessen

submitted by

Nagarjun Malagol

from Sankeshwar, India

Gießen, 2023

With the permission of the Faculty of Agricultural Sciences, Nutritional Sciences and Environmental Management of the
Justus Liebig University of Giessen

Board of Examiners:

1st supervisor:	Prof. Dr. Reinhard Töpfer
2nd supervisor:	Prof. Dr. Rod Snowdon
Examiner:	Prof. Dr. Karl-Heinz Kogel
Examiner:	Prof. Dr. Michael Frei
Chairperson:	Prof. Dr. Jan Siemens

Date of the Disputation: 16.11.2023

Declaration in accordance with the Doctoral Regulations of the Faculty 09 in the version of 29.05.2019 § 17 (2)

“I declare that the dissertation here submitted is entirely my own work, written without any illegitimate help by any third party and solely with materials as indicated in the dissertation. I have indicated in the text where I have used texts from already published sources, either word for word or in substance, and where I have made statements based on oral information given to me.

At all times during the investigations carried out by me and described in the dissertation, I have followed the principles of good scientific practice as defined in the “Statutes of the Justus Liebig University Gießen for the Safeguarding of Good Scientific Practice”

Date:

Signature:

Table of Contents

List of figures

List of tables

List of abbreviations

2D	2 dimensional
2n	diploid chromosome number
AI	Artificial intelligence
ANN	Artificial neural network
ATP	Adenosine 5‘-triphosphate
Avr	avirulence effector
BLAST	Basic Local Alignment Search Tool
bp	base pair
cDNA	complementary DNA
COxGT2	*V. coignetiae* x ’Gewürztraminer’
cv.	cultivar
DAMP	Damage or danger-associated molecular pattern
DNA	Deoxyribonucleic acid
DCNN/CNN	Deep Convolutional Neural Network
DE	Differentially expressed
dpi	days post inoculation
ETI	Effector-triggered immunity
ETS	Effector-triggered susceptibility
flg	Flagellin
FRC	Fungus-resistant cultivar
gDNA	Genomic DNA
ger.	german
Gf.	Geilweilerhof
GWAS	Genome wide association studies
hpi	hour(s) post inoculation
hL	hectolitre
HR	Hypersensitive response
HTP	High Throughput
IM	Interval mapping
LDA	Leaf disc assay

LG	Linkage group
LOD	Logarithm of the odds
LRR	Leucine rich repeat
MAPK	Mitogen-activated protein kinase
MAMP	Microbe-associated molecular pattern
MAS	Marker-assisted selection
NBS	Nucleotide-binding-site
NLR	Nucleotide-binding site leucine-rich repeat domain receptor
OIV	Organisation Internationale de la Vigne et du Vin
PAMP	Pathogen-associated molecular pattern
PCD	Programmed cell death
PIWI	ger.: *pilzwiderstandsfähig* (fungus resistant)
PRP	Pathogenesis-related proteins
PRR	Pattern recognition receptors
PTI	PAMP triggered immunity
PTS	Pathogen triggered susceptibility
QTL	Quantitative trait locus
ReLU	Rectified linear unit
Ren/Run	Resistance to *Erysiphe necator*
ResNet	Residual neural network
RGAs	Resistance gene analogs
rhAmpSeq	RNase H2-dependent amplicon sequencing
RMSE	Root Mean Square Error
Rpv	Resistance to *Plasmopara viticola*
SCNN	Shallow convolutional neural network
ROS	Reactive oxygen species
SNP	Single-nucleotide polymorphism
ssp	Subspecies
SSR	Simple sequence repeats
*V*IVC	*Vitis* International Variety Catalogue

Summary

Downy mildew of grapevines is one of the most destructive diseases caused by an obligate biotrophic oomycete *Plasmopara viticola*, triggering severe yield loss. Regular applications of fungicides are necessary to prevent such losses, but this leads to severe environmental issues and decreased social acceptance. As a potential equivalent to traditional downy mildew management strategies, cultivars with durable resistance could contribute to sustainable and environmentally friendly viticulture. It is, therefore, common for grapevine breeders to develop fungus-resistant varieties utilizing naturally occurring resistance from wild species. Therefore, the primary breeding goal is to identify new resistances with different defence mechanisms and stack them in new varieties to prevent disease outbreaks and resistance-breaking isolates, thus minimizing fungicides in viticulture. Heretofore, more than 30 resistance loci against *P. viticola* have been already discovered. In this study, the bi-parental F1 population (‘Morio Muskat’ x COxGT2 (*V. coignetiae* x ’Gewürztraminer’)) Gf.2018-063 was investigated to identify and map resistance to *P. viticola*. The source of resistance is the East Asian wild species *Vitis coignetiae*. In addition to 109 simple sequence repeats (SSR) markers, 647 transferrable RNase H2-dependent amplicon sequencing (rhAmpSeq) markers are implemented in the creation of a genetic map. The resulting high-resolution rhAmpSeq map spanned a total map length of 1147.36 cM, comprising 19 linkage groups and an average distance between loci of 3.2 cM. Using each linkage map separately and three years of leaf disc assay based phenotypic data, quantitative trait locus (QTL) analysis was performed resulting in a consistent and highly significant QTL on chromosome 14 with an explained phenotypic variance of up to 36.4 %. This QTL does not share any SSR marker alleles with the pre-existing East Asian *V. amurensis* derived *Rpv8* and *Rpv12* QTLs on chr. 14. Therefore, it was designated as *Rpv32* (Resistance *Plasmopara viticola* 32) (Malagol et al., 2023, in preparation). SSR and rhAmpSeq markers identified in this research work can be exploited in Marker-assisted selection (MAS) for introgression of *Rpv32* into breeding lines and stacking resistances.

Furthermore, microscopic staining studies at various time intervals and quantitative analysis of *P. viticola* (5 dpi) demonstrated and confirmed that the genetically identified resistant parental genotype (COxGT2), in contrary to the second parental genotype (‘Morio Muskat’), prevents pathogen proliferation.

Moreover, the population utilized in this study showed segregation for the morphological trait leaf hair and a significant QTL was identified on LG 5 with an explained variance of 24 % (ribbon trichome). The hypothesis that leaf hair serves as physical barrier against *P. viticola* was tested in all three years. However, no strong association was observed between the leaf hair density and *P. viticola* infection on the leaf discs.

When different people work on phenotypic data evaluation in various years, traditional phenotyping methodologies turn out not only to be time-consuming and labor-intensive, but also immensely subjective. This subjectivity tends to introduce statistical noise and bias into the final analytical result. Therefore, this research also focused on training and developing a high-throughput SCNN (shallow convolutional neural network) based model for downy mildew disease quantification (Zendler et al., 2021). The model achieved an overall prediction accuracy of 97 %. The SCNN model performance was demonstrated by a strong and significant correlation with independently evaluated experts' data. This SCNN model in combination with an automated imaging system, shows accuracy and potential reduction in time spent on phenotyping. This pipeline serves as a valuable tool in grapevine breeding research.

As an additional aspect of this research, a Residual Networks-based Convolutional Neural Network (ResNet-CNN) for leaf hair quantification was developed due to the lack of accurate and precise tools available (Malagol et al., 2023, in preparation). The model achieved an overall prediction accuracy of 95.41 %. The validation and cross validation with two expert and two non-experts showed exceptional correlation ($R = 0.98$ and $R = 0.92$, RMSE 8.20 and 14.18, respectively). The absolute errors calculated clearly indicated bias introduced due to the subjectivity. To conclude, the developed ResNet-CNN is capable of enhancing objective phenotyping accuracy for leaf hair density, allowing for a more precise analysis of this trait (refer to Annex III & Annex IV).

Zusammenfassung

Der Falsche Mehltau der Rebe, der durch den obligat biotrophen Oomyceten *Plasmopara viticola* verursacht wird, gehört zu den gefährlichsten Erkrankungen der Rebe, da er zu erheblichen Ertragsverlusten führen kann. Der regelmäßige Einsatz von Fungiziden ist notwendig, um Ertragseinbußen zu verhindern, führt aber zu nachteiligen Umweltauswirkungen und geht einher mit einer geringen gesellschaftlichen Akzeptanz. Resistente Rebsorten können eine Ergänzung zu den herkömmlichen Strategien in der Bekämpfung des Falschen Mehltaus darstellen und zu einem nachhaltigen und umweltfreundlichen Weinbau beitragen, indem durch ihre Nutzung die Ausbringung von Pflanzenschutzmitteln drastisch reduziert werden kann. Daher ist es naheliegend, dass die Rebenzüchtung den Fokus auf pilzresistente Sorten legt und dabei natürlich vorkommende Resistenzen von Wildarten der Rebe nutzt. Die primären Zuchtziele sind daher die Identifizierung neuer Resistenzen mit unterschiedlichen Abwehrmechanismen, um einen Krankheitsausbruch und resistenzbrechende Isolate zu verhindern. Bis heute wurden mehr als 30 Resistenzloci gegen *P. viticola* identifiziert.

In dieser Studie wurde die bi-parentale F1-Population ('Morio Muskat' x COxGT2 (*V. coignetiae* x 'Gewürztraminer')) Gf.2018-063 untersucht, um Resistenzen gegen *P. viticola* zu identifizieren und zu kartieren. Als Resistenzquelle diente die bisher ungenutzte ostasiatische Wildart *Vitis coignetiae*. Es wurde eine genetische Karte basierend auf 109 *simple sequence repeats* (SSR)-Markern erstellt sowie eine weitere genetische Karte mit 647 Markern auf Grundlage der RNase-H2-abhängigen Amplikon-Sequenzierung (rhAmpSeq). Die daraus resultierende hochauflösende rhAmpSeq-Karte umfasst eine Gesamtlänge von 1147,36 cM, mit 19 Kopplungsgruppen und einem durchschnittlichen Abstand zwischen den Loci von 3,2 cM. Die phänotypischen Daten (Blattscheiben-Test) wurden über drei Jahre erhoben und in Quantitative Trait Locus (QTL)-Analysen unter Verwendung jeder einzelnen Kopplungskarte eingesetzt. Es konnte ein konsistenter und hoch signifikanter QTL auf Chromosom 14, mit einer erklärten phänotypischen Varianz von bis zu 36,4 % ermittelt werden. Dieser QTL teilt keine SSR-Markerallele mit den bereits existierenden, von *V. amurensis* abgeleiteten, QTLs *Rpv8* und *Rpv12* auf Chr. 14. Daher wurde er als *Rpv32* (Resistenz *Plasmopara viticola* 32) bezeichnet (Malagol et al., 2023, in Vorbereitung). SSR- und rhAmpSeq-Marker, die in dieser Forschungsarbeit identifiziert wurden, können in der markergestützten Selektion für die Introgression von *Rpv32* in Zuchtlinien und die Pyramidisierung von Resistenzen genutzt

werden. Darüber hinaus zeigen und bestätigen mikroskopische Färbungsstudien in verschiedenen Zeitintervallen und quantitative Analysen von *P. viticola* (5 dpi), dass der resistente parentale Genotyp (COxGT2) im Gegensatz zum anfälligen Genotyp ('Morio Muskat') die Vermehrung des Pathogens verhindert. Weiterhin zeigt die in dieser Studie verwendete Population eine Segregation für das morphologische Merkmal Blattbehaarung, für das ein signifikanter QTL auf Chr. 5 mit einer erklärten Varianz von 24 % (ribbon trichome) identifiziert wurde. Die Hypothese, dass die Blattbehaarung als physische Barriere gegen *P. viticola* dient, wurde in allen Jahren analysiert. Jedoch wurde kein Zusammenhang zwischen der Dichte der Blatthaare und dem Befall der Blattscheiben mit *P. viticola* im vorliegenden Fall festgestellt.

Herkömmliche Methoden der Phänotypisierung sind sowohl zeit- und arbeitsintensiv, als auch subjektiv, wenn unterschiedliche Personen solche Daten erheben. Diese Subjektivität kann zu statistischem Rauschen und zu Verzerrungen im Ergebnis führen. Daher konzentrierte sich die vorliegende Forschungsarbeit zusätzlich auf das Training und die Entwicklung eines auf künstlicher Intelligenz (SCNN: Shallow convolutional neural network) basierenden Hochdurchsatzmodells zur Quantifizierung der Resistenzeigenschaften gegen den Erreger des Falschen Mehltaus (Zendler *et al.*, 2021). Das Modell erreicht eine Gesamtvorhersagegenauigkeit von 97 %. Die Leistung des SCNN-Modells wurde durch eine hohe und signifikante Korrelation mit den Daten von unabhängig bewertenden Experten nachgewiesen. Dieses SCNN-Modell, in Kombination mit einem automatisierten Bildgebungssystem, bietet eine hohe Genauigkeit und verringert den Zeitaufwand für die Phänotypisierung. Die Pipeline ist daher ein wertvolles Instrument für die Forschung in der Rebenzüchtung.

Als zusätzlicher Aspekt dieser Arbeiten wurde ein auf Convolutional Neural Network (ResNet-CNN) basierendes Analysemodell für die Quantifizierung von Blatthaaren entwickelt, da bisher keine genauen und präzisen Werkzeuge zu deren Phänotypisierung zur Verfügung standen (Malagol et al., 2023, in Vorbereitung). Die Gesamtvorhersagegenauigkeit des Modells beträgt 95,41 %. Die Validierung und die Kreuzvalidierung mit zwei Experten und zwei Nicht-Experten zeigten eine außergewöhnliche Korrelation (R = 0,98 und R = 0,92, RMSE 8,20 bzw. 14,18). Die berechneten absoluten Fehler weisen eindeutig auf eine durch die Subjektivität bedingte Verzerrung hin. Zusammenfassend lässt sich sagen, dass das entwickelte ResNet-CNN in der

Lage ist, die objektive Phänotypisierungsgenauigkeit für das Merkmal „Dichte der Blatthaare“ zu verbessern und eine präzisere Analyse des Merkmals zu ermöglichen (Annex III & Annex IV). Damit steht ein neues Werkzeug zur Verfügung, das die Voraussetzungen für die genetische Analyse der Dichte der Blattbehaarung als physische Barriere gegen *P. viticola* schafft.

1. Introduction

1.1 The grapevine *Vitis vinifera* ssp. *sativa* and viticulture

Grapevine is one of the economically most important horticultural fruit crops, botanically a berry, mainly grown in temperate and subtropical areas. Grapevine contributes to the global gross production value of 67.8 US billion dollars (FAO-United Nations, 2022). However, in addition to producing wine, grapevines are also consumed as fresh fruit, juice, and raisins (Ren and Wen., 2007; Wan et al., 2013), resulting in a total annual production of 74.08 million tons of grapes for the year 2022 and a value that has been steadily rising over the previous years (International Organisation of Vine and Wine, 2022). In the European Union (EU), wine production is anticipated to reach 157 million hectoliter in 2022, representing a 3.5 million hectoliter (+2 %) rise compared to 2021 (International Organisation of Vine and Wine, 2022).

Next to beer, wine is one of the oldest alcoholic beverages humans have produced and established between 6600-7000 BCE (McGovern, 2003; Chojnacka, 2010). The genus *Vitis* comprises of more than 70 species and is further subdivided into the Eu*Vitis* (2n = 38) and *Muscadinia* (2n = 40) subgenera, with about 40 Asian and 30 American *Vitis* species, respectively (Wan et al., 2008; Liu et al., 2012). The origin of the domesticated grapevine *Vitis vinifera ssp. sativa* probably lies in the region known as Transcaucasia, between the Caspian and Black Seas (Vavilov, 1930; Töpfer et al., 2011b). The effect of early domestication of *V. vinifera ssp. sylvestris* originated *V. vinifera ssp. sativa*, lead to larger berry size, a greater sugar content, and a shift in sexuality from dioecious to hermaphrodite (Vavilov 1930; Kole, 2011, p. 9; Myles et al., 2011; Töpfer et al., 2011a; Zhou et al., 2017). However, paleobotanical discoveries in Spain from 3000 BC highlighted the issue of additional domestication hubs in the western Mediterranean (Nunez & Walker 1989). Based on the microsatellite analysis, it is assumed that there was a secondary domestication of cultivated vines from locally occurring wild vines in Europe (Arroyo-Gracia et al., 2006; Imazio et al., 2006). The first cultivation of grapevines in Europe may have occurred about 2800 years ago under the influence of the Greeks (Bouquet, 1982). The quality of the cultivated European grapevine could not be compared to its closely related Eurasian wild species *V. vinifera ssp. sylvestris* for two significant reasons: because the European cultivated vines can be optimized and selected in terms of high yield and faster growth, and the noticable berry quality (Alleweldt & Possingham, 1987;

Mullins et al., 1992; Zohary, 2003; Keller, 2015a; Grassi & Arroyo-García, 2020). This is demonstrated by the fact that practically all cultivated vines which are cultivated today are based on the *V. vinifera ssp. sativa* species (Zohary & Hopf, 1994; This et al., 2006).
In 2007, grapevine became the fourth flowering plant (Magnoliopsida) to have its genome entirely sequenced and assembled. A new era in grapevine research resistance and breeding began with sequencing the nearly homozygous inbred grapevine line PN40024 derived from *V. vinifera cv.* 'Pinot Noir' / 'Helfensteiner' (Jaillon et al., 2007). Currently, different updated versions of PN40024 are available. The latest improved annotated version of the grapevine reference genome called PN40024.v4 is available while defining estimated genes up to 35,230 (Velt et al., 2022).

In addition to European *V. vinifera* other *Vitis* species exist outside of Europe covering the geographical location of North America and Asia. About 70 wild species of *Vitis* have been described thus far (This et al., 2006). The most important representative species of the American continent include *Muscadinia rotundifolia, V. labrusca, V. riparia, V. cinerea, V. aestivalis* and *V. rupestris*. In Asia species include *V. amurensis, V. romanetii, V. davidii, V. chungi, V. adenoclada* and *V. piasezkii* (This et al., 2006; Li et al., 2021). These wild species represent valuable genetic resources due to their close affinity and possibility to hybridize with European *V. vinifera spp. sativa* (Staudt and Kassemeyer, 1995; Maul et al., 2021). Hybridization between non-European grapevine species (e.g. *V. amurensis, V. labrusca* etc.) and *V. vinifera*, and several backcrosses over time resulted in a new group of cultivars, so called PIWIs (ger. *pilzwiderstandsfähige Rebsorten (fungus resistant grapevine varieties)* or pioneer wines/vines). Common to the PIWIs is their resistance to the mildew diseases (powdery mildew and downy mildew) originating from the wild *Vitis* species. One of the most popular and regularly planted grape varieties with resistances is the 'Regent', crossed in 1967, covering it´s maximal average of 2,200 ha of vineyards by 2008 (Töpfer et al., 2011a; Maul et al., 2021).

1.2 Grapevine diseases

International commerce was made feasible by technological advancement, explorers' expeditions, and transportation networks, which served as the potential drivers behind global distribution and contributed to the spread of many animal and plant species (McKinney & Lockwood, 1999). As a result, infectious diseases and pests often spread unknowingly by travelling with the appropriate

host (Brown & Hovmoller, 2002; Meyerson & Mooney, 2007; Hulme, 2009; Bebber et al., 2014). Thus, many natural settings currently contain assemblages of alien species that endanger native species populations and change ecosystem function, whether as a result of intentional or unintentional introduction (McGeoch et al., 2010).

As an example, invasive grapevine diseases and pests established themselves in Europe in the middle of the 19th century by transatlantic trade of vines of diverse *Vitis* species between Europe and North America (Töpfer et al., 2011a; Vezzulli et al., 2022). The most prevalent pathogens with American origin have been posing an increasing hazard to the susceptible European grapevines *(V. vinifera).* The diseases included, powdery mildew, caused by *Erypsiphe* (syn. *Uncinula*) *necator* (Anamorphic *Oidium tuckeri* Berk., 1834) which was first observed and reported in 1845 (Berkely, 1847; Wilcox et al., 2015; Töpfer et al., 2011). In the middle of the 1860s, the grape phylloxera (*Daktulosphaïra vitifoliae*) was first identified in France (Ordish, 1972; Walker et al., 1991; Ferris et al., 2012). The rapid proliferation implied that the pathogen was widely dispersed before being discovered, most likely on a contaminated greenhouse, equipment, and infected rooting from growers and nurseries (Walker et al., 1991). However, to overcome this crisis, decades later, phylloxera infestations could be combat by grafting *V. vinifera* cultivars onto rootstocks of American wild grapevines exhibiting root phylloxera tolerance (Weaver, 1976; Kocsis et al., 1999; Granett et al., 2001). The first introduction of downy mildew (*Plasmopara viticola* (Berk. & Curt) Berl. & de Toni) occurred in Europe in the 1870s (Fontaine et al., 2021), known to cause severe yield loss of up to 90 % (Calonnec et al., 2004). In addition, the ongoing climate change and increased global warming enhance these catastrophic disease outbreaks affecting the grapevines (Coakley et al., 1999; Salinari et al., 2007; Chakraborty et al., 2000b; Zyprian et al., 2018; Delrot et al., 2020).

1.2.1 Downy mildew

Plasmopara viticola ((Berk & Curt.) Berl. & de Toni), an obligate biotrophic oomycete, is the underlying cause of grapevine downy mildew and contributes to devastating yield losses worldwide. Despite fungus-like structures, oomycetes are more closely linked to brown algae producing septate hyphae in contrast to fungi (Karling, 1981; Dick, 2001; Judelson & Ah-Fong, 2019). In addition, they produce their cell walls predominantly from β-1,3 and 1,6-glucans, arachidonic acid and cellulose, and possess diploid cell phases throughout the mycelium's

vegetative phase (Beakes, 1987 and 1989; Gessler et al., 2011; Fawke et al., 2015; Robinson and Bostock, 2015; Judelson & Ah-Fong, 2019). Due to the absence of genes in nitrogen metabolism and aminobutyric acid catabolism, *P. viticola* evolved from a pathogen similar to *Phytophthora* species that adopted a biotrophic lifestyle (Brilli et al., 2018).

P. viticola, in particular, is widespread in all temperate or tropical regions and infects all the green tissues of the grapevine, especially invading the stomata on the abaxial surface of leaves (Moriondo et al., 2005). Under optimal circumstances, infections can also be seen on inflorescences and immature bunches (Lafon & Clerjeau, 1988). Early signs include yellow oil spots on the upper leaf surface and white cottony growth (Figure 1B) on the lower leaf surface. As disease progresses the affected area becomes necrotic and eventually leads to defoliation of the host plant (Koblet et al., 1994; Ollat & Gaudillere, 1998; Kassemeyer, 2017) (Figure 1C). Therefore, developing optimal disease control strategies and predictive models requires a thorough understanding of the pathogen's life cycle.

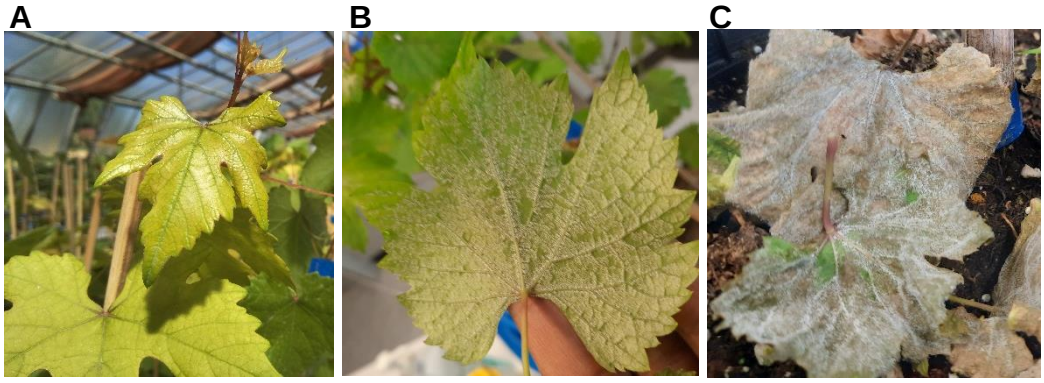

Figure 1 Downy mildew infection/symptoms. (A) Healthy susceptible ‘Müller Thurgau’ leaf; (B) White cottony growth due to *P. viticola* infection on the abaxial surface of the leaf; (C) Defoliation to downy mildew infection.

1.2.2 Life cycle of *P. viticola* causing downy mildew disease

P. viticola depends on living plant tissue and spreads via sexual and asexual reproductive cycles (Figure 2) (Park et al., 1997; Caffi et al., 2013). For infection, downy mildew requires optimal environmental conditions like warm and humid weather conditions (Mendgen & Hahn, 2002). Therefore, during the late spring and early summer (t >8 °C), the oospores germinate under wet soil conditions and form macrosporangia. The primary sporangium formed produces up to

60 diploid zoospores, which are dispersed via wind and rain (Kortekamp et al., 1998; Kiefer et al., 2002; Gessler et al., 2011). Zoospores create germ tubes that enter the stomata and grow into a sub-stomatal vesicle forming primary hyphae and mycelia (Walker et al., 2007; Buonassisi, 2017). The mycelium expands via the intercellular spaces of mesophyll cell and the plasma membrane of the parenchyma cells, forming a nutrient feeding structure called haustorium (Langcake & Lovell, 1980; Jones et al., 2006; Fröbel & Zyprian 2019b). As signs of early symptoms, yellow oil spot lesions start appearing on the adaxial surface of the leaves. The incubation period ranges from 5 to 21 days, depending on the temperature. White cottony growth appears on the abaxial leaf surface after the post-inoculation stage. At this point, sporangiophores spread by wind or rain, causing secondary infections and a successful primary pathogen life cycle (Caffi et al., 2007; Delmas et al., 2014; Velasquez-Camacho et al., 2022). Under optimal weather condition, the pathogen continues to repeatedly proliferate by encysting and germinating through new tissue for asexual reproduction (Figure 2).

During the end of the asexual reproduction, the thick-walled oospores produced by fertilization of oogonia by antheridia, act as survival spores. The oospores are lodged in dead leaves and other host tissues on the vineyard soil's surface (Figure 1C) (Rouzet et al., 2003). The pathogen is known to persist in the soil for several years in this hibernating stage of oospores. Oospores develop into one germ tube that matures in a sporangium. In order to complete the life cycle, the zoospores mature inside the sporangia and represent primary inoculation for the next late spring (Buonassisi, 2017).

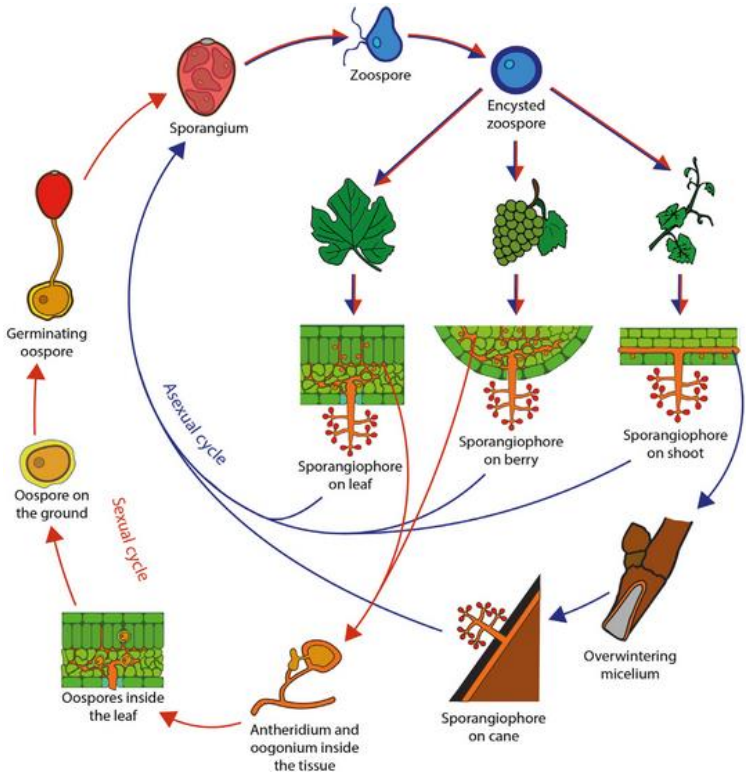

Figure 2 Life cycle and epidemiology of *P. viticola* (Velasquez-Camacho et al., 2022). Red arrows refer to the sexual cycle. Blue arrows refer to the asexual cycle.

1.3 The plant immune system

The study of defence mechanisms has long been a research topic since plants serve as hosts for various pathogens and pests (Bentham et al., 2020). During evolution, plants have developed several defence mechanisms such as physical barriers, secondary metabolites and antimicrobial compounds to combat phytopathogens (Gindro et al., 2006, Zhang et al., 2019; Zhou & Zhang, 2020). Plants possess structural defence through an impermeable waxy cuticle and thorns that serve as their first line of defence by a non-host resistance strategy (Paris et al., 2016; Nishad et al., 2020; Han & Tsuda, 2022). The widely distributed diversity of trichomes also contributes to plant resistance (Kortekamp et al., 1999; Ma et al., 2016; Xing et al., 2017; Barba et al., 2019). Grapevine research, including investigations on leaf hair, demonstrates that the hydrophobic properties of leaf hair structures serve as an effective physical barrier against fungal pathogens (Kortekamp & Zyprian, 1999; Barba et al., 2019) (Figure 3). Pathogens entering the apoplast naturally enter through stomata, and some studies have shown the role of stomata in plant defence (Wang and Gou et al., 2021). The plant's immune system is a network of interactions between

several defense systems inside the cell and the primary protective barriers outlined above (Tsuda & Katagiri, 2010). This depends on the innate immunity of each cell, systematic signalling from the infection sites and the systemic acquired resistance (SAR) (Ausubel et al., 2005; Dangl & Jones, 2001 and 2006; Dodds & Rathjen, 2010; Ali et al., 2018).

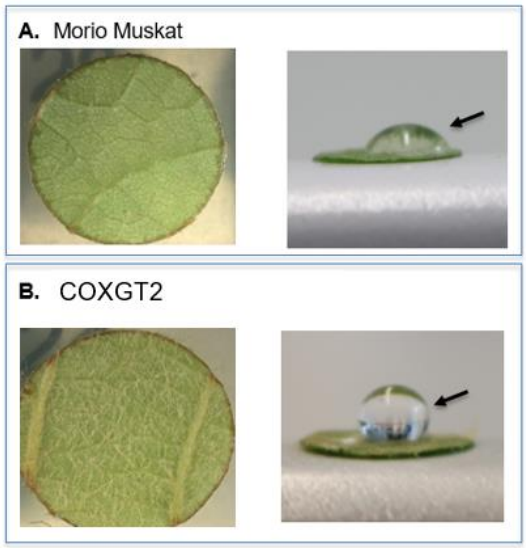

Figure 3 Hydrophobic characteristics; (A) wettable susceptible 'Morio Muskat' and (B) non-wettable genetic resistant donor COxGT2 leaf disc.

The 'ZigZag model', which describes the evolution of plant-pathogen interactions of biotrophic and hemibiotrophic diseases, speculates a reduction in the host immunity due to the co-evolution between plant and pathogen (Figure 4) (Dangl & Jones, 2006; Keller et al., 2016; Kanyuka & Rudd, 2019). In plants, two complementary strategies are involved in pathogen recognition, although both are initiated in different host cell compartments (Lu et al., 2021). Firstly, a pattern recognition receptor (PRR) present on the cell surface detects pathogen-associated molecular patterns (PAMPs)/microbial associated patterns (MAMPs) and induces PAMP-triggered immunity (PTI) (Figure 4; Step 1). Pathogens possess PAMPs and effector proteins. PAMPs are genera-specific structural molecules such as flagellin, chitin, glucans and peptidoglycan (Felix et al., 1993; Gust et al., 2007; Erbs et al., 2008; Thomma et al., 2011). Whereas effectors are known to be species-specific molecules triggered to suppress the primary PTI (Chisholm et al., 2006; Bent et al., 2007). To supress the innate immunity (PTI) exhibited by the plants, pathogens deploy the

effector molecules into the extracellular spaces of plant cells leading to pathogen triggered susceptibility (PTS) (Figure 4; Step 4). However, some plants have evolved and have directly or indirectly developed proteins (NBS-LLR) to recognize isolate-specific pathogen effectors leading to effector-triggered immunity (ETI), an enhanced variant of PTI that is frequently linked to hypersensitivity response (HR) and programmed cell death (PCD) (Zänker, 2008; Rivas, 2012) (Figure 4; Step 3). As counteract, certain evolved pathogens retrigger effector triggred susceptibility (ETS) in plants, by deploying effector variants. The reactivation of the ETI, however, occurs in some plants as a result of adaptation to the evolved pathogen-specific effectors (Jones & Dangl, 2006) (Figure 4; Step 4).

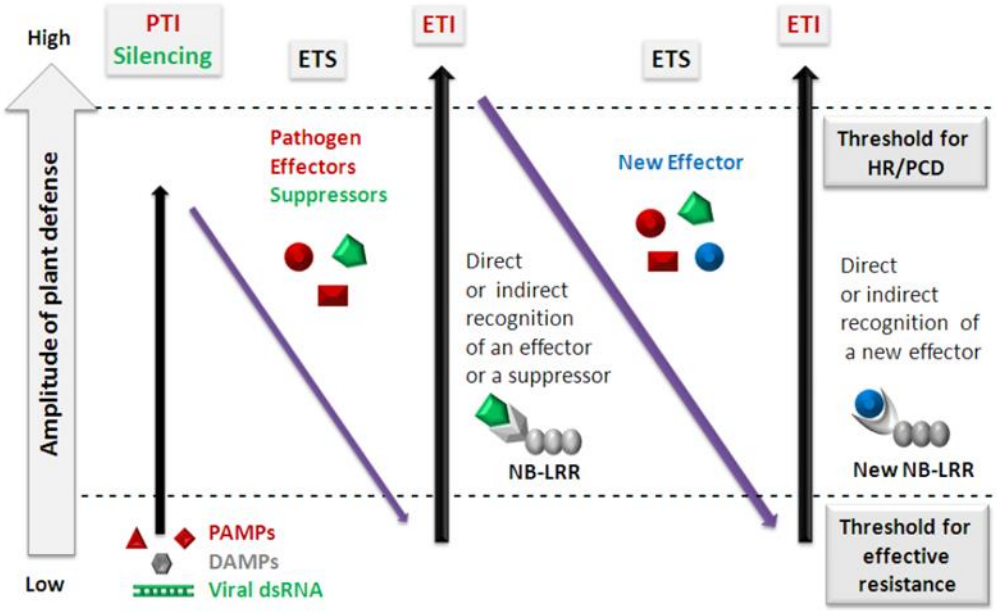

Figure 4 Zigzag model for the evolution of plant innate immunity. The following four phases are illustrated: Step 1: Pathogen/Microbe associated molecular patterns (PAMPs/MAMPs) (red and dark grey) bind to the transmembrane pattern recognition receptors (PRR), initiating PAMP triggered immunity (PTI) in plants. Step 2: Pathogens secrete effector molecules (red and green) into the extracellular spaces of a plant cell to inhibit/suppress the PTI leading to effector-triggered susceptibility (ETS). Step 3: In specific cases, evolved plants directly or indirectly recognise the effector molecules by NBS-LRR receptors leading to activation of effector-triggered immunity (ETI) (Grey). Step 4: Certain pathogens with effector variants that retrigger an ETS in the plant and the reactivation of the ETI as a result of an adaptation of the plant to recognise these new effectors (red and green). The intensity and effectiveness of the defence reaction (amplitude of defence) are indicated as a function of a scale and by exceeding specific limit values (the threshold for effective resistance, the threshold for hypersensitive response/programmed cell death) (Jones & Dangl 2006; Zvereva & Pooggin, 2012).

1.3.1 PTI: PAMP-Triggered Immunity

PTI is commonly referred to as a broad-spectrum primary immune response used by plants to recognize a wide range of features of various intruding pathogens (Ezzat, 2014; Boutrot & Zipfel, 2017; Wan et al., 2019). Pathogens contain conserved range of motifs called 'Pathogen associated molecular patterns' that play a major role in activating PTI in plants. These PAMP molecules, for example, bacterial lipopolysaccharide (LPS)/ endotoxins/ protein subunit of flagellum, are identified by the toll-like receptors (TLRs) and pattern recognition receptors (PRRs) (Chisholm et al., 2006; Ingle et al., 2006; Kato & Svensson, 2015). Structurally, both receptor types have an ectodomain for recognizing pathogenic ligands outside the cell, a simple transmembrane domain for anchoring in the membrane, and a cytoplasmic domain for intracellular signalling (Couto & Zipfel, 2016). In general, the possible defence reactions that can be elicited as a result of a PTI response include, such as an apoplastic oxidative burst, a calcium influx channel, rapid responses of the cytoskeleton, activation of mitogen-activated protein kinase signalling (MAPKs) and activation of a transcriptional cascade. Evidently, which includes stress-related hormone like ethylene and jasmonic acid are all triggered (Chinchilla et al., 2007; Boller & Felix, 2009; Héloir et al., 2019). The PRR-interacting protein identification offers information on the immediate downstream signalling activities (Bigeard et al., 2015). For instance, the RLK family member FLAGELLIN-INSENSITIVE (FLG) is a well-researched PRR in *Arabidopsis thaliana*. The FLS2 gene identified in *A. thaliana*, which codes for an LRR-RLK type receptor, is associated with an immune response to the flg22 elicitor (Gómez-Gómez & Boller, 2002).

The flagellin polypeptide flg22, identified as a bacterial elicitor, triggeres a PTI for representative species of the genus *Vitis* (Felix et al., 1999; Chang & Nick, 2012). The molecular mapping of the cell system of the wild American grapevine *V. rupestris* revealed cell death-independent defence triggered by PAMP flg22 and the cell death-related ETI activated by an elicitor called Harpin (Chang et al., 2017). Studies by Luo et al., 2019 on Chinese wild grapevine varieties revealed that the elicitor flg22 activated and participated in the promoter MYB15-induced basal immunity (PTI). Sulfated laminarin (PS3) has been demonstrated to induce resistance to *P. viticola* in susceptible grapevine cultivars (*V. vinifera cv. Marselan*) (Ménard et al., 2004; Trouvelot et al., 2008). In the same study, it was also demonstrated that the cell wall component β-1,3 glucan sulfate triggers a series of defence mechanisms against *P. viticola* (Trouvelot et al., 2008). Another study by Guan

et al. (2020) showed that a modulator compound called O-methylmellein, in addition to specific elicitors, plays a role in triggering basal immunity against grapevine trunk diseases.

Additionally, one of the initial forms of defence in grapevine is the fast contraction of actin filaments and removal of microtubules (Qiao et al., 2010; Guan et al., 2014). In conclusion, Thomma et al. (2011), however, draws attention to the fact that individual forms of defence reactions often need to be more clearly attributable to PTI or ETI processes. For instance, recent research has shown that the EDS1-PAD4-ADR1 node serves as the foundation for defensive signalling cascades that are activated by both surface-resident and intracellular LRR receptors (Pruitt et al., 2021).

1.3.2 ETI: Effector Triggered Immunity

Effector-triggered immunity (ETI), commonly referred to as gene-for-gene resistance, is a different strategy for inducing plant immunity (Flor, 1971; Jones & Dangl, 2006). As a result of evolution, adaptive microbial pathogens secrete chemical factors or "effectors," that suppress and block PTI, eventually reactivating and promoting infection and leading to effector triggered susceptibility (ETS) (Nürnberger & Kemmerling, 2009; Tsuda & Katagiri, 2010). In some plants, these effector molecules are recognized via intracellular receptors resulting in ETI. Resistance genes (*R*-genes) encode the majority of these intracellular receptors, which are nucleotide binding site (NBS) and leucine-rich repeat (LRR) domain-containing proteins (NBS-LRR), and are expressed on the basis of the perception of the pathogen effectors (Dangl & Jones, 2001; McHale et al., 2006; Dodds et al., 2010; Kourelis & Van Der Hoorn, 2018; Shao et al., 2019). Unquestionably, utilizing *R*-genes to provide disease resistance to the plants is the most successful, ethical, and commonly employed approach in breeding. Furthermore, breeding more robust, sustainable and long-lasting resistance is to stack many *R*-genes in single genotype (Douglas & Halpin, 2010; Chepsergon et al., 2021).

According to structural differences and localization in the N-terminal region, plants have two primary types of NB-LRRs, i. e., TIR-NB-LRR and CC-NBLRR proteins (Takken & Joosten, 2000; Dangl & Jones, 2001; Inohara et al., 2005; Shao et al., 2019). Avirulence (Avr) protein is the identified effector perceived by a receptor that initiates a particular or specific resistance response in plant cytoplasm, explaining the gene for gene model (Oort, 1944; Luderer and Joosten et al., 2002). The investigation of ‘R-protein' function in signal transduction during the plant

resistance response to pathogens was made possible by recently found additional domains (e. g. RPM1, RPS2, RPS5 and WRKY) (Bent et al., 1994; Grant et al., 1995; Mindrinos et al., 1994; Warren et al., 1998; Glowacki et al., 2011). The "guard hypothesis", according to which R-proteins "guard" certain host proteins (referred to as "guardees") that are modified by pathogen effectors (Dangl & Jones, 2001; Luderer & Joosten, 2002). As an example, PBS1 (Guardee) is targeted by bacterial effector protein 'AvrPphB' and guarded by 'RPS5' (van der Hoorn & Kamoun, 2008; Shao et al., 2019).

According to Feechan et al. (2013), only two TIR-NBS-LRR receptor-coding *R*-genes have been found in the North American grapevine *M. rotundifolia* species, mediating resistance to powdery mildew (*Run1*) and downy mildew (*Rpv1*), respectively. It's well studied that *P. viticola*-related infections result in the introduction of cytoplasmic effectors of motif type, i. e., RxLR (Arginine-xxx-Leucine-Arginine), crinkling and necrosis-inducing families (CRN) and cysteine, histidine, x, cycteine (CHXC) into the plant cytoplasm through particular signals (Stassen & Van den Ackerveken, 2011; Lan et al., 2019; Chepsorgen et al., 2021). ETI was activated in leaves of *V. vinifera* after infection with the oomycete *P. viticola* and secretion of RxLR- and CRN-type effector molecules (Jiang & Tyler, 2012). Hence, concluding the association of RxLR effectors in triggering ETI and they also represent potential avirulence proteins (Avr proteins) (Xiang et al., 2016; Yin et al., 2017).

In general, plants initiate defensive reactions after effectors are recognised, including the hypersensitive response (HR) and systemic acquired resistance (SAR) (Brader et al., 2017; Esmaeel et al., 2018; Koledenkova et al., 2022). A recent study showed the recognition of Avr proteins by the induction of an ETI-dependent immune response led by Caspase-like proteases, causing HR and preventing further colonization of the pathogen in resistant grapevine cultivars (Gong et al., 2022). Whereas rapid influx of calcium ions causing HR, it in turn, induces the production of reactive oxygen species (ROS), triggering intracellular signalling pathway causing oxidative burst, finally leading to PCD (Kim et al., 2011; Hatsugai et al., 2015; Wang et al., 2018). Furthermore, the downstream signalling leads to early stomatal closure, accumulation of pathogenesis-related proteins (ex: β-1–3 glucanase), triggering the production of callose and lignin synthesis, and secondary antimicrobial metabolites (e. g. phenols, phytoalexins) (Godfrey et al., 2007; Bigeard et al., 2015; Patel et al., 2020). Jasmonic and salicylic acids mediate resistance to

biotrophic and necrotrophic pathogens, respectively (Zhou & Zhang, 2020). 'VaRPP13' protein identified in *Arabidopsis*, tobacco and grapevine (*V. amurensis* 'Shuang Hong') is known to contribute broad-spectrum resistance to oomycetes via activating SA signalling pathway (Chen et al., 2022).

Evidence of *P. viticola* isolates known to overcome *Rpv3.1, Rpv10, Rpv12,* and *Rpv29* mediated resistance (Peressotti et al., 2010; Eisenmman et al., 2019; Paineau et al., 2022; Marone Fassolo et al., 2022) are the classical examples that demonstrate the Avr effector's adaptation of *P. viticola* leading to ETS response in plants. Nevertheless, the interaction of PTI and ETI to provide plant immunity has yet to be understood entirely. However, research on *Arabidopsis*, tobacco and tomato suggests that the PTI and ETI receptors may coexist in the same protein complex with speculation of early-stage interaction between PTI and ETI signalling (Dodds & Rathjen, 2010; Qi et al., 2011; Li et al., 2019).

1.4 Current status of downy mildew resistance

Resistance to *P. viticola* opens up new breeding opportunities for grapevines. Finding new sources of naturally existing *P. viticola* resistance is paramount in breeding (Eibach et al., 2007; Töpfer et al., 2011). Additionally, to prevent the selection of pathogen strains capable of overcoming these resistances, pyramiding these resistance loci is one of the effective strategies in grapevine breeding (Zini et al., 2019; Töpfer & Trapp et al., 2022). To date, numerous QTLs (quantitative trait loci) are identified in different genetic backgrounds of *Vitis* species and hybrids. These loci vary in their strength, from weak to providing strong resistance to *P. viticola* (Koledenkova et al., 2022; Possamai & Wiedemann-Merdinoglu, 2022; www.vivc.de/loci accessed on 10th December 2022). To date, identified loci and their allelic forms include: *Rpv1* and *Rpv2* from *M. rotundifolia* (Merdinoglu et al., 2003; Wiedemann-Merdinoglu et al., 2006); *Rpv3* and *Rpv19* in American *V. rupestris* (Welter et al., 2007; Bellin et al., 2009; Di Gaspero et al., 2012; Divilov et al., 2018; Foria et al., 2020); *Rpv3.1, Rpv3.2* and *Rpv3.3* (Fischer et al., 2004; Zyprian et al., 2016; Vezzulli et al, 2018; Possamai et al., 2020; Ciubotaru et al., 2021). *Rpv4, Rpv7, Rpv11, Rpv17, Rpv18, Rpv20, and Rpv21* from interspecific hybrid (North American species) (Fischer et al., 2004; Welter et al., 2007; Bellin et al., 2009; Van Heerden et al., 2014; Divilov et al., 2018); *Rpv15* and *Rpv16* in *V. piasezkii* Maxim. (Pap et al., unpublished). *Rpv5, Rpv6 , Rpv9,* and *Rpv13* in *V. riparia* (Marguerit et al., 2009; Moreira et al., 2011*); Rpv14* in *V. cinerea* (Ochssner et al., 2016*); Rpv8,*

Rpv10, *Rpv12*, *Rpv22*, *Rpv23*, *Rpv24*, *Rpv25*, and *Rpv26* in *V. amurensis* (Blasi et al., 2011; Schwander et al., 2012; Venuti et al., 2013; Song et al., 2018; Lin et al., 2019; Schneider et el., 2019; Fu et al., 2020); *Rpv27* in *V. aestivalis* (Sapkota et al., 2015, 2019). *Rpv28* in *V. rupestris* cv. Scheele and *V. riparia* 'Michaux' (Bhattaria et al., 2021). *Rpv29* from 'Mgaloblishvili' (*V. vinifera*) and *Rpv30* and *Rpv31* in other varieties from Georgia (Sargolzaei et al., 2020). Figure 5 illustrates the physical/genomic position of all the resistance loci mentioned above (Figure 5).

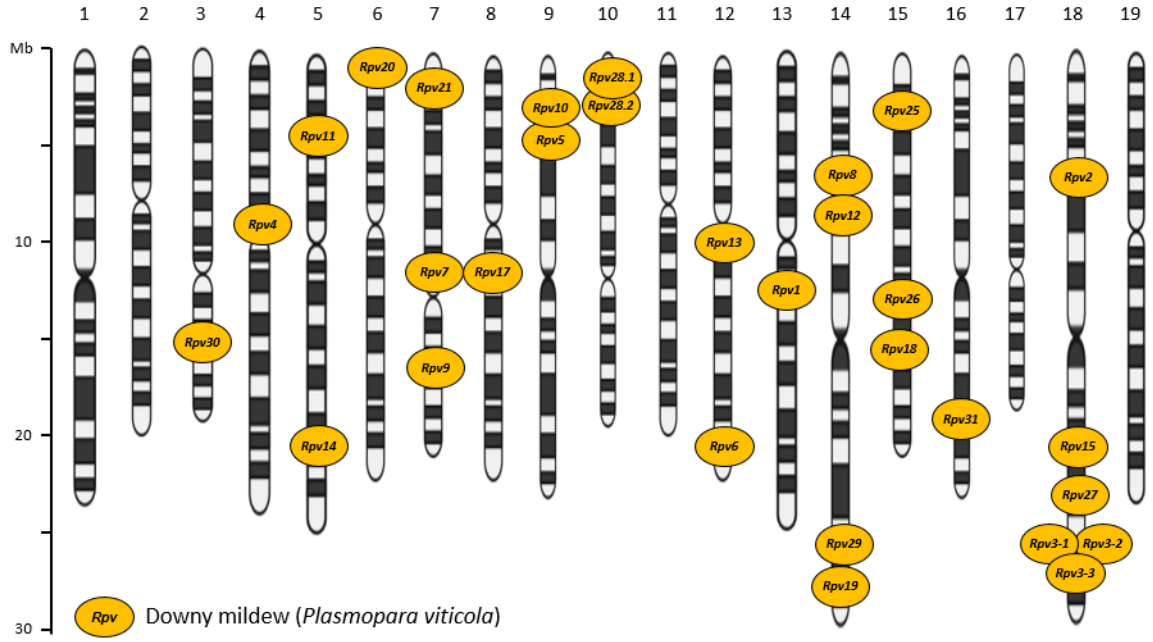

Figure 5 Illustration of the chromosomal location of up to date identified resistance loci to *P. viticola* (*Rpv*) according to www.vivc.de/loci (n = 19; length in [Mb]). The black and white bands on chromosome do not resemble any information.

1.4.1 Wild species: *Vitis coignetiae*

The *V. coignetiae* also called the crimson glory grapevine, is native to Far East Asia (Japanese Islands, Korea, Sakhalin island of Russia) (Figure 6). Some genetic diversity in the *V. coignetiae* grapevines has been observed and reported in Hiruzen, Japan (Okamoto et al., 2002). Furthermore, research reveals current attempts in the last two decades to domesticate *V. coignetiae* in Japan to produce wine (Okamoto et al., 2002). In addition, *V. coignetiae* is used as an ornamental plant in many parts of the world due to its vigorous, mildew tolerance, deciduous climber, lush growth

characteristics and striking red colours in autumn. However, *V. coignetiae* has not been exploited in any resistance investigations thus far although it is cross-fertile with *V. vinifera*.

Figure 6 *Vitis coignetiae* (♂) as an ornamental vine at the Institute for Grapevine Breeding.

1.5 Grapevine resistance breeding

1.5.1 Artificial Intelligence-based phenotyping

In addition to genomics, phenotypic information, which is still a bottleneck in plant breeding, is a critical factor in accelerating plant breeding (Furbank & Tester, 2011; Crossa et al., 2017; Singh et al., 2019). Revolutionizing phenomics with artificial intelligence (AI) has successfully classified various plant traits. Machine learning (ML), a discipline of artificial intelligence, is recognized for executing specific tasks by building algorithms models (Singh et al., 2016; Zhou, 2021). The field of ML is further divided into supervised and unsupervised ML. Supervised learning aims to determine the output for a given object based on a set of provided input features. At the same time, unsupervised ML involves fitting predictive model's parameters to perform well on labelled training data, consisting of inputs and known outputs (Mahesh, 2020; van Dijk et al., 2021). ML or training computers to learn from structures and patterns in large datasets has been widely utilized in plant breeding research to identify, classify and interpret observable dynamic phenotypic traits (Andrade-Sanchez et al., 2013; Yang & Guo, 2017; Niazian and Niedbala et al.,

2020). AI-based, non-invasive, and high throughput phenotyping systems are in great demand, contributing to precision plant breeding. Recent studies have shown the effectiveness, efficiency, and accuracy of sensor and computer-based vision phenotyping approaches in many agricultural systems (Lau et al., 2014; Tardeiu et al., 2017; Mahlein et al., 2019; Van Es et al., 2019; Schramowski et al., 2022; Ren et al., 2022). In grapevine research, AI has been implemented in modelling and predicting phenotyping traits to the AI-based fermentation process (Florea et al., 2022; Fraiwan et al., 2022). In general, when processing sensor data, ML plays a vital role in measuring traits on different levels (van Dijk et al., 2021). Both ground and aerial high throughput (HTP) ML platforms equipped with sensors are utilized to fast and precisely quantify different traits, diseases and vineyard management (van der Heijden et al., 2012; Oerke et al., 2016; Virlet et al., 2017; Romero et al., 2018; Bendel et al., 2020; Rist et al., 2018 & 2022). Based on the recent advancements in machine vision and its application in phenotyping, it is possible to develop a tool for automated image acquisition and analysis (Bock et al., 2010; Mutka & Bart, 2015).

1.5.1.1 The Convolutional Neural Networks

Several ML models have been implemented under vision-based image classification depending on the model's layer depth, including the first Convolutional Neural Network (CNN) architecture AlexNet to Inception and its variant, and from ResNet (Residual neural Network) to the latest YOLO family (You Only Look Once) (Jiang et al., 2022). CNN was invented in 1995 by LeCun and Bengio. Deep Convolutional Neural Networks (DCNNs) are well known for their image classification using deep learning techniques due to the larger number of layers and capability to simultaneously process red, green and blue (RBG) elements of an image (Canziani et al., 2016; Sewak et al., 2018). In general, features are extracted by different convolution layers repeatedly during an image classification and simultaneously combined with mathematical imputation, and the network finally produces an output label (Sewak et al., 2018). CNNs have been extensively reviewed in computer vision reviews, which summarize the basis of their use, their history and their future applications (Rawat et al., 2017; Gracia-Gracia et al., 2018). Deep learning advancements have improved to the point that they can compete with humans in correctly identifying and classifying pictures. However, according to the studies, it is worth to note training CNN with high-quality images might be difficult owing to the constraints of the Graphical Processing Unit and computer memory. Whereas training using low-resolution images may result in the loss of features, ultimately leading to poor accuracy (Véstias, 1997).

In recent years, CNNs have been enthusiastically embraced, and an exponentially developing trend is predicted for CNN-based plant phenotyping. The review articles presented by Saleem et al. (2019) and Lu et al. (2021), provide detailed insights into implementing CNNs in plant phenotyping. Yang & Xu et al. (2021) provides extensive information on deep learning methodologies in horticulture research. Deep learning has been implicated in the identification of different grapevine cultivars (Liu et al., 2021). Studies conducted in grapevine breeding research have shown that CNNs have outperformed traditional phenotyping methods for improved image processing and precision (Lauguico et al., 2020; Nasiri et al., 2021; Mohimont et al., 2022; Fraiwan et al., 2022). Grapevine breeding research and investigations like linkage and association mapping rely heavily on precise phenotypic data (Zendler et al., 2021). Breeding for disease resistance traits (powdery mildew and downy mildew) mainly involves artificial inoculation experiments (leaf disc assays) followed by manual phenotyping (Huang et al., 2020; Possamai & Merdinoglu, 2022). When more than one individual works on a traditional phenotypic method involving a score-based system, the subjectivity is intense, effecting the overall output.

Furthermore, phenotyping thousands of samples using biological replicates makes the entire procedure not only time-intensive but also laborious (Lu et al., 2021). This indicates that there is a requirement for HTP, accurate and objective phenotyping tools. However, it is possible to develop algorithms capable of learning complex features which can be implemented in laboratory-based phenotyping models. Eventually, it can speed up breeding studies by boosting phenotyping accuracy and minimizing manpower requirements. Bierman et al. (2019) presented a CNN-based GoogLeNet model with 94 % accuracy for HTP quantification of powdery mildew. Accurate and precise downy mildew evaluation tools are crucial for QTL analyis. Whereas, traditional methodologies tend to produce bais and are time intensive. In addition, no laboratory based image analysis tools are currently available for downy mildew disease assessment. In this study, a shallow convolutional neural network (SCNN)-based grapevine downy mildew disease quantification model (Zendler et al., 2021) involving less hidden layers in comparison to DCNN and a Residual Neural Network (ResNet) based model for grapevine leaf hair quantification was developed.

1.5.2 Genotyping

*1.5.2.1 PIWI cultivars (*ger. *pilzwiderstandsfähige Rebsorten)*

Grapevine (*V. vinifera L.)* has enormous agricultural and commercial importance globally, with several million hectares invested in viticulture (OIV, 2021; Sosa-Zugina et al., 2022). Some of the major devastating fungal diseases of grapevine include downy mildew (*Plasmopara viticola*) and powdery Mildew (*Erysiphe necator*) effecting the quality and quantity (refer to section 1.2). In a broader spectrum, severe yield and financial losses have been observed over the years (OIV, 2020; OIV, 2021; Jermini et al., 1997, 2010). The management strategies for the diseases in traditional *V. vinifera* cultivars necessitate the extensive use of fungicides regularly. Over the years, fungicide use has become increasingly widespread since the mid-19th century and is widely considered to offer the best protection against grapevine diseases (Nicholas et al., 1994). In the European Union, viticulture uses nearly 60-70 % of fungicides to control downy and powdery mildew infection (Furiosai et al., 2022). In additon to the synthetic fungicides for controlling downy mildew, copper sulfate has been used successfully utilized in the form of sulfate in organic viticulture. According to EU regulations, maximum of 6 kg/ha of copper is used for viticulture. In the last two decades, the German ministry for agriculture spent about €10.2 million for research on a copper minimisation strategy (Kühne et al., 2017; Tamm et al., 2018a, 2018b).

However, despite their usefulness, they potentially pose a significant threat to humans and the environment (Steeland and Bofetta, 2000; Carausu et al., 2016; Li et al., 2018; Dimuitriu et al., 2022). Moreover, copper is a heavy metal and according to the recent studies the negative impact of copper sulfate residues found in soil and aquifers give rise to eco-toxicological effects (Ruyters et al., 2013; Ballabio et al., 2018; Karimi et al., 2021). In addition, studies have shown a negative impact on non-target organisms due to the fungicide application in viticulture (Bereswill et al., 2012; Marhino et al., 2020).

Viticulture's sustainability depends on finding a critical balance between controlling fungal diseases and protecting the environment. Naturally available resistances from American wild grapevine species were apparently used in generating the first fungus resistant cultivars known as 'French/ American Hybrids' as early disease control options (Kole, 2011, p. 10; Eibach & Töpfer, 2007; Blaser & Scherz, 2011). These early varieties were particularly resistant but had poor wine quality, prompting France to restrict these fungal-resistant cultivars in 1953 (Alleweldt & Possingham, 1988; Di Gaspero et al., 2012). However, contemporary PIWI varieties (ger.

pilzwiderstandsfähige Rebsorten (fungus-resistant cultivars)) established through multiple repeated backcrosses with *V. vinifera* varieties are particularly beneficial in terms of sustainability, in addition to excellent resistance and wine quality (Alleweldt & Possingham, 1988; Töpfer et al., 2011a; Di Gaspero et al., 2012; Rousseau et al., 2013; Finger et al., 2022). Since 2008 (Germany and Europe), cultivar 'Regent' is one of the most cultivated PIWI and an excellent successful story of grapevine resistant breeding (DeStatis, 2016; Pedneault & Provost, 2016; Maul et al., 2021). Recent data suggest a minor reduction in 'Regent' cultivation (1,917 ha), although it remains one of Germany's most extensively grown PIWI cultivars (DeStatis, 2016; Müllner, 2021). Some of the impactful representative cultivars increasing in demand include 'Cabernet Blanc', 'Calardis Blanc', 'Muscaris', 'Sauvitage', 'Sauvignac' and 'Souvignier Gris' (Richter, 2022). Over the last few years, there has been a gradual growth in PIWI cultivation. In 2019, the total area under PIWI wine cultivation was approximately 2,600 ha; in 2020, approximately 2,650 ha and in 2021 2,713 ha. This corresponds to 2.62 % of the German vineyard area (103,421 ha) (Richter, 2022). Private entities and public research institutes have launched grapevine-breeding activities for fungus-resistant cultivars (Spring & Dupraz, 2021).

1.5.2.2 Marker-Assisted Selection

American/French hybrids opened up new perspectives in grapevine breeding. However, using classical hybridization principles and conventional selection processes, the decision to include resistance and viticultural traits from a particular parentage was mainly based on long-term visual evaluation and micro-vinification results (Töpfer et al., 2011; Eibach & Töpfer et al., 2015). In addition, a further obstacle was grapevine's woody perennial nature, with their long generation cycle (3-5 years) due to a long juvenile period, strong inbreeding depression, and require plenty of resources and time (Kole, 2011, p. 160; Töpfer et al., 2011; Töpfer & Trapp, 2022). Furthermore, breeding a new cultivar using traditional selection techniques took approximately 25 – 30 years from the initial cross to its release (Eibach & Töpfer et al., 2015).

Molecular tools and the sequencing of the grapevine genome have revolutionized grapevine breeding in the 21st century (Jaillon et al., 2007; Velasco et al., 2007; Smit et al., 2020). Linkage (QTL) and association mapping (GWAS), based on DNA marker information from a specific parental cross, have made it possible to introduce molecular markers and then assist in selecting desirable traits, a process commonly referred to as Marker-Assisted Selection (MAS) (Paterson et al., 1988; Tanksley, 1993; Kearsey, 1998). The introduction of polymorphic SSR-based DNA

markers made an early contribution to creating linkage maps (Riaz et al., 2006 & 2008). The QTL analysis, involving phenotypic and genotypic correlation, assisted in the identification of new resistance loci associated with the traits and subsequently developing markers for MAS (Dalbo et al., 2000; Kole 2011, p. 112).

MAS is exploited by breeders to accelerate the breeding process and select genotypes more effectively with minimal use of resources (Collard, 2005; Collard & McKill, 2008). In addition, in contrary to the empirical breeding, MAS assists in selecting prospective young seedlings early on, improving genetic gain by rapid development of varieties with targeted traits and reduce the time of breeding process by 5-10 years (Eibach & Töpfer 2015; Töpfer & Trapp, 2022). Several marker systems have been developed based on the method of detection and mode of transmission that help in linkage or association mapping and successfully applied in plant breeding activities (Agarwal et al., 2008; Grover & Sharma, 2016; Nadeem et al., 2018). The PCR-based DNA marker techniques include: RFLP (restriction fragment length polymorphism) earlier used to identify polymorphic loci due to different DNA restriction patterns, RAPD (random amplified polymorphic DNA, AFLP (amplified fragment length polymorphism), and SSR (simple sequence repeats).

The genome-wide distribution, codominant, highly transferable, polymorphic, and cost-efficient features of SSR markers made them reliable in linkage studies (Töpfer et al., 2011b; Vieira et al., 2016). The latest genetic studies in grapevine involved the usage of genotyping-by-sequencing (GBS) and amplicon-based SNP markers, enabling the detection of point mutations, insertion and deletion (InDels) of individual nucleotides (Lijavetzky et al., 2007; Laucou et al., 2018; Negus et al., 2021; Vervelle et al., 2022). A recent SNP study revealed genome-wide variation linked to the early ripening of grape mutants (Pei et al., 2021). Furthermore, SNP-based genotyping has been employed in assessing genetic variability, diversity, population structure and genetic architecture of multiple traits in grapevines (Mercati et al., 2016; De Lorenzes et al., 2019; D'Onofrio et al., 2021; Bianchi et al., 2022). The *Vitis* genus presents a significant degree of structural variation, challenging the transferable marker development (Zou et al., 2020). Hence, marker transferability remains an additional concern in grapevine breeding research. The latest rhAmpSeq marker system was designed especially for the core *Vitis* genome. It offers high marker transferability of up to 92 %, high throughput, and the detection of multi-allelic SNPs (Zou et al., 2020). In addition, the rhAmpSeq markers system provides highly specific binding of markers and obtain high multiplexing avoiding primer dimer formation. The implication of the rhAmpSeq markers and its

transferability has been successfully shown in recent studies (Yin et al., 2021; Olson et al., 2021; Karn et al., 2021; Reshef et al., 2022; Alhakoon et al., 2022; Buck et al., 2022; Park et al., 2022).

1.5.2.3 Pyramiding resistance loci

The resistant PIWI cultivars allow for a reduction of fungicide application depending on the strength of their resistance (Töpfer & Trapp, 2022). The ultimate aim of grapevine breeding is to develop grapevine cultivars with durable resistance without compromising the wine quality (Töpfer et al., 2011a). As a new dimension, climate change plays a vital role and a deciding factor in terms of the quantity of fungicides applied and the outbreak of diseases (Töpfer & Trapp, 2022). Eventually, finding new resistance loci is of high importance and value. However, single locus imparting resistance is broken due to the continuous adaptation of the pathogen (Peressotti et al., 2010; Töpfer et al., 2011). Recent studies have shown the existence of different isolates of *P. viticola* and their capability of overcoming host resistance, i. e., *Rpv3, Rpv10,* and *Rpv12* (Delmotte et al., 2006, 2014; Gómez-Zeledón et al., 2013, 2017; Eisenmann et al., 2019; Wingerter et al., 2021; Paineau et al., 2022). Therefore, stacking loci from different resistant donors with diverse resistance mechanisms might be a feasible strategy to durable resistant cultivars (Töpfer et al., 2011 and 2011a). A first example of resistance pyramiding in grapevine was shown by Eibach et al. (2007), combining resistances of line VRH3082-1-42 carrying *Run1/Rpv1* locus with resistance found in 'Regent,' i. e., loci *Ren3/Rpv3*. The offspring of this cross was screened using MAS to identify the presence of pyramided loci, followed by corresponding phenotyping assessments. A recent study conducted by Ciubotaru et al. (2021) showed that, contrary to mono-locus genotypes, an early (12 h) synthesis of metabolites (phenolic compounds, acids, aldehydes, etc.) was observed in pyramided genotypes (*Rpv3.1* and *Rpv12*; *Rpv3.1, Rpv3.2* and *Rpv10*) in response to *P. viticola* infection. As a result, it was concluded that pyramided resistance involves many mechanisms that inhibit pathogen growth and are helpful for genetic improvements in grapevine.

1.6 Research objectives

As previously stated, traditional grapevine cultivars derived from *V. vinifera* are in high demand due to their exceptional wine quality. However, they are also highly vulnerable to downy mildew, a catastrophic disease caused by the host-specific oomycete *P. viticola,* that necessitates the extensive and regular application of fungicides. This research's primary and fundamental aim is to

reduce the usage of fungicides that are applied to control downy mildew incidences by identifying the novel resistances from an unexploited wild species. Since the world demands sustainable viticulture, the elimination of the detrimental impact of fungicides on human health and the environment is crucial. Existing resistant grapevine cultivars are developed through long-term breeding strategies, and several resistance loci to *P. viticola* have been identified (www.vivc.de). However, only a few of these resistance loci have been exploited in developing cultivars showing promising resistance to downy mildew.

The research objective is identifying naturally occurring new resistance loci from the unexploited wild *Vitis* species *V. coignetiae* by applying genetic mapping with classical QTL analysis. Greenhouse grown potted plants of a bi-parental F1 population ('Morio Muskat' x COxGT2 (*V. coignetiae* x 'Gewürztraminer')) were utilized for genetic and phenotypic analysis (leaf disc assay). Field resistance to downy mildew was observed in the *V. coignetia*e derived cross 'COxGT2' individual. In addition, the F1 population shows quantitative seggregation for the morphological trait leaf hair, know to act as a physcial barrier against downy mildew. Therefore, the association between the leaf hair and downy mildew will be determined in this study. Markers linked tightly to the resistance loci shall be identified as a prerequisite for MAS in breeding programs. Furthermore, the comparison of identified resistance loci to some of the already existing resistance loci will be carried out. Moreover, *P. viticola* proliferation in different resistance carrying genotypes (*Rpv8, Rpv12*) and microscopic analysis of pathogen mycelium development in the parental genotypes ('Morio Muskat' and COxGT2) will be evaluated at different time points (1, 3, and 5 days post inoculation).

Additionally, due to a large number of F1 individuals (#496) and replicates (approx. 2000 leaf discs/single experiment/year), manual scoring phenotyping results are time-consuming, tedious, and highly subjective. Nevertheless, revolution in machine learning has led to the development of accurate and precise measurement of phenotypic traits. This research work also focused on developing a low-cost artificial intelligence-based high throughput (HTP) downy mildew disease severity and leaf hair quantification models. Both the CNN-based models will be trained, tested, and validated on the F1 population Gf.2018-063.

2 Materials and Methods

2.1 Materials

2.1.1 List of chemicals and kits

Chemicals	Application	Supplier
2-Mercaptoethanol (≥ 99 %)	Total genomic DNA extraction	Carl Roth GmbH + Co. KG, Karlsruhe
Agar	Gel electrophoresis	Gustav Essig GmbH & Co. KG, Mannheim
	Leaf disc assays	Essig GmbH & Co. KG, Mannheim, Germany
Agarose	Gel electrophoresis	Axon Labortechnik GmbH, Kaiserslautern
Aniline blue	Microscopic staining	Merck KGaA, Darmstadt
DNeasy® Plant Mini Kit	Total genomic DNA extraction	Qiagen, Venlo, Netherlands
Ethanol, absolute	DNA extraction	Th. Geyer GmbH & Co. KG, Renningen
GeneRulerTM 1 kb DNA Ladder Mix	DNA ladder	Thermo Fisher Scientific Inc., Waltham, MA, USA
GeneRulerTM LR	DNA ladder	Thermo Fisher Scientific Inc., Waltham, MA, USA
KAPA2G Fast Multiplex Mix	Multiplex kit for SSR marker analysis	KAPA Biosystems, Wilmington, Massachusetts, USA
NucleoSpin® 96 Plant II	Total genomic DNA extraction	Macherey-Nagel GmbH & Co. KG, Düren
peqGOLD Plant DNA Mini Kit	Total genomic DNA extraction	VWR International GmbH, Randor, PA, USA
Trypan blue	Microscopic staining	PanReac AppliChem ITW Reagents, Darmstadt

50x TAE Puffer pH 8,3	Total genomic DNA extraction	Carl Roth GmbH + Co. KG, Karlsruhe
50x TE Puffer (pH 8,0)	Total genomic DNA extraction	Carl Roth GmbH + Co. KG, Karlsruhe
EDTA-Na_2	Total genomic DNA extraction	Carl Roth GmbH + Co. KG, Karlsruhe
TRIS	Total genomic DNA extraction	Carl Roth GmbH + Co. KG, Karlsruhe

2.1.2 List of laboratory equipments

Application	**Equipments**	**Suppliers**
Agarose gel documentation	QUANTUM ST5 with UV light	Vilber Lourmat GmbH, Eberhardzell
Centrifugation	Table top centrifuge 5452	Eppendorf AG, Hamburg
	Sigma 6-16KS	Sigma Laborzentrifugen GmbH, Germany
Incubator	Thermomixer compact	Eppendorf AG, Hamburg
Leaf disc assay	Stereo microscope Axio Zoom.V16	Carl Zeiss AG, Oberkochen
	Corning® 245 mm Square BioAssay Dish with Handles, not TC-treated Culture (no. 431111)	Corning, Arizona, USA
	Hemocytometer (counting chamber)	Paul Marienfeld GmbH & Co. KG, Lauda Königshofen
	Thermo Fischer scientific Cork borer (10mm)	Thermo Fischer scientific, Houston, USA
Plant Tissuelyser	Paint Shaker-SK450	Fast & Fluid Management B. V., Sassenheim, NL
	Tissuelyser RETSCH	Qiagen GmbH, Hilden
Photometer	Microplate-Reader CLARIOstar	BMG Labtech GmbH, Ortenberg
PCR	ABI 9700 Thermocycler	Applied Biosystems, Darmstadt

	GeneAmp PCR system 9700	Applied Biosystems, Darmstadt
PCR fragment analysis	ABI 3130xl Genetic Analyser	Applied Biosystems, Darmstadt
	Agagel Mini	BiometraR GmbH, Göttingen
	EC360 Midi Cell Electrophoretic Gel System	E-C Apparatus Corporation, Milford, USA
	Power Supply EC105	E-C Apparatus Corporation, Milford, USA
Microscopy	Stereo microscope Leica M205FA 1x – 160x	Leica Camera AG, Wetzlar
	Microscope specimen slide	Thermo Fisher Scientific Inc., Waltham, MA, USA
	Micro slide and cover glass	Waldemar Knittel Glasbearbeitungs GmbH, Bielefeld
Miscellaneous	384-Well-Plate	Biozym Scientific GmbH, Hessisch Oldendorf
	96-Well-Plate	Kisker Biotech GmbH & Co. KG, Steinfurt
	Deep freezer -20°C GNP 4166	Liebherr, Bulle, CH
	Eppendorf micro tube (0.2,0.5,1,1.5,2,15,50 ml)	Eppendorf AG, Hamburg
	Eppendorf table centrifuge	Eppendorf AG, Hamburg
	Refrigerator +4°C ,KS36VAW41	Siemens, München
Vortex	Vortex Genie 2TM	Scientific Industries, Bohamia, NY USA
Weigh balance	Weighing balance PB3015	Sartorius, Göttingen
	Kern ABJ-NM	KERN & SOHN GmbH, Hamburg

2.1.3 List of software and online tools

Application	Softwares and online tools	Suppliers/links
SCNN/ResNet CNN	Python 3.10.7	Python Software Foundation License
	Unix/Linux	Debian
Data Bank	BLAST	Basic local alignment search tool https://blast.ncbi.nlm.nih.gov/Blast.cgi Altschul et al., 1990 Altschul et al., 1997
	BUSCO	Benchmarking Universal Single-Copy Orthologs https://busco.ezlab.org/ Simão et al., 2015 Waterhouse et al., 2018
	National Center for Biotechnology Information (NCBI)	NCBI Bethesda MD, USA www.ncbi.nlm.nih.gov
	Phytzome Version 13	https://phytozome-next.jgi.doe.gov/
	GBVitis	JKI/DV S. Kecke, G. Marx, A. Ganesh v6.4
	Vitis International Variety Catalogue (*V*IVC)	www.vivc.de Maul et al., 2021
Genetic map - SSR	Join Map 5.0	Kyazma, Wageningen, Netherlands
Genetic map - rhAmpSeq	Lep-MAP3 (Genetic map)	https://sourceforge.net/p/lep-map3/wiki/LM3 %20Home/
	Unix/Linux	Debian
	Perl	https://www.perl.org/
	Java	Oracle (https://www.java.com/download/ie_manual.jsp)

GWAS - rhAmpSeq	Tassel 5.0	BUCKER LAB (Ed Buckers laboratory) https://tassel.bitbucket.io/
PCR fragment analysis	Gene Mapper 5.0	Applied Biosystems, Darmstadt
QTL analysis - SSR	Map QTL 5 and 6	Kyazma, Wageningen, Netherlands
Respository	GitHub	© 2022 GitHub, Inc., https://github.com
Statistical analysis	R and R-studio	Version 4.0.3 https://www.R-project.org/ R Core Team, 2020

2.1.4 Plant material

The breeding line COxGT2 (also denominated as 'PIWI süd') plant material described to exhibit a high level of field resistance to downy mildew was obtained from the nursery of grapevine breeder Edwin Schrank, Dackenheim, Germany. A biparental segregating F1 population 'Gf.2018-063' (Figure 7) consisting of 496 individuals derived from the crossing of 'Morio Muskat' x COxGT2 was utilized in resistance mapping studies. The crossing was completed in 2018 and the seedlings were planted in 2019.

A 'Cabernet Dorsa' ('Blaufränkisch' x 'Dornfelder') x Couderc 13 (*Vitis aestivalis* var. *lincecumii* x Couderc 162-5) population, 'Gf.2018-074', consisting of 314 F1 individuals, was used in addition to the 'Gf.2018-063' population to develop a SCNN-based downy mildew quantification system. The ResNET-based leaf hair quantification model was developed using the populations Gf.2018-063 and validated using three well-known hairy ('Pinot Meunier', 'Tigvoasa', and *V. thunbergii*) and non-hairy ('Riesling', 'Merlot', and 'Cabernet Sauvignon') genotypes.

All the experimental plants utilized in this study are maintained in the greenhouses at the Institute for Grapevine Breeding Geilweilerhof with a single shoot of approx. 30-40 cm in height and a pot diameter of 20 cm. The plants were regularly irrigated and sprayed with sulphur-containing fungicides to prevent powdery mildew incidences. No spraying was carried out a week before the artificial leaf disc inoculation experiment.

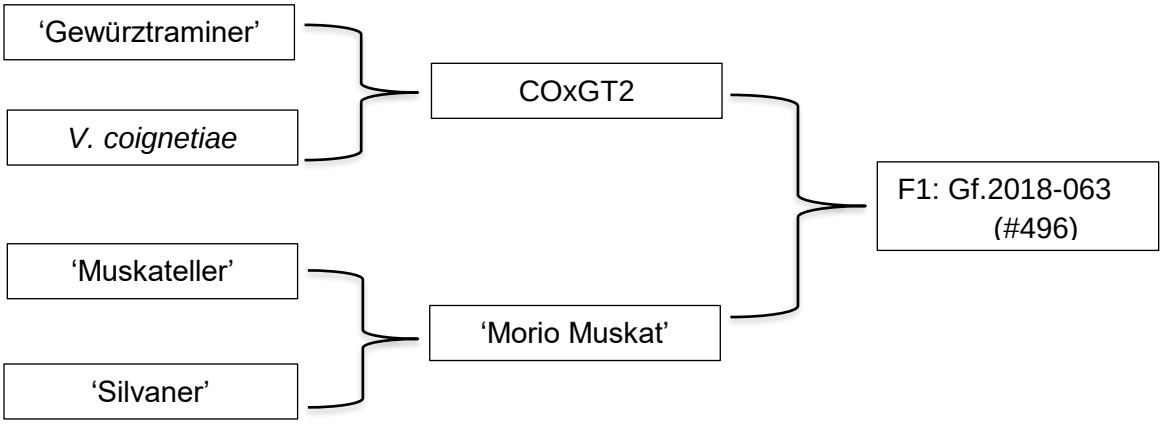

Figure 7 A bi-parental F1 population ‘Gf.2018-063’ (N = 496) derived from the cross of ‘Morio Muskat’ x COxGT2 (*V. coignetiae* x ’Gewürztraminer’).

2.1.5 *Plasmopara viticola* spore material

P. viticola spores were collected using a filter-based suction tip from the naturally infected susceptible grapevine varieties ‘Müller Thurgau’ and ‘Riesling’ from untreated fields. Some of the spore material was propagated on ‘Müller Thurgau’ and ‘Riesling’ leaves under controlled laboratory conditions (32 °C, 72 % rH). The collected material was stored at -20 °C and was thawed at room temperature before use.

2.2 Methods

2.2.1 Phenotypic assessment

2.2.1.1 Leaf disc assay

The phenotypic assessment of resistance was carried out using artificially inoculated leaf disc assays (LDA). To achieve an uniform physiological leaf age for all the genotypes, the fourth or fifth leaf from the apical node was collected. Four leaf discs per genotype were excised using a stainless steel cork borer (1 cm diameter) and were placed upside-down on 1 % water agar in 245 mm Square BioAssay Dishes and were placed according to a template of two 96 sample grids as shown in the Figure 8A and 8B. Control leaf discs were sprayed with autoclaved ddH_2O. The grid template was designed to suit the Zeiss AxioZoom v16 (see 2.2.1.2) motorized table's specifications. The leaf discs were artificially infected by placing 30 µl of sporangia suspension of concentration approximately 22,000 sporangia/ml. The water-diluted sporangia density was

determined before infecting discs using a hemocytometer and the concentration was adjusted accordingly. Infected leaf discs were incubated overnight in dark at 24 °C, the spore suspension drops were removed the next day using a water-jet pump, and further incubation was carried out at 22 °C with a photoperiod of 16 h (full spectrum light) and high relative humidity of 72 %. Leaf discs were evaluated post five days of inoculation.

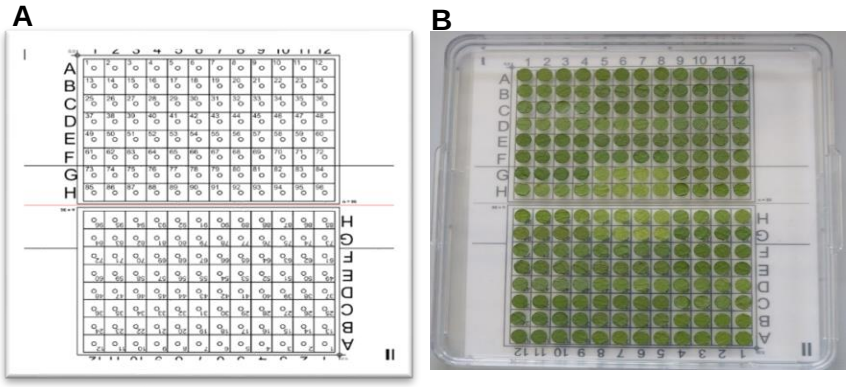

Figure 8 Grid template (A) used for placing leaf discs on a square 24.5 cm × 24.5 cm petri dish filled with 1 % water agar and a picture of square dishes with leaf discs on them (B).

2.2.1.2 High throughput imaging

A Zeiss Axio Zoom V16 (Jena, Germany) with a motorized table and a 0.5 magnification lens (PlanApo Z 0.5/0.125; Free Working Distance 114 mm) was utilized for automated imaging of post five days inoculated leaf discs with *P. viticola*. All the leaf disc images were recorded at 10.5-fold magnification. The program ZenBlue version 3.4 (Zeiss, Jena, Germany) was used to create a movement template that automatically accessed the 96 places with one cm diameter spacing (Figure 8). The leaf discs were lit using a backlight, two gooseneck lights, and an LED ring light. To appropriately illuminate sporangiophores growing from the leaf discs, the gooseneck lights were angled at a 45° angle. The combined exposure period of the three lights was adjusted and fixed to default at 18–20 ms, making the whole imaging process high throughput. The Zeiss Axio Zoom (Jena, Germany) V16 is integrated with a software-autofocus, which was utilized to determine the ideal focal height for each individual leaf disc before imaging. Lowest suitable aperture of 39 % was utilized to get feasible maximum focal depth. For the trained CNN to accurately classify images, consistent illumination of leaf discs was essential. The plate was turned

180° after imaging the first 96 samples, and the second half of the plate was captured. It took around 15 minutes to image all 96-leaf discs. For additional analysis, images were exported as JPEG files with a resolution of 2752 x 2208 dpi and original files were saved as .czi format. With the use of a Python script and a naming template, the exported photos were renamed (available in the GitHub repository). A sample template which can be directly loaded into Zen Blue 3.0 is available in the below link (https://github.com/Daniel-Ze/Leaf-disc-scoring).

2.2.1.3 Manual phenotyping: Downy Mildew

Downy mildew phenotypic evaluation was based on the number of sporangia formed on the leaf disc images captured at 5 dpi (days post-inoculation). A reversed five-class OIV 452-1 descriptor (OIV, 2nd edition 2001, https://www.oiv.int/) scale was utilized for the visual phenotypic assessment (Figure 9). The density of sporangia developed on the leaf discs defined disease severity. Where score 1: no sporangiophores (highly resistant), score 3: one to five sporangiophores (resistant), score 5: six to twenty sporangiophores (moderate), score 7: more than twenty (susceptible), and score 9: a dense uniform cottony cloud of sporangiophores (highly susceptible).

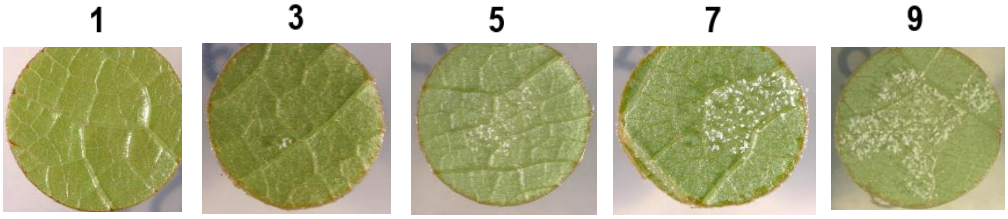

Figure 9 A reversed five-class OIV 452-1 descriptor for downy mildew resistance.

2.2.1.4 Manual Phenotyping: Leaf hair

The leaf hair evaluation was based on the density of abaxial (lower surface) leaf hair present on the leaf discs. A well-established OIV-086 descriptor was utilized for leaf hair evaluation (OIV, PGRI; 6.1.37, https://www.oiv.int/). Where class, 1: None/Very low hair; 3: Low; 5: Medium; 7: High; 9: Very high (Lanate/ dense cover of hair) (Figure 10).

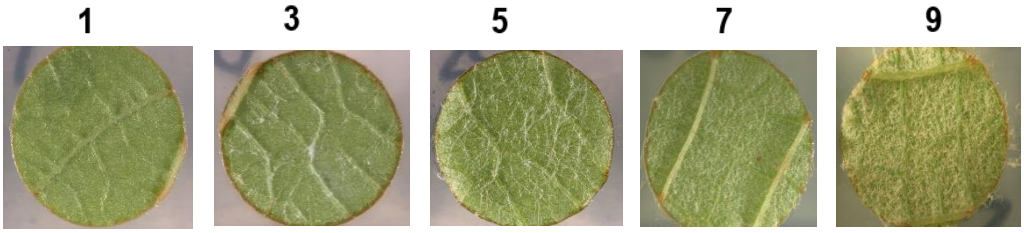

Figure 10 A five-class OIV 086 descriptor for leaf hair density.

2.2.1.5 Correlation of Phenotypic data: Downy Mildew vs. leaf hair

According to the hypothetical question, the influence of leaf hair density on *P. viticola* infection decrement was investigated by correlating at both molecular and phenotypic level. The manually evaluated phenotypic data of downy mildew resistance were correlated with the phenotypic data of leaf hair each year with individual experiments using Spearman correlation coefficient (rSp), using the statistical program 'R' software, v. 3.4.5 (R Core Team 2017).

2.2.2 DNA extraction

To extract the genomic DNA from the young and healthy grapevine leaf material, about 1 cm² of leaf from the third leaf of a shoot tip were harvested in 96 deep well plates containing steel beads, frozen in liquid nitrogen and ground using a TissueLyser mill (Qiagen GmbH, Hilden, Germany). The genomic DNA utilized for the SSR marker was isolated using the protocol of Nucleospin 96 II DNA Kit (Macherey Nagel, Germany). Whereas, the genomic DNA for rhAmpSeq marker analysis was extracted using the protocol of peqGOLD Plant DNA Mini Kit (VWR).

2.2.3 Marker analysis

The concentration and the quality of all the extracted genomic DNA samples were analyzed on the agarose gel and spectrophotometric measurements (CLARIO STAR) at 260 nm (A260). For further marker analysis, the average concentration of all the DNA samples was set to 1 ng/µl by dilution.

2.2.3.1 SSR markers

Preexisting Simple Sequence Repeats (SSR) markers available at the institute were utilized in the initial genetic map creation and fine mapping of the population Gf.2018-063. The SSR markers used were selected from published mapping work (Thomas & Scott, 1993; Bowers et al., 1996;

Bowers et al.,1999; *Vitis* Microsatellite Consortium; Sefc et al., 1999; Scott et al. 2000; Scott et al., 2000; Dalbo et al., 2001; Adam-Blondon et al. 2004; Merdinoglu et al., 2005; Doligez et al., 2006; Di Gaspero et al., 2005 and 2007; Welter et al., 2007; Cipriani et al., 2008; Salmaso et al., 2008; Coleman et al., 2009; Fournier-Level et al., 2009; Di Gaspero et al., 2011; Blasi et al., 2011; Schwander et al., 2012; Fechter et al., 2012 and 2014; Venuti et al., 2013; Van Heerden et al., 2014; Zyprian et al., 2016; Zendler et al., 2017) and were chosen based on their functionality standard and fluorescent dye (FAM, HEX, TAMRA and ROX). These markers were tested on a subset of the population for testing their suitability for multiplexing and their segregation pattern. Up to eight markers with suitable segregation, patterns were multiplexed further and run on the overall population.

2.2.3.2 PCR

PCR was performed in 96 or 384 well plates using the GeneAmp PCR System 9700 (Applied Biosystems) thermocyclers, according to the Kapa2G Fast Multiplex PCR Mix kit protocol and following approach given in Table 1. The fragments (between 35 – 500 bp) of the size standard mixed post PCR reaction were marked with LIZ® and identical to the commercially available GeneScan™ 500 LIZ®.

Table 1 PCR approach and protocol.

Master mix 5 µl approach	
Component	**Amount [µl]**
gDNA (1 ng)	1
Forward primer	0.015 – 0.03
Reverse primer	0.015 – 0.03
PeqLab-Mastermix	2.5
H_2O	5

PCR protocol		
Temperature [°C]	**Time [min]**	
95	3:00	
95	0:15	
60	0:30	X 30
72	0:30	
72	7:00	
4	∞	

After performing the PCR, the amplified products were diluted with 10 µl of H_2O and 1 µl of the diluted reaction was transferred to a new 96 or 384-well plate. 12.5 µl of LIZ solution (0.5 µl LIZ

size standard and 12 µl H_2O LiChrosolv) were then added to the DNA followed by denaturation at 95 °C for 5 min and cooled down to 4 °C. To analyze genetic markers, the plate was transferred to a capillary sequencer (ABI 3130 xl, Applied Biosystems, Invitrogen, Foster City, California, USA) of the 16-channel capillary (36 cm) filled with polymer POP-7™. Each SSR marker's primer has a fluorescent dye (6-FAM, HEX, TAMRA, or ROX) tagged at the 5' end for detection (the primers were created and marked by Metabion, Planegg-Martinsried). The fragment length was analyzed using the GeneMapper® 5.0 software program (Applied Biosystems, Invitrogen, Foster City, California, USA).

2.2.3.3 RNase H2-dependent amplicon sequencing markers

The population Gf.2018-063 including parental and grandparental DNA were genotyped utilizing 2057 amplicon-based SNP markers referred to as RNase H2-dependent amplicon sequencing markers (rhAmpSeq markers). The Cornell University, Geneva, New York, service providers carried out rhAmpSeq marker-based sequencing (Zou et al., 2020).

2.2.4 Genetic mapping

The genetic map was created using two separate marker technologies: first, SSRs was used to build the initial map, and SNP based rhAmpSeq was used for the fine mapping.

2.2.4.1 Simple Sequence Repeats based genetic map

An integrated genetic map was produced using the JoinMap 4.1 tool (Van Ooijen, 2006), which also produced independent maternal and paternal genetic maps. The allele combinations of the relevant F1 individuals identified through the analysis with GeneMapper® 5.0 were coded in accordance with the five potential segregation patterns (Table 2) and were submitted in this format to the JoinMap 4.1 tool.

Table 2 JoinMap program's recommended possible segregation patterns and F1 genotypes in a full-sib family of an outbreeding species.

Segregation pattern	Description	Possible F1 genotypes
<abxcd>	With four alleles, the locus is heterozygous in both parents	ac, ad, bc, bd
<efxeg>	With three alleles, the locus is heterozygous in both parents	ee, ef, eg, fg
<nnxnp>	Maternal locus is homozygous with paternal heterozygous locus (Paternally segregating marker)	nn, np
<lmxll>	Paternal locus is homozygous with maternal heterozygous locus (Maternally segregating marker)	lm, ll
<hkxhk>	With two alleles, the locus is heterozygous in both parents (bi-parentally segregating)	nn, np

The maps were constructed using the "Double Pseudo-Testcross" Strategy (Grattapaglia & Sederoff 1994). Based on the "Grouping Tree", the markers were combined into coupling groups. The program's default settings were utilized with the "Maximum Likelihood Mapping" (ML-mapping) approach. The Chi-square test validation was used to determine the markers' segregation in the F1 individuals. The Integrated Genetic Map computation excluded markers with more than 40 % deviation. The grouping of markers into the linkage groups was performed using the "independence LOD score" with minimum LOD value of eight (according to Adam Blondon et al. (2004)). The number of markers (M), the maximum, flows into the formula E(G) = M(M-1)X/K Distance between two markers (X) and the number of locus pairs above the LOD significance limit (K).

2.2.4.2 RNase H2-dependent amplicon sequencing marker based genetic map

The raw rhAmpSeq sequencing data for the mapping family Gf.2018-063 was initially sliced (keep minor allele frequency > 0.05) using the script 'slice.py' offered by the service provided (Zou et al. 2020). Perl program-based script 'to_lep_map.pl' was used to convert the raw 'hap genotype' containing four most frequent haplotype alleles for each marker into a Variant Calling Format file (.vcf), where each haplotype allele of a marker was converted to a pseudo A, T, G, or C allele. As quality control (QC) analyses, multidimensional scaling (MDS) and Mendelian error detection

were carried out using TASSEL 5.0 software to identify self-fertilization, contamination, or mislabeling of the genotypes. The genetic map creation and QTL analysis did not include the QC tests failed samples.

Lep-MAP3 v.0.2 (LM3; Rastas, 2017) was used to construct the genetic map. The following LM3 modules were used in creating the genetic maps: (1) ParentCall2 - used to call parental genotypes; (2) Filtering2 - for filtering (dataTolerance = $1.00E^{-6}$) the distorted / monomorphic markers based on a $\chi 2$ test (chi-squared to determine if a significant deviation of the allele ratio from the expected mendelian ratio has occurred, based on the above tolerance threshold); (3) SeparateChromosomes2 module - used to split the markers into 19 linkage groups (LG); (4) OrderMarkers2module - used to order the markers within each LGs (iterations/group = 20), and computing parental and sex averaged genetic distances. Marker collinearity was estimated using the physical position of the markers based on the reference genome "PN40024" (version12X.v2) (Zou et al. 2020) and their genetic positions in the genetic map, in order to check structural variation and genome organization. The 'map2genotypes.awk' script was used to transform the phased output data from the OrderMarkers2 step into phased genotype data followed by converting the data into 1 1 = AC = 1, 1 2 = AD = 2, 2 1 = BC = 3 and BD = 2 2 = 4 for QTL analysis. QTL analysis was performed using package 'R/qtl' (R version 3.6.3; Broman et al., 2003).

2.2.5 QTL analysis

2.2.5.1 Simple Sequence Repeats

MapQTL 6 software was implemented in the detection of QTL. The analysis included Kruskal-Wallis test, an interval mapping and a multiple QTL mapping. An automated cofactor selection (ACS) with a p-value of less than 0.005 was carried out before the MQM mapping. Chromosome-specific significance threshold (p = 0.05) of the LOD value was determined using a permutation test (1000 repetitions).

2.2.5.2 RNase H2-dependent amplicon sequencing markers

R software, version 3.4.5, and the 'R/qtl2' package (Broman et al. 2003) were used for all analyses (R Core Team 2007). Using 'calc.genoprob' with step = 0 (probabilities calculated at the marker sites), the genotype probabilities were estimated under the 1.0e-4 genotyping error rate assumption. To find the significant LOD thresholds, 1,000 permutation tests at alphas of 0.1 and

0.05 were carried out using the one-dimensional 'scanone' function and expanded Haley-Knott (HK) (Feenstra et al. 2006) method to confirm the relevance and to detect the QTLs. The "AID" package's boxcoxnc function was used to power transform the phenotypic data of all the years that were identified to be non-linear or skewed. In addition, the confidence interval test was determined as Bayesian credible intervals 'lod integer', 1.5 - LOD support intervals for QTLs were calculated. The overall phenotypic variation described by the QTL was determined using the 'Fitqtl' tool, which was also used to test for qtl-qtl interactions.

2.2.6 Microscopy: Aniline blue staining

In order to monitor *P. viticola* intracellular mycelial development within the leaf discs, three biological replicates of each genotype leaf discs were artificially infected using spore suspension. Leaf discs were collected at different time points 1, 3, and 5 days post inoculation (dpi), and were incubated for 3-6 h in 1N KOH solution at 65 °C. The leaf discs were rinsed thrice in deionized H_2O and placed upside down (adaxial surface facing the glass slide) on a glass slide. The leaf discs were treated with 50 µl of aniline blue solution (0.05 % aniline blue, 0.067 mol^{-1} K_2HPO_4, pH 9). After 10 min of bench incubation, the aniline blue solution was carefully rinsed using deionized H_2O and the excessive remaining solution was removed using a paper towel until streaks were no longer visible. The samples were documented and analysed using Zeiss axio zoom V16 fluorescence microscopy (GFP filter at λ=470 nm).

2.2.7 Growth and sporulation

To observe the *P. viticola* growth and development on five days post inoculation, two susceptible genotypes 'Morio Muskat' and 'Müller Thurgau' and three *P. viticola* resistance carrying genotypes, COxGT2 (*Rpv32*), *V. amurensis* (*Rpv8*), 'Kunbarat' (*Rpv12*) and *V. coignetiae* were utilized in the experiment. Two leaves per genotypes were harvested (4^{th} and 5^{th} from the apical node) and six biological replicate leaf discs (three discs each leaf) were produced representing each genotype. The leaf disc assay was performed using section 2.2.1 of methods. Post five days inoculation, leaf disc images were captured using Zeiss Axio zoom stereo microscope V16 followed by washing each leaf disc in 1.5 ml Eppendorf tubes. If required a needle was used to remove the rest pathogen on the leaf discs and washing was repeated. The tubes were vortexed and the sporangia were observed and counted using the hemocytometer. The average of six leaf discs

were utilized in the statistical analysis. Multiple pairwise comparison tests were run to compare the difference between the genotypes.

2.2.8 Artificial Intelligence-based phenotyping

2.2.8.1 SCNN: Training and performance evaluation

According to Zendler et al., 2021, for the training of the neural network-based classifier, five leaf discs representing reversed five-class OIV 452-1 descriptor were selected (Figure 9) belonging to the F1 population Gf.2018-063. The single leaf disc images were sliced into 506 equal segments and were manually classified into respective classes as background, leaf and sporangiophores (Figure 11) using a python-based script 'image-sorter2'. The SCNN model was trained using sliced images as the labelled input images.

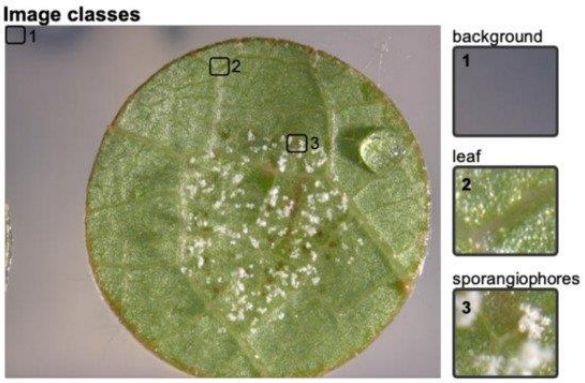

Figure 11 Leaf disc image and respective input image classes (1: water agar background, 2: leaf and 3: infected leaf with sporangiophores) obtained by slicing (Zendler et al., 2021).

For training and validation, a Python script was used to randomly select input image slices from the corresponding classes. The CNN1 (Figure 12) was trained to distinguish between 'background' and 'leaf' with 2919 images and validated with 947 images per class. Whereas, the CNN2 (Figure 12) was trained to distinguish between infected and non-infected. In total, 968 images per class were used for training and 437 images per class were used for validation in the final dataset. All SCNN trainings were conducted on a desktop computer with a 24-thread CPU, 32 GB of RAM on an Ubuntu 20.04 operating system. Three image convolutions and a fully linked dense layer with 512 nodes were utilized to create the CNN1 model. Stochastic gradient descent (SGD) with 'Nesterov momentum', with 0.1 learning rate and 0.4 dropout were chosen as the optimizer. CNN2

was structured slightly different, ‘Nadam’ optimizer with a learning rate of 0.0001 and a dropout of 0.5 were chosen, with two dense layers of ‘512’ and ‘1024’ nodes, respectively, and an additional extra convolution layer. Each convolutional layer compromises of convolution (Cov2D), activation (ReLU = rectified linear unit activation function) and pooling (MaxPooling2D). ReLU activation is also present in the dense layers, which are completely linked. The Sigmoid activation function necessary for the binary output of the CNNs is present in the last ‘Dense 1’ layer.

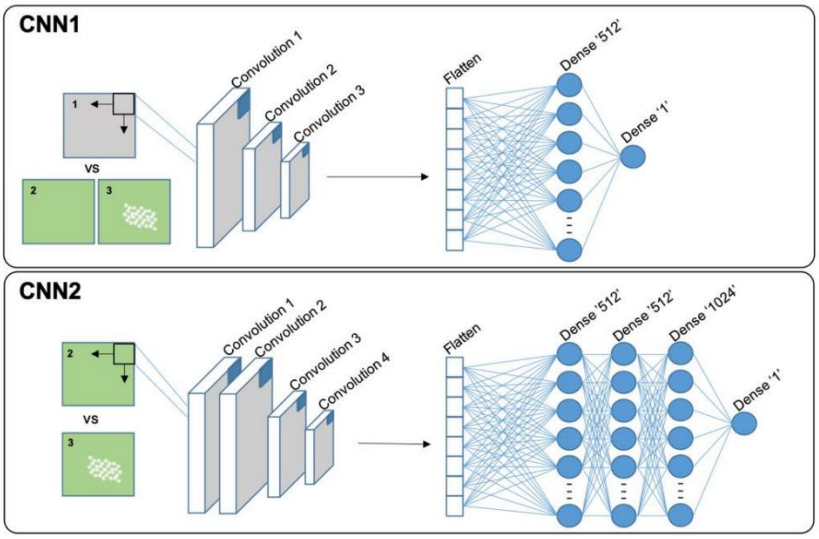

Figure 12 Block diagram of CNN1 (back vs. leaf) and CNN2 (infected vs. non-infected) including the input layer (convolution), hidden layer (convolution+ReLU and pooling) and binary output layer (Dense) (Zendler et al., 2021).

2.2.9 Statistics

All the statistical tests conducted in this work were run using the statistical program ‘R’ software, v. 3.4.5 (R Core Team, 2020).

3 Results

3.1 SCNN-based downy mildew quantification

All the results associated to SCNN on the grapevine downy mildew quantification system are published as second author in Zendler et al., 2021 (https://doi.org/10.3390/agronomy11091768).

3.1.1 SCNN: Training results

Suitable CNN models were chosen, trained and validated to calculate the overall validation accuracy. The model training and validation accuracy results of CNN1 and CNN2 are shown in the Figure 13. The CNN1 (background vs. leaf disc) achieved an overall validation accuracy of 98 % with a minimum validation loss of 6 %. The CNN2 (infected vs. non-infected leaf disc) achieved an overall accuracy of 95 % with a slightly higher validation loss of 15 %. The discrepancies between the validation loss of CNN1 and CNN2, are due to the feature complexities of the image slices. Since it can be seen, the classification of background vs. leaf disc (CNN1) is much easier compared to infected vs. non-infected leaf discs (CNN2). As indicated by the overlapping of the training and validation curves, both models are accurate in predicting the classes in the leaf disc classification pipeline.

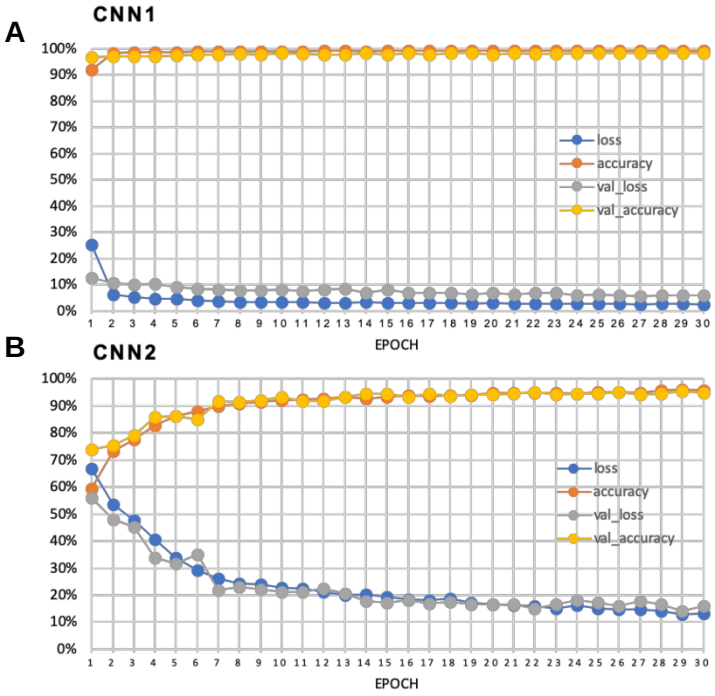

Figure 13 CNN model training results. (A) CNN1 (background vs. leaf disc), (B) CNN2 (infected vs. non-infected leaf disc). Val_accuracy: Validation accuracy; accuracy: training accuracy; val_loss: validation loss; loss; training loss plotted for 30 epochs (Zendler et al., 2021).

3.1.2 Experts generated ground truth data

A leaf disc set compromising of 15 leaf disc images from the cross of 'Morio Muskat' x COxGT2 and a second population of 'Cabernet Dorsa' x Couderc 13 were selected and manually classified into respective OIV classes (3 images/class). This set of selected leaf disc images was run through the CNNs and leaf disc slices were independently evaluated by three experts. As shown visually in the RGB images (Figure 14), there is a substantial degree of similarity between the three expert manual ratings and the CNN results. In addition, the expert's data significantly resemble and are in accordance with the CNN-classified leaf disc images.

The CNN1 shows consistently efficient results in classifying the background and the leaf disc for all the images in both the cross populations. However, very slight discrepancies between the slices were observed, which often have no impact on the final results. In addition, some minor differences were also observed between the three expert's results indicating subjectivity. The images from the population 'Cabernet Dorsa' x Couderc 13 utilized for model validation

exhibited a high number of discrepancies from the population used for model development ‘Morio Muskat’ x COxGT2, primarily as a result of a change in image quality specification and possibly due to a dissimilar genetic background. There is a chance that a neighboring leaf disc cross the grid when they are arranged on the agar plate. For instance, a second leaf disc that is only partially visible in the image class7_3 has been recognized, and results of this leaf disc are added too the final findings, thus it is important to take care of this. When comparing the ‘leaf with sporangiophores’ image slices to the RGB images and the ground truth data, it is clear that they are consistently predicted in the appropriate places of the leaf disc (Figure 14). However, it appears that not all image slices with sporangiophores are detected by the second CNN. The leaf disc images from the ‘Cabernet Dorsa’ x Couderc 13 cross, which were not utilized for neural network training, appear to have this problem more noticeably.

Figure 14 Randomly selected original pictures of three leaf disc belonging to each of the five OIV classes. The results of two different segregating populations are shown. (A) ‘Cabernet Dorsa’ x Couderc 13 and (B) ‘Morio Muskat’ x COxGT2. The ground truth data generated by three experts and the results of the CNN classification of the image slices. (Black = background (1), dark blue = sporangiophores (2), light blue = no sporangiophores (3) (Zendler et al., 2021).

3.1.3 Overall performance evaluation

The validation of the leaf disc image set was evaluated using the OIV scale (Figure 9) and the SCNN pipeline. The percentage of true positives was calculated for each individual image compromising 506 sub-images (slices) as shown in Figure 15A. For the 15 'Morio Muskat' x COxGT2 leaf disc images, the median percentage of true positive classifications ranged between 96-97 % and the overall percentage of true positives ranged from an average between 92–100 %. Whereas, in the 'Cabernet Dorsa' × Couderc 13 leaf disc images, the median percentage of true positive classifications ranged between 92 – 94 % and the overall percentage of true positives ranged from an average between 89 – 99 % (Figure 15A). To evaluate the performance of the SCNN, the inverse OIV452-1 classes scoring and the manual percentage scoring of whole leaf disc data by three experts were independently correlated with SCNN-based estimations. The correlation coefficient (r) of 0.92 and 0.91 was obtained for the population 'Morio Muskat' x COxGT2 and 'Cabernet Dorsa' × Couderc 13 respectively ($p < 0.01$). The results are indicated in Figure 15B and 15C. The correlation coefficient was 0.91 for the 'Cabernet Dorsa' x Couderc 13 leaf disc pictures, lower in contrary to 'Morio Muskat' x COxGT2 leaf disc pictures but still very significant.

The final correlation was run using the OIV452-1 classes assigned leaf disc scores and the SCNN-based evaluation in percentage. One linear regression is suggested since all three experts assigned the same classifications to the various leaf disc pictures. The cross 'Morio Muskat' x COxGT2 and 'Cabernet Dorsa' x Couderc 13 yielded a correlation coefficient of 0.96 and 0.92 respectively ($p < 0.001$). Thus, according to the results for true positives and the two distinct correlations, the output of the CNN classification appears to reflect the values evaluated by individual experts independently.

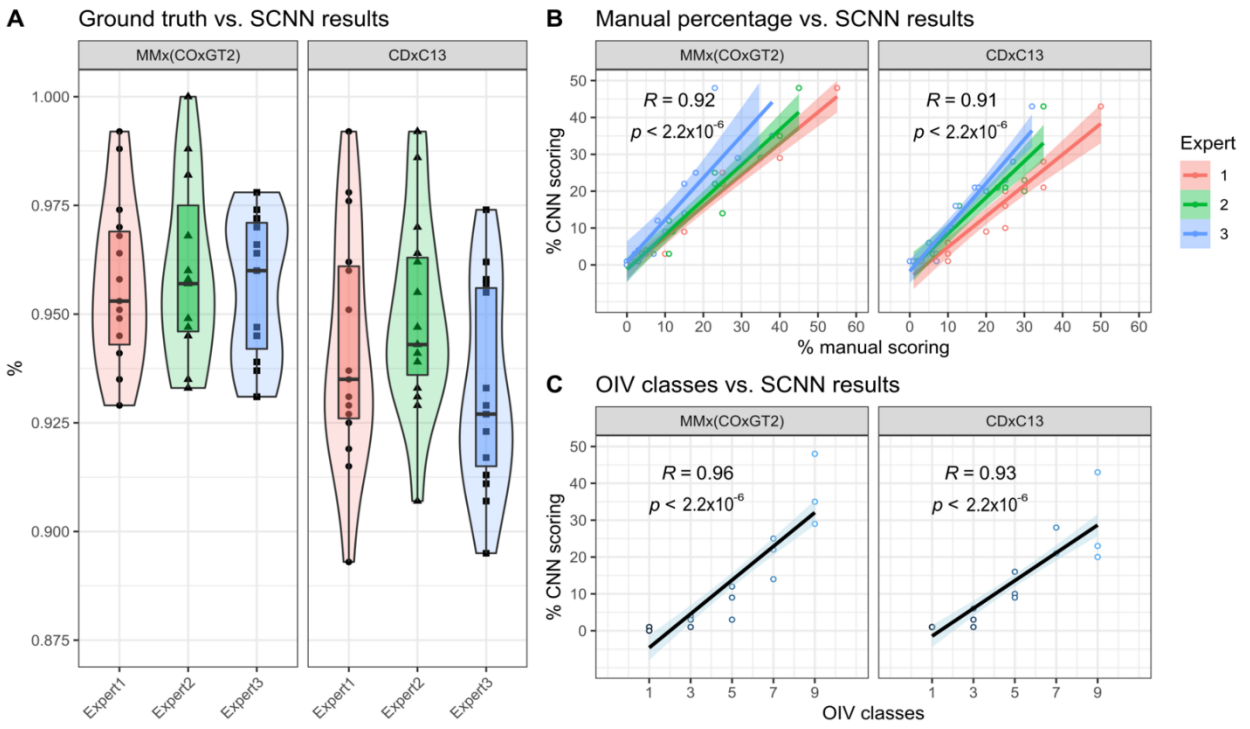

Figure 15 (A) Ground truth vs. SCNN results; Comparison between the SCNNs true positive classifications and three experts' independent manual classification. (B) Manual percentage vs. SCNN; Pearson's correlation (R) results between the manual scoring [%] of experts vs. CNN output [%] ($p < 0.05$) including the confidence intervals for each linear regression. (C) OIV classes vs. SCNN results; Pearson's correlation (R) results between OIV scale based evaluation of the leaf discs vs. the SCNN results. Populations utilized for CNN training and validation are 'Morio Muskat' x COxGT2 and 'Cabernet Dorsa' x Couderc 13 respectively (Zendler et al., 2021).

3.1.3.1 Classification pipeline: SCNN and ResNet

A leaf disc picture is first virtually divided into 506 parts, which were categorized as either leaf disc or water agar (background) by CNN1. CNN2 further classifies leaf disc pictures into 'leaf discs with sporangiophores' and 'leaf discs without sporangiophores'. The pipeline iterates over each image in a given folder to classify each image and then runs an R script to plot the recognized slices of sporangiophores on the original RGB image (Figure 16). A similar workflow of the pipeline was followed in the case of the ResNet model (Figure 17). A plot showing the proportion of leaf disc area covered by sporangiophores and an excel file of all the values are generated is presented in Figure 16. As a measure of control, each image of categorized sporangiophores is kept in a separate folder for manual review. One can access the SCNN pipeline and thorough installation instructions at www.github.com/Daniel-Ze/Leaf-disc-scoring.

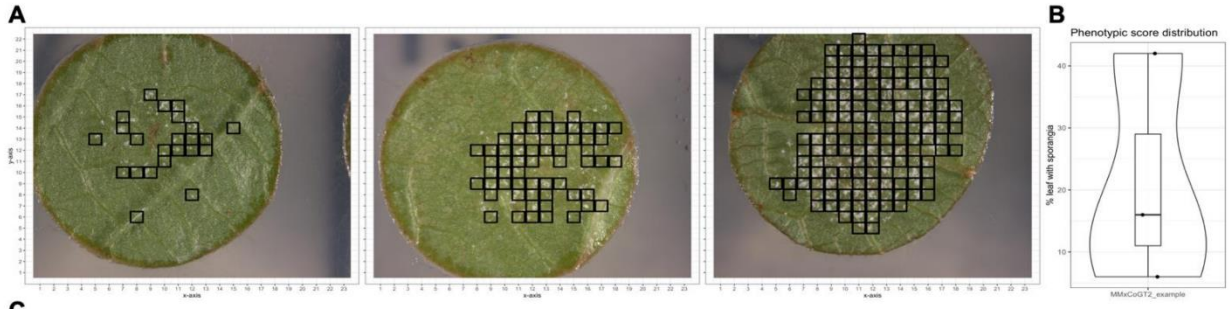

Exp_name	Sample	Number	Leaf_disc	Agar	perc_leaf_disc	perc_agar	spo	no_spo	perc_spo	perc_no_spo
MMxCOxGT2	score5_Plate_5_I_s77.jpg	1	362	144	72	28	23	339	6	94
MMxCOxGT2	score7_Plate_4_I_s24.jpg	2	354	152	70	30	58	296	16	84
MMxCOxGT2	score9_Plate_11_II_s30.jpg	3	352	154	70	30	147	205	42	58

Figure 16 Example of the leaf disc scoring pipeline's output. (A) Three original RGB images recognized "with sporangiophores" leaf disc slices. (B) Summary of the [%] leaf disc areas determined for the collection of photos under analysis. X-axis indicates: the population evaluated; Y-axis: [%] of sporangiophores on the leaf disc (C) A tab delimited table produced by the leaf disc scoring process (Exp name_experiment name; Sample: Sample ID utilized in the analysis; Number: serial number; Leaf disc: slices identified as being from leaves; Agar: slices identified as being from agar/background; Spo: slices identified as being infected with sporangiophores; no_spo: slices without spores; perc: indicates percentage) (Zendler et al., 2021).

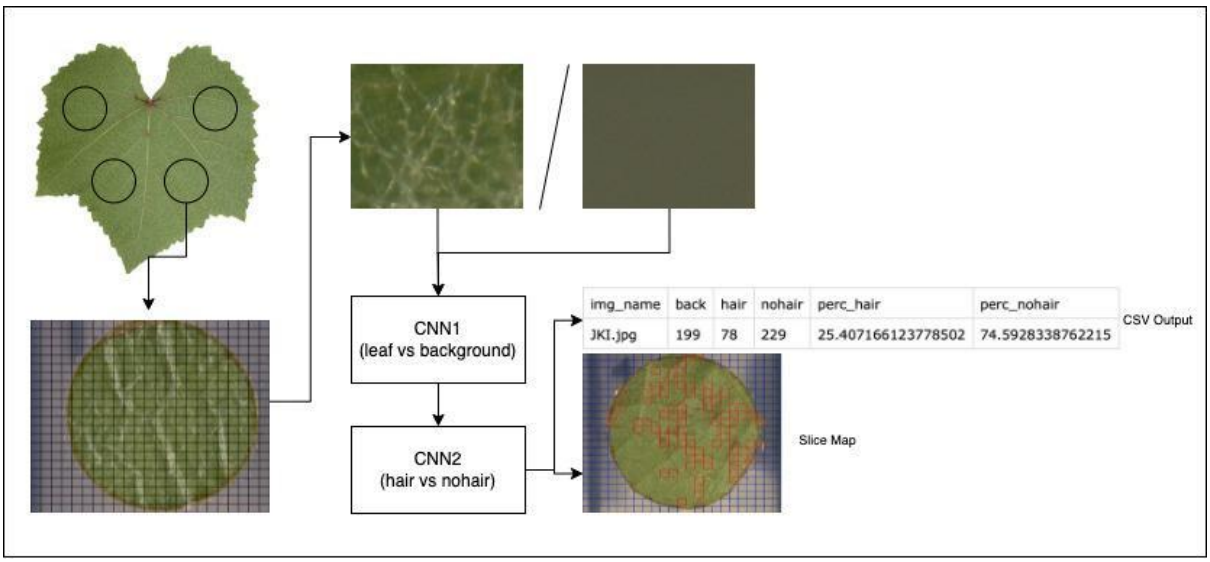

Figure 17 Leaf hair classification pipeline. Slice map - The original RGB images recognized "with hair" leaf disc slices (red color). A CSV output delimited table that produced by the leaf disc scoring process (img name: image name; back: slices identified as back; hair: slices identified as hair; nohair: slices identified as no hair; perc hair: hair percentage; perc_nohair: no hair percentage) (Malagol et al., 2023 in preparation).

3.2 Summary of phenotypic data

3.2.1 Downy mildew resistance and morphological trait leaf hair (trichrome) density

The Gf.2018-063 bi-parental population with 496 individuals was phenotyped for resistance to downy mildew by performing independent laboratory-controlled LDAs (leaf disc assay) in 3 years. The leaf discs were manually evaluated according to the reversed scale of the well-established OIV 452-1 descriptor (Figure 9). The phenotypic data distribution and the trait segregation for the years 2020 (three experiments), 2021 (four experiments) and 2022 (single experiment) are shown as bar plots (Figure 18). Based on the number of sporangia the resistant donor (COxGT2) was assigned the OIV score 3 and the susceptible parent ('Morio Muskat') was assigned the OIV score 9. As can be seen, in all the years the data roughly reflects a bimodal distribution and indicates the difference between the susceptible and the resistance genotypes. At this point, the rejection of a normal distribution was expected, since the sample shows a splitting of the individuals concerning the resistance characteristic. However, in the phenotypic data distribution for the years 2020 and 2022, the number of individuals varies being resistant or susceptible from individual experiment to experiment, and year to year. Additionally, in the year 2020, the first two leaf disc experiments showed 38 % of individuals belonging to the class score 1, i. e. resistant in comparison to the third experiment and similar to the results in the year 2022 due to the indirect adverse effect of spraying (powdery mildew control).

The population Gf.2018-063 showed quantitative segregation of the trait leaf hair density, known to be involved in physical resistance to downy mildew due to its hydrophobic characteristic. In general, it can be seen in the Figure 3 (refer to section Introduction), that the resistant donor COxGT2 shows hydrophobic characteristics of lower leaf side hairs in comparison to the susceptible non-hairy parent 'Morio Muskat'. In the years 2019, 2020, and 2022, the individual leaf discs from single evaluations were manually rated for morphological trait leaf hair using the OIV-086 scale represented below as bar plots (Figure 19). All the independent evaluations of trait leaf hair density appeared to be consistent throughtout the years. In general, about $1/4^{th}$ of the population showed low leaf hair density in all the years. All the independent experiment's non-linear data were rank/box cox transformed and tested for normality using Shapiro-Wilk test before the QTL analysis.

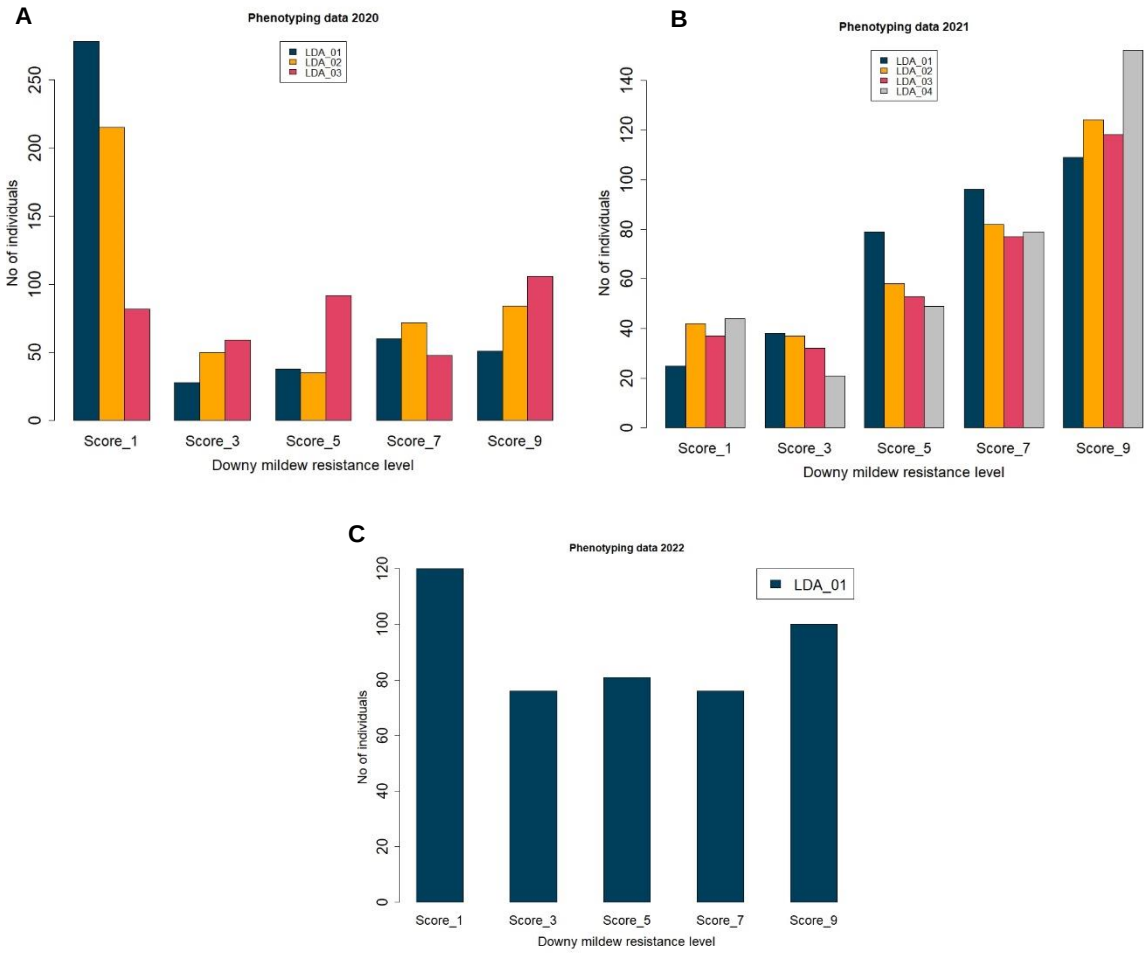

Figure 18 Phenotypic data distribution of the mapping population Gf.2018-063 for the year 2020 (A), 2021 (B) and 2022 (C) associated with resistance to *P. viticola* scored 5 days post inoculation (dpi). X-axis represent the reversed OIV 456-1 scores from 1 = highly resistant to 9 = highly susceptible. Y-axis represent the number of individuals per score. LDA_01, LDA_02, LDA_03 and LDA_04 indicate the number of independent leaf disc assay/ experiments performed per year (season).

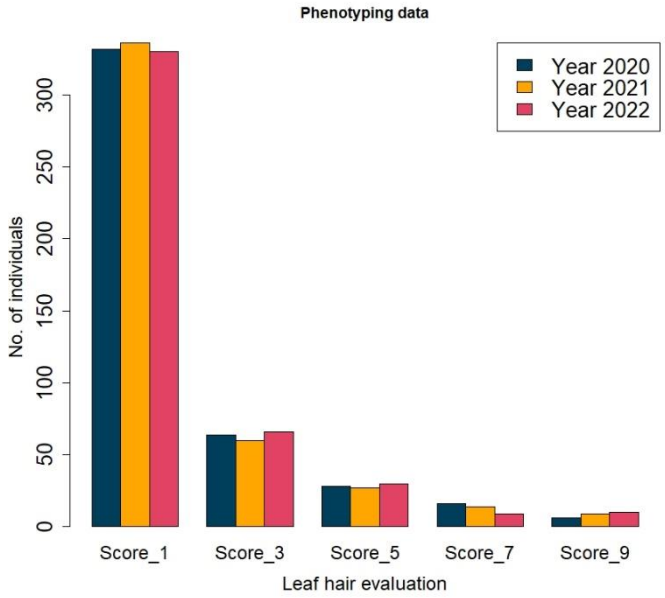

Figure 19 Phenotypic data distribution of the mapping population Gf.2018-063 representing evaluation of the trait leaf hair of three single experiments in the year 2020, 2021 and 2022. X-axis representing the OIV-086 score, Where class 1: None/Very low hair; class 3: Low; class 5: Medium; class 7: High; class 9: Very high (lanate / dense cover of hair) and Y-axis representing the number of individuals per score.

3.3 Genetic map

3.3.1 Initial map: SSR marker

As per the objective, SSR marker-based initial framework map was generated for the bi-parental population Gf.2018-063 (384 individuals). In total, 297 SSR markers were selected based on thier available physical position (reference genome PN40024) and were tested on the entire population, thus the coverage was reached with reduced efforts. In total 109 markers were mapped and used to calculate the final integrated map. The map comprises of 19 linkage groups (LGs) with homogeneously distributed makers on an average marker density of 5.05 per chromosome and covering total map length of 1899 cM (Figure 20). In addition, parental maps for maternal parent 'Morio Muskat' and paternal COxGT2 were created. In comparison to the integrated map, a smaller number of markers were used for the individual parental maps. In general, it can be observed that the LGs (2, 7, and 12) with fewer number of markers showed larger gaps between the markers. Table 3 provides an overview of the mapping in terms of total number of markers per chromosome, marker distance and length of the LGs.

Table 3 Summary of the SSR based integrated and the parental maps (‘Morio Muskat’: maternal; COxGT2: paternal) including total number of markers, marker distance [cM] and length [cM] of the linkage group (LG).
(Σ = Sum and $\bar{x}$ = Average).

SSR marker-based linkage map									
LGs	Integrated map			Maternal map of ‘Morio Muskat’			Paternal map of COxGT2		
	Length [cM]	No. of markers	Avg. distance [cM]	Length [cM]	No. of markers	Avg. distance [cM]	Length [cM]	No. of markers	Avg. distance [cM]
1	97.8	8	12.2	93.4	8	11.7	38.2	5	7.6
2	183.6	2	91.8	183.6	2	91.8	0	1	0.0
3	84.3	3	28.1	76.3	3	25.4	92.4	3	30.8
4	55.5	4	13.9	55.5	4	13.9	55.5	4	13.9
5	90.4	4	22.6	134.7	2	67.4	46.1	4	11.5
6	141.1	5	28.2	166.5	3	55.5	145.7	5	29.1
7	89.5	3	29.8	101.6	3	33.9	77.4	3	25.8
8	130.4	4	32.6	105.6	4	26.4	155.2	4	38.8
9	70.8	6	11.8	1.0	2	0.5	71.1	6	11.9
10	167.6	11	15.2	28.7	6	4.8	189.9	11	17.3
11	60.1	5	12.0	38.1	3	12.7	76.2	4	19.1
12	153.2	6	25.5	151.0	5	30.2	36.1	3	12.0
13	139.4	6	23.2	0.0	1	0.0	139.4	6	23.2
14	57.7	5	11.5	71.9	4	18.0	39.8	5	8.0
15	70.9	4	17.7	70.9	4	17.7	70.9	4	17.7
16	71.5	5	14.3	75.8	4	19.0	67.3	5	13.5
17	61.4	3	20.5	0.0	1	0.0	61.4	3	20.5
18	58.9	4	14.7	31.2	2	15.6	48.2	4	12.1
19	115.1	8	14.4	89.6	4	22.4	134.7	8	16.8
$\bar{x}$	99.99	5.05		77.63	3.42		81.31	4.63	
Σ	**1899.2**	**96**	**440.2**	**1475.4**	**65**	**466.7**	**1545.5**	**88**	**329.5**

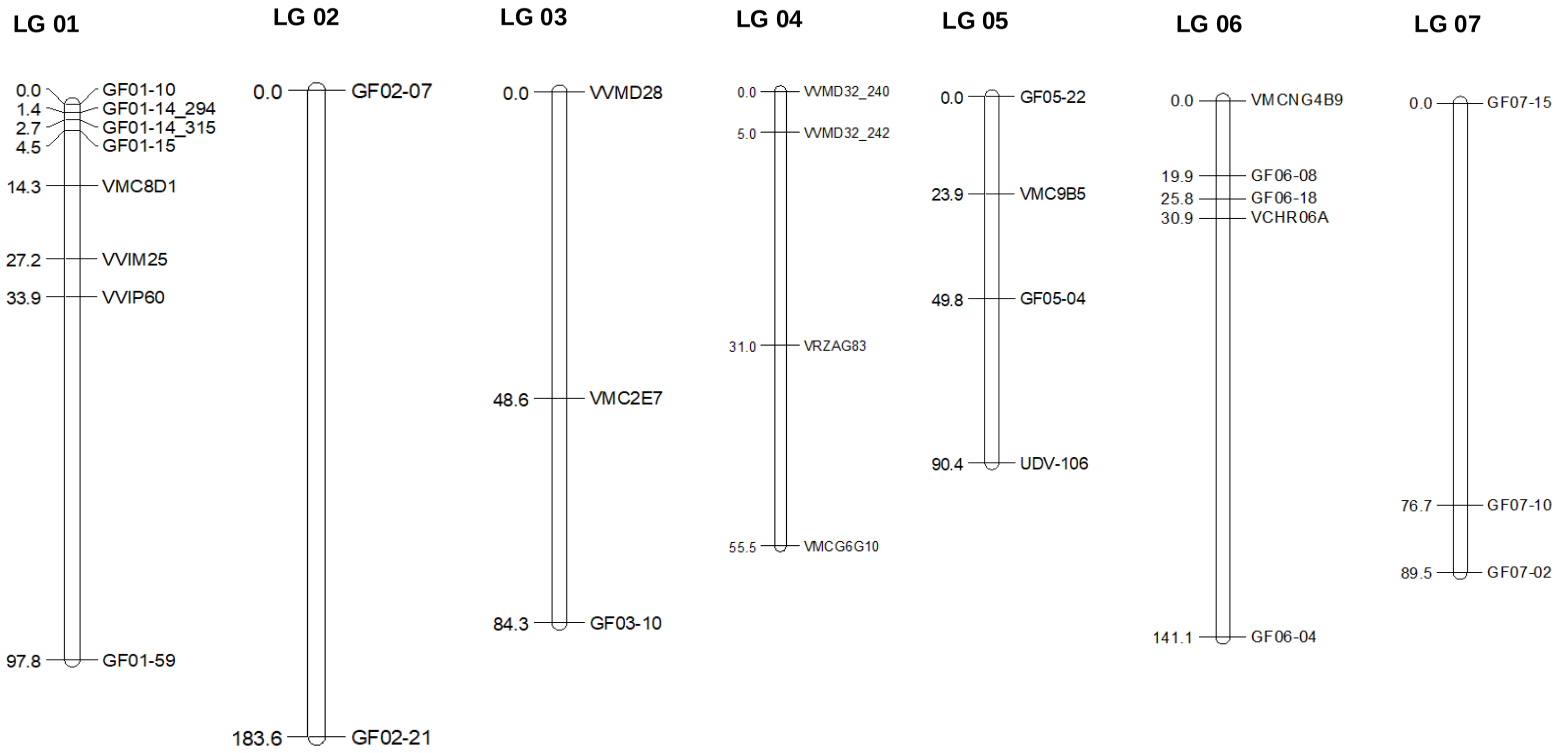
LG 01
0.0 GF01-10
1.4 GF01-14_294
2.7 GF01-14_315
4.5 GF01-15
14.3 VMC8D1
27.2 VVIM25
33.9 VVIP60
97.8 GF01-59
LG 02
0.0 GF02-07
183.6 GF02-21
LG 03
0.0 VVMD28
48.6 VMC2E7
84.3 GF03-10
LG 04
0.0 VVMD32_240
5.0 VVMD32_242
31.0 VRZAG83
55.5 VMCG6G10
LG 05
0.0 GF05-22
23.9 VMC9B5
49.8 GF05-04
90.4 UDV-106
LG 06
0.0 VMCNG4B9
19.9 GF06-08
25.8 GF06-18
30.9 VCHR06A
141.1 GF06-04
LG 07
0.0 GF07-15
76.7 GF07-10
89.5 GF07-02

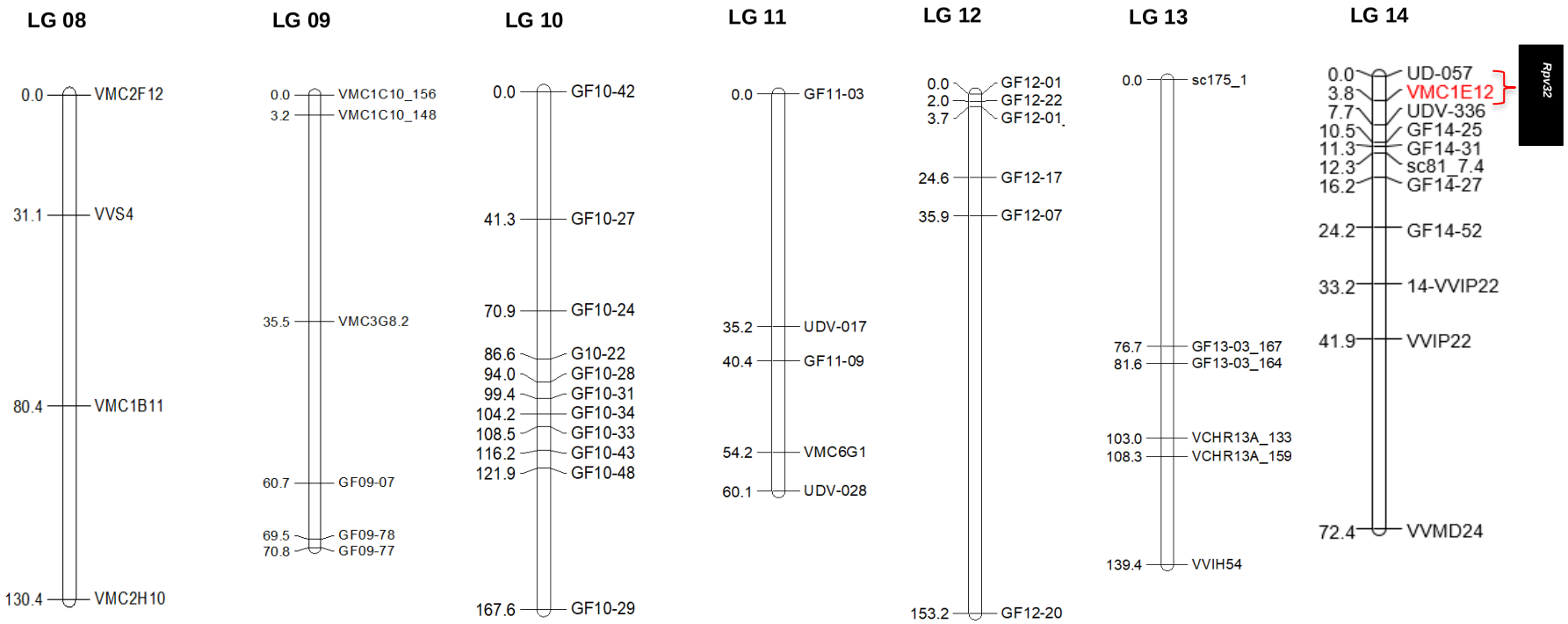
LG 08
0.0 VMC2F12
31.1 VVS4
80.4 VMC1B11
130.4 VMC2H10
LG 09
0.0 VMC1C10_156
3.2 VMC1C10_148
35.5 VMC3G8.2
60.7 GF09-07
69.5 GF09-78
70.8 GF09-77
LG 10
0.0 GF10-42
41.3 GF10-27
70.9 GF10-24
86.6 G10-22
94.0 GF10-28
99.4 GF10-31
104.2 GF10-34
108.5 GF10-33
116.2 GF10-43
121.9 GF10-48
167.6 GF10-29
LG 11
0.0 GF11-03
35.2 UDV-017
40.4 GF11-09
54.2 VMC6G1
60.1 UDV-028
LG 12
0.0 GF12-01
2.0 GF12-22
3.7 GF12-01
24.6 GF12-17
35.9 GF12-07
153.2 GF12-20
LG 13
0.0 sc175_1
76.7 GF13-03_167
81.6 GF13-03_164
103.0 VCHR13A_133
108.3 VCHR13A_159
139.4 VVIH54
LG 14
0.0 UD-057
3.8 VMC1E12
7.7 UDV-336
10.5 GF14-25
11.3 GF14-31
12.3 sc81_7.4
16.2 GF14-27
24.2 GF14-52
33.2 14-VVIP22
41.9 VVIP22
72.4 VVMD24
Rpv32

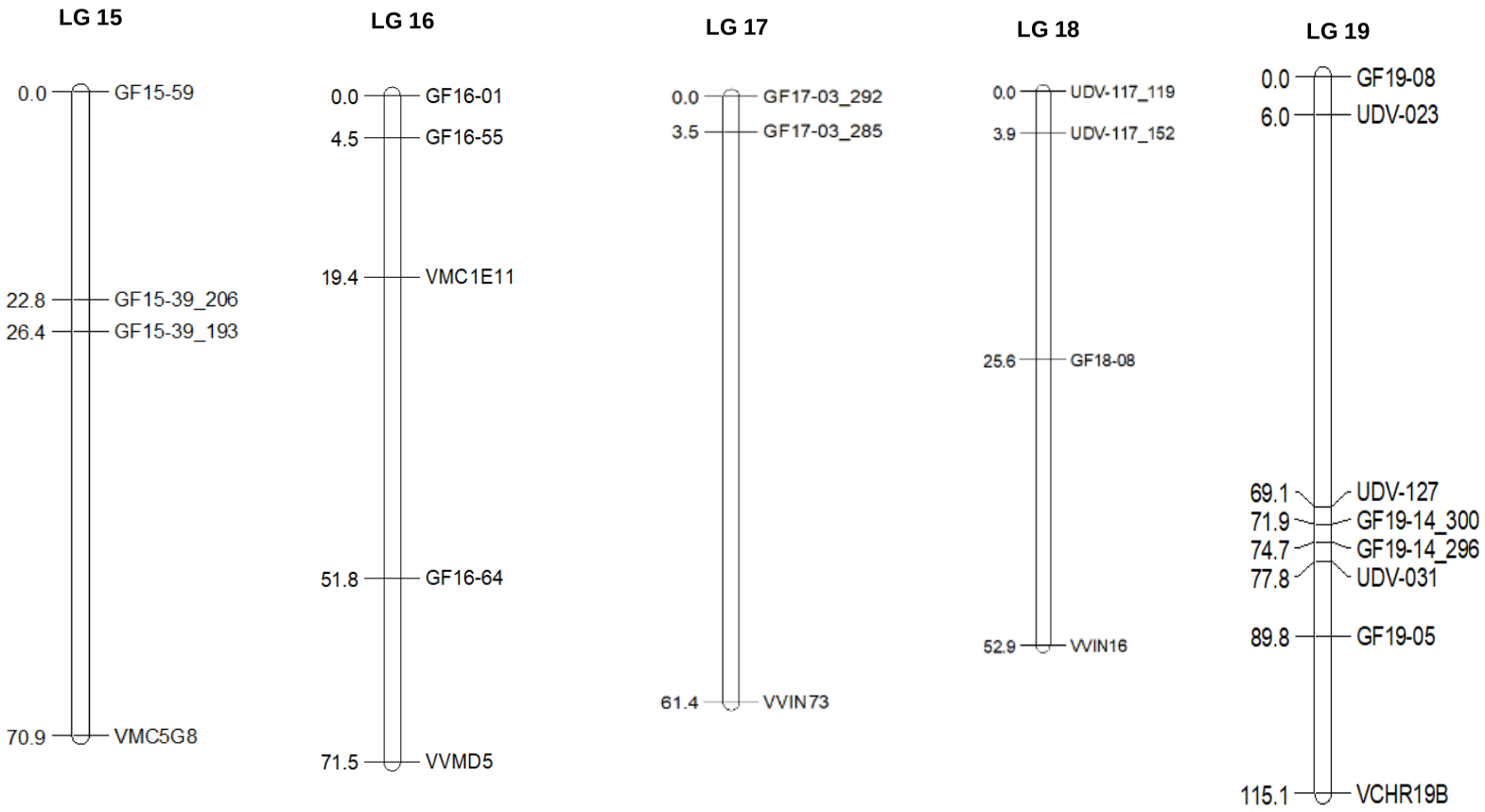

Figure 20 Integrated SSR marker based genetic map of the population 'Morio Muskat' x COxGT2. The positions of the 96 SSR markers are shown distributed over 19 Linkage groups (LGs) in [cM]. Black box indicates the identified resistance locus *Rpv32*.

3.3.2 Fine mapping: rhAmpSeq marker

In total, 2057 rhAmpSeq core genome markers were tested on the entire population (Gf.2018-063) of 496 individuals. The quality control failed individuals (41) and markers were discarded in the final genetic map construction, leading to 455 individuals and only 32 % (639) of the markers were mapped and utilized in the final map creation. To verify the genome organization and overall genome coverage of the mapped rhAmpSeq markers, the genetic positions calculated for each marker of the LGs were tested for their collinearity. The genetic positions were correlated to the physical position from the version 12x.V2 of the PN40024 reference genome. According to the results, the marker order and the positions on the genetic maps had a high correlation ($r > 0.90$) to their physical position (Figure 21). Structural variation and some inconsistencies that appear to be more frequent in the wild *Vitis* genotypes than in *V. vinifera* that are to be responsible for some physical gaps (chr. 3, chr. 10, chr. 12 and chr. 17) can be clearly seen in the genome coverage of the rhAmpSeq markers as indicated by Zou et al., 2020. All the expected 19 LGs were identified covering total map length of 1147.3 cM on an average of 53 loci per LG (Figure 22). The LG 07 covered with the highest number of markers (49) and LG 12 covered with lowest number of markers (12). The linkages groups' lengths ranged between 46 cM (LG 15) to 70.4 cM (LG 01), from lowest to highest, respectively. Table 4 provides the summary of rhAmpSeq based genetic map in terms of total number of markers per chromosome, average distance between the markers and length of each linkage group.

Table 4 Overview of the rhAmpSeq marker-based genetic map including total number of markers, average marker distance [cM] and length [cM] of the linkage group (LG) (Σ = Sum and $\bar{x}$ = Average).

LGs	No. of Markers	Length of LG [cM]	Avg. distance between markers [cM]
LG 01	49	70.4	1.06
LG 02	35	53.3	0.79
LG 03	25	48.2	0.77
LG 04	36	54.8	1.48
LG 05	46	57.9	1.09
LG 06	33	51.1	1.16
LG 07	54	80.6	1.48
LG 08	47	60.6	1,37
LG 09	31	51.3	1.12
LG 10	22	50	1.21
LG 11	37	52	1.36
LG 12	12	66.8	2.38
LG 13	33	64.5	1.84
LG 14	23	57.6	1.69
LG 15	29	46.5	1.40
LG 16	30	48.4	1.51
LG 17	22	53.6	1.57
LG 18	42	73	2.43
LG 19	33	51.7	1.47
$\bar{x}$	33.63	54.4	1.77
Σ	639	1147.3	

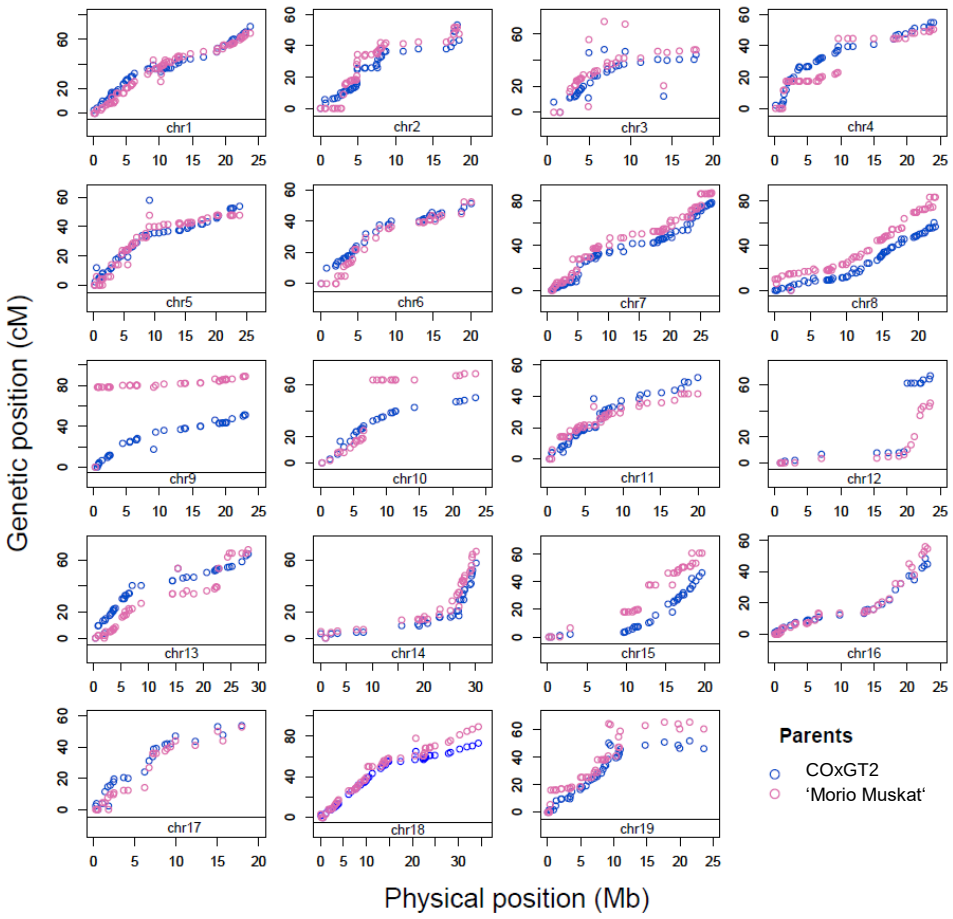

Figure 21 Dot plots depicting the collinearity relationship between the genetic [cM] and the physical position [Mb] for the population Gf.2018-063 genetic map. X-axis indicates the physical position in mega base from the version 12x.V2 of the PN40024 reference genome. Y-axis indicates the genetic position in centiMorgan of each marker derived from the rhAmpSeq based genetic map of the population Gf.2018-063. (chr: chromosome; blue color refers to the parent COxGT2; pink refers to the parent 'Morio Muskat').

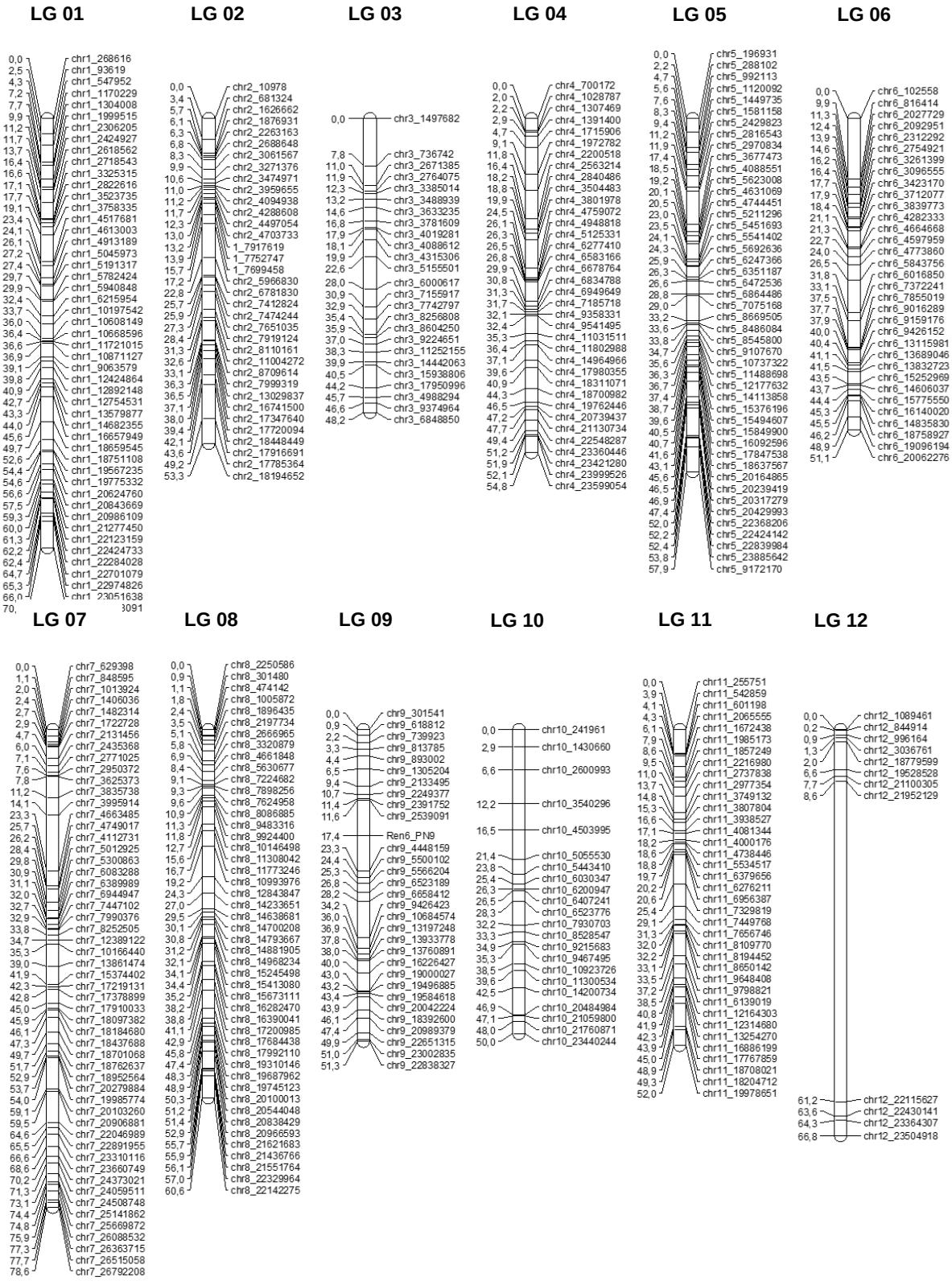
LG 01
LG 02
LG 03
LG 04
LG 05
LG 06
LG 07
LG 08
LG 09
LG 10
LG 11
LG 12

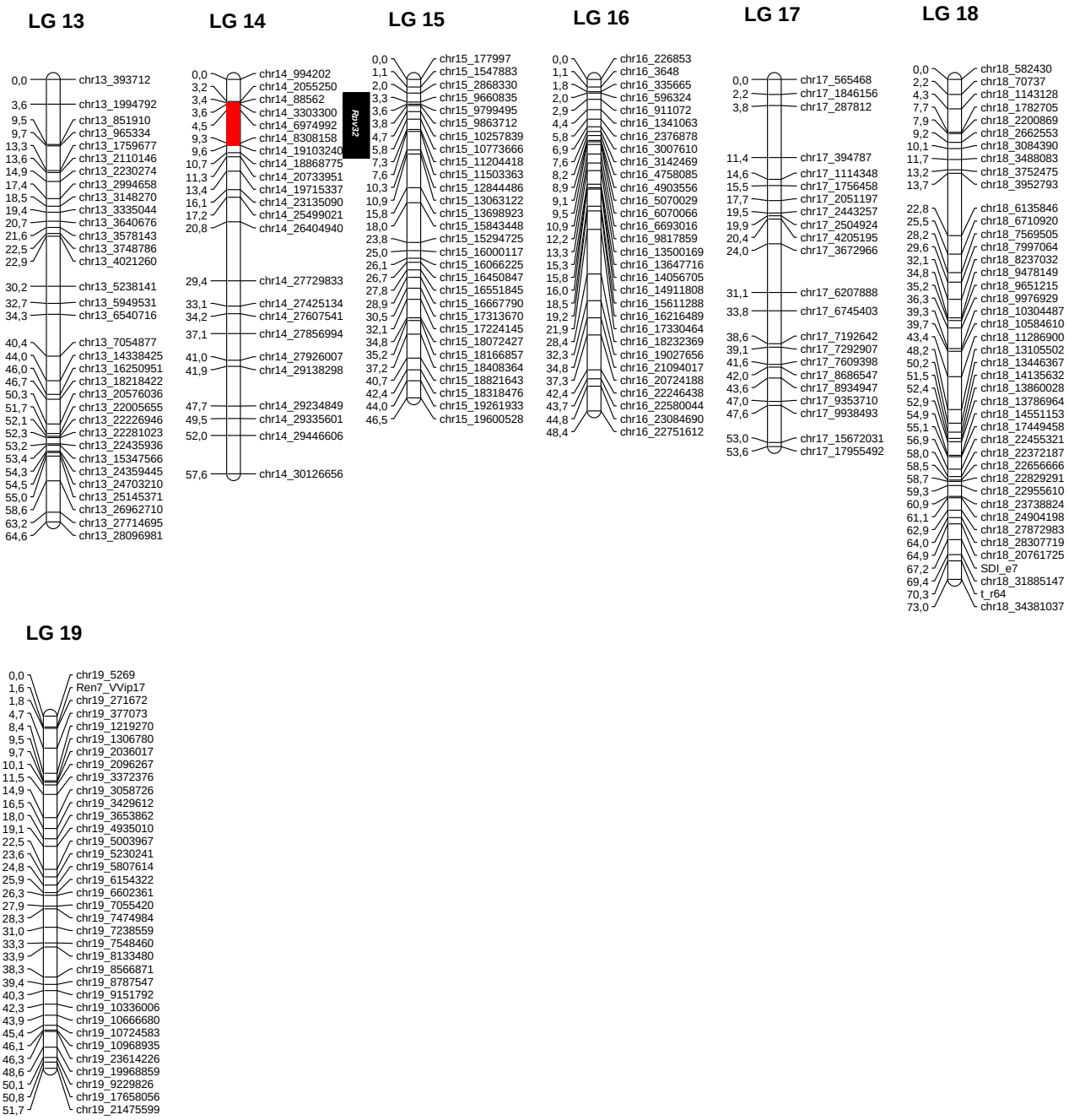

Figure 22 rhAmpSeq marker-based genetic map of the population 'Morio Muskat' x COxGT2. The positions of the markers are shown distributed over 19 linkage groups (LG) in [cM]. Black box (red colour) indicates the identified resistance locus *Rpv32* on LG 14.

3.4 QTL analysis

After the phenotypic data evaluation and a genetic map generation, mapping of downy mildew disease resistance was performed. In the year 2020, the QTL analysis was carried out for three independent experiments using the SSR-based initial genetic map. No QTLs were detected in the year 2020 due to a large gap on the chr. 14. Later, fine mapping of SSR based genetic map in the year 2021 followed by QTL anaylsis showed a significant QTL on LG 14. Nevertheless, the overall density of the SSR marker per LG was too low. In order to increase the overall marker density, a rhAmpSeq marker based genetic map was created in the year 2021 and henceforth rhAmpSeq-based genetic map was employed in the QTL analysis of the year 2020, 2021, and 2022. Genetic maps based on rhAmpSeq and SSR were kept separate and were not combined due to lack of reliable marker conversion tools.

3.4.1 SSR marker data

Interval mapping (IM) and Multiple QTL Mapping (MQM) type was utilized to locate the regions of the genetic map linked to the expression of downy mildew resistance. Based on the integrated map of the population Gf.2018-063, a highly significant and strong QTL was identified on LG 14 in one of the downy mildew phenotypic evaluations conducted in the year 2020 (Table 5). In addition to IM (green, whiskers box plot), a multiple-QTL mapping (MQM) (red, whiskers box plot) indicating the LOD ± 1 (whiskers) confidence intervals was performed for the population using a co-factor selection (Figure 23). Subsequently, no additional QTLs were identified by setting the LODmax marker as cofactor in MQM analysis and the area of QTL could not be narrowed down. However, the LODmax marker ‘VMC1E12’ remained as the potential marker associated to the trait (Figure 23). In both the mapping types conducted, marker ‘VMC1E12’ determined on LG 14 reached a maximum LOD value of around 8.08, explaining the percentage phenotypic trait variance of up to 10.5 %. The confidence intervals determined for this QTL (LODmax-1) ranged between 0.2 cM to 5.4 cM (Figure 23).

Table 5 Overview of the QTL analysis based on the phenotypic data of LDA for the year 2020 of three independent experiments. Linkage group (LG); LOD maximum marker; position in cM; LOD maximum value determined by Interval Mapping (IM) and MQM (Multiple QTL Mapping); VMC1E12 selected as co-factor for the MQM analysis; PEV: explained phenotypic variance for the trait downy mildew resistance for the LODmax marker "VMC1E12" in percentage. * Physical position of the SSRs in the reference genome PN40024 12X.v2 in Mega base pairs [Mb]; Confidence intervals calculated as Bayesian credible intervals (CI) with a probability of coverage of 0.95. Determined significance of genome wide threshold of LOD values is 3.2 for 1000 permutations (at $\alpha = 0.05$). "--"; No QTL/data found for the LDA experiment 1 and 2, respectively.

Mapping type	No. of Expt (year 2020)	LG	LODmax marker	LODmax value	PEV [%]	Genetic Position [cM]	Physical Position* [Mb]	CI (cM) $[LOD_{max} - 1]$
IM	1	14	--	--	--	--	--	--
	2		--	--	--	--	--	--
	3		VMC1E12	8.08	10.5	3.8	7.1	0.2 - 5.4
MQM	1	14	--	--	--	--	--	--
	2		--	--	--	--	--	--
	3		VMC1E12	8.07	10.5	3.0	7.1	0.2 - 5.4

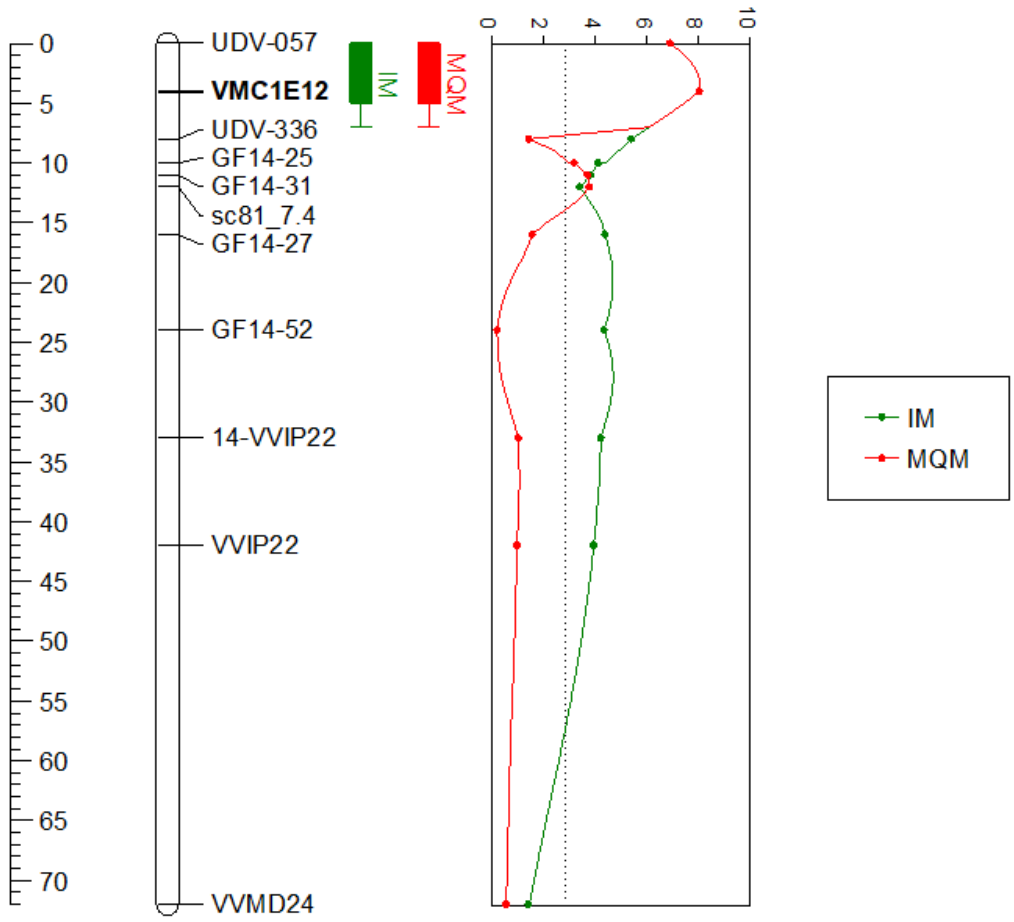

Figure 23 QTL for (LOD) *P. viticola* resistance identified on LG 14 of the integrated map; Marker distances in [cM]; IM (green, whiskers box plot) and MQM (red, whiskers box plot) indicating the LOD ± 1 (whiskers) confidence intervals. The LG specific significance level of 2.4 is indicated by the dotted line.

3.4.2 rhAmpSeq marker data

The aim was to create an initial genetic map using SSR markers and perform QTL analysis. However, the development and release of highly transferable rhAmpSeq markers (Zou et al. 2020) gave an opportunity to establish a high marker density genetic map utilizing the most recent haplotype SNP markers and conduct QTL analysis.

3.4.2.1 QTL analysis: downy mildew resistance

The rhAmpSeq genetic map with the phenotypic data of all the years showed a consistent, single and strong QTL in all the independent LDA evaluations over three years (2020, 2021, and 2022). The highly significant downy mildew resistance locus detected on the upper arm of chr. 14 was

designated as '*Rpv32'.* In the year 2020, the QTL was identified in two experiments with LOD value of 11.6 and 4.6, explaining the total phenotypic variance of 11.5 % and 4.7 % respectively, spanning the region between 3.2 cM to 4.5 cM. In the year 2021, all the experiments yielded the same QTL with improved LOD value ranging from 7.82 – 31.6, and with explained variance between 7.8 % and 28.15 %. LODmax marker 'chr14_6974992' at 4.5 cM was found to be significantly associated to the trait with the left and right flanking markers 'chr14_88562' and 'chr14_19715337', respectively (Figure 24A). The QTL was identified consistently in all the experiments of 2020 and 2021 (Figure 24B and C). Similarly, the QTL was also detected in the year 2022 (Figure 24D), conclusively proving the existence of natural genetic resistance to downy mildew in COxGT2 (Table 6). The position of the QTL shifted slightly in the year 2022, however, covering a wider interval with the same flanking markers. The allele responsible for the trait was inherited from the *V. coignetiae,* which has not been examined and exploited in breeding. The QTLs of all the three years are always located between the same left flanking markers chr14_88562 (3.4 cM) and chr14_3303300 (3.6 cM), and right flanking markers chr14_8308158 (9.3 cM) and chr14_19103240 (9.6 cM), respectively (refer to Table 6).

3.4.2.2 QTL analysis: Leaf hair

Segregation for leaf hair density was observed in the population Gf.2018-063, previously used to identify a QTL for downy mildew resistance on chr. 14. A highly significant and stable QTL associated to the morphological trait leaf hair was identified on chr. 5 located between the interval 4.3 to 8.7 cM. The explained phenotypic trait variance ranged between 24.23 % and 25.36 % with a highest LOD value of 28.33 (Table 6 and Figure 25C). The QTL associated to the trait leaf hair density identified in all the years (2020, 2021 and 2022) and the LODmax marker with flanking markers are shown in Figure 25B. In all years, the interval was consistently flanked by chr5_196931 and chr5_2429823 markers. The allele responsible for the trait leaf hair density was contributed by the maternal parent 'Morio Muskat'.

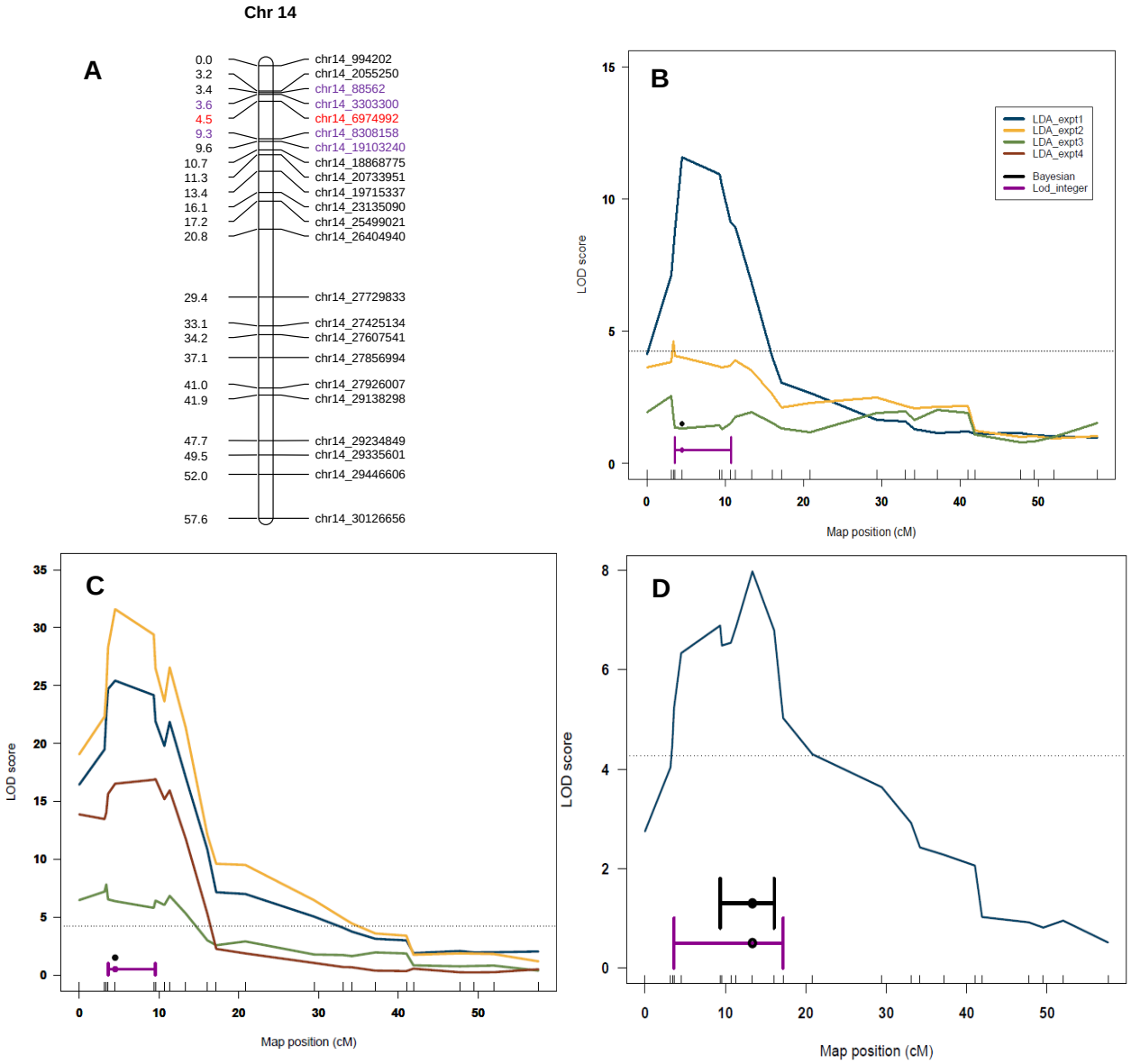

Figure 24 QTL analysis for downy mildew resistance using rhAmpSeq marker-based genetic map. (A) The physical position of peak marker (bold red) and their LOD interval (marked purple) on the upper part of chr. 14. Logarithms of the odds (LOD) score for genetic markers distributed across the chr. 14 for the individual experiments (B) year 2020, (C) 2021 and (D) 2022. The dotted line (black) indicates the 95 % confidence threshold. 'LDA_expt1' indicates the number of the independent experiment conducted in ascending order. Bayesian (black colored interval) and LOD integer (purple colored interval) based interval are shown separately.

Table 6 Summary of the QTL analysis of the F1 population 'Morio Muskat' x COxGT2 (Gf.2018-063) based on the downy mildew resistance phenotypic data of LDA and leaf hair density performed in three years (2020, 2021 and 2022). Linkage group (LG); LOD maximum marker; Peak marker position in [cM]; LODmax: LOD maximum value; PEV: explained phenotypic variance for the trait downy mildew resistance and leaf hair density in percentage. * Physical position of the rhAmpSeq marker in Mega base pairs [Mb]; Confidence intervals calculated as Bayesian credible intervals (CI) with a probability of coverage of 0.95. Determined significance of genome wide threshold of LOD values is 4.2 for 1000 permutations (at α = 0.05). "--"; No QTL/data found for the LDA experiment 3 for the year 2020, respectively. Common LODmax marker/significant marker shown in red colour; Left and right flanking markers for each LODmax marker are also indicated. In the bottom section, the summary of the QTL analysis of the population "Gf.2018-063" is shown based on the single experiment of leaf hair phenotypic data collected in three years (2020, 2021 and 2022), using multiple imputation and Haley–Knott (HK) method of scanone Rqtl with 95 % Bayesian interval.

Trait: Downy mildew resistance							
Year	**LG**	**LODmax marker**	**Peak marker position [cM]**	**LOD value**	**PVE [%]**	**Left flanking marker**	**Right flanking marker**
2020	14	chr14_6974992	4.5	11.6	11.56	chr14_3303300	chr14_18868775
		chr14_88562	3.4	4.61	4.77	chr14_994202	chr14_23135090
		--	--	--	--	--	--
2021		chr14_6974992	4.5	25.42	23.32	chr14_88562	chr14_19103240
		chr14_6974992	4.5	31.6	28.16	chr14_3303300	chr14_8308158
		chr14_88562	3.4	7.82	7.83	chr14_994202	chr14_19715337
		chr14_19103240	9.57	16.9	16.37	chr14_88562	chr14_19715337
2022		chr14_19715337	13.4	7.98	8.13	chr14_3303300	chr_25499021
Trait: Leaf hair							
2020	5	chr5_1449735	7.63	28.33	25.36	chr5_196931	chr5_2429823
2021		chr5_1449735	7.63	26.92	24.26	chr5_1120092	chr5_2429823
2022		chr5_1449735	7.63	26.88	24.23	chr_196931	chr5_2429823

.

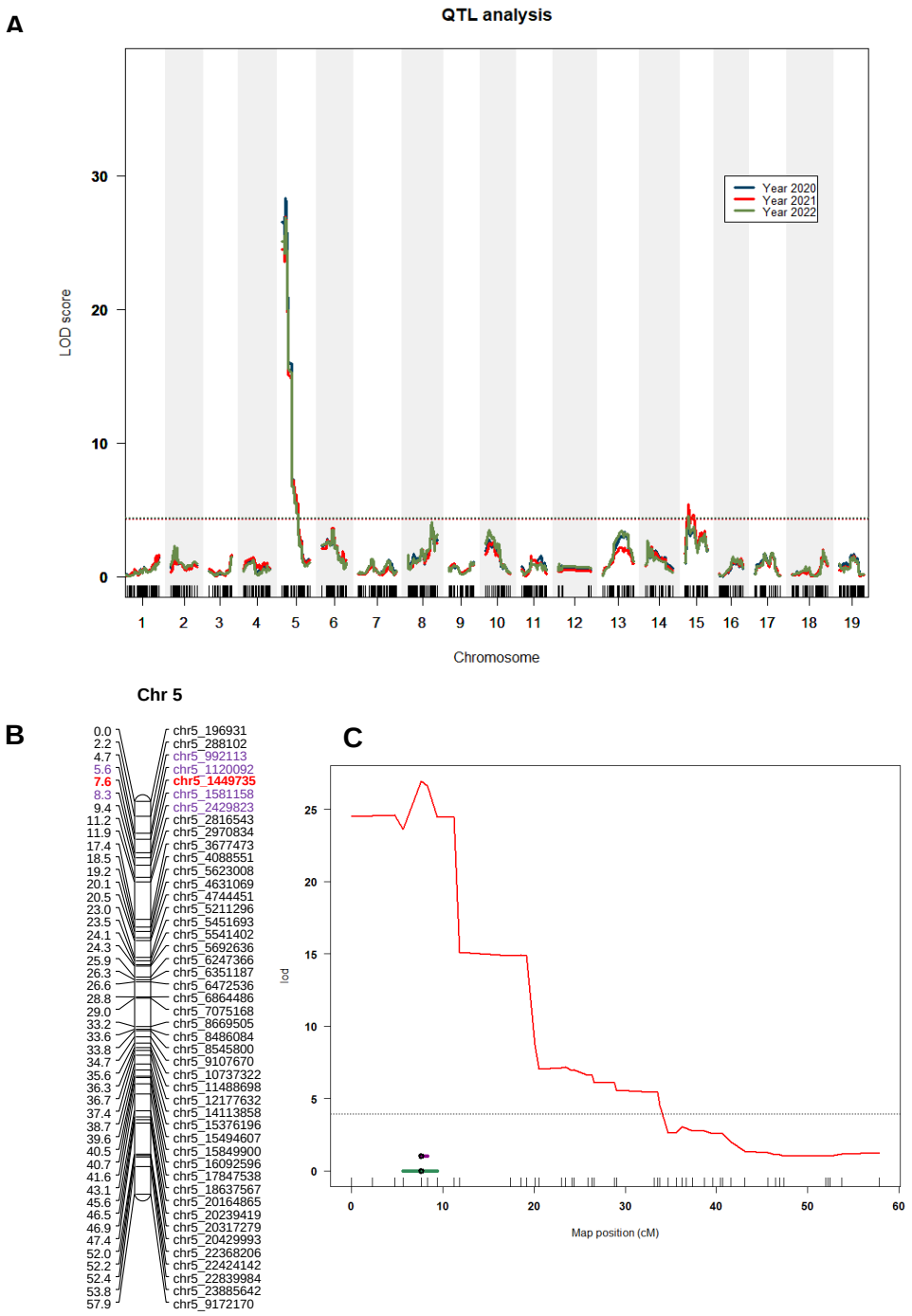

Figure 25 QTL analysis for the morphological trait leaf hair. **(**A) Logarithm of the odds (LOD) score for genetic markers distributed across the 19 chromosomes for the year 2020 (blue), 2021 (red) and 2022 (green). (B) The physical position of peak marker (bold red) and their LOD interval (marked purple) on the upper part of chr. 5. (C) QTL analysis of the experiment conducted in 2020 showing the highest LOD value. X-axis indicates the map position and Y-axis indicates the LOD score [cM]. The dotted line (black) indicates the 95 % confidence threshold. Bayesian (purple colored interval) and LOD integer (green colored interval) based interval are shown separately.

3.4.3 Marker analysis to differentiate *Rpv8, Rpv12* and *Rpv32* locus

The new resistance locus *Rpv32* was identified on the upper part of chr. 14 in the vicinity of marker VMC1E12 (7136678 bp) close to *Rpv8* and *Rpv12*. However, *Rpv32* origin is from wild *V. coignetiae*, whereas *Rpv8* and *Rpv12* were identified in *V. amurensis* genetic background. Therefore, *Rpv8* and *Rpv12* locus-associated published markers were tested on *Rpv8, Rpv12* and *Rpv32* resistance-carrying genotypes. Table 7 clearly shows significant differences in the marker data of *Rpv8* (Blasi et al., 2011) and *Rpv32* for the marker Chr14V015. Similarly, significant differences between all the marker data of *Rpv12* (Venuti et al., 2013) and *Rpv32* showed no genetic relation of this chromosomal region, indicating a new resistance locus. However, no differences were observed between *Rpv12* and *Rpv8* except for a 2 bp difference of the allele sizes for marker UDV-350 at 8.963.620 bp.

Table 7 Comparative analysis with *Rpv8* (Blasi et al., 2011), *Rpv12* (Venuti et al., 2012), and *Rpv32* (this work) allel size of associated SSR markers on genotypes carrying *Rpv8, Rpv12* and *Rpv32* resistance. Physical positions of markers in base pairs (bp).

Publication	**Marker**	**Physical position 12x.V0 [bp]**	***V. amurensis* (*Rpv8*)**	**'Kunbarat' (*Rpv12*)**	**COxGT2 (*Rpv32*)**
Blasi et al.,	Chr14V015	6.641.772	212	212	207
Venuti et al.	Sc81_7.4	8.426.630	275	275	322
Venuti et al.	Sc81_8.2	8.741.251	--	265	--
Venuti et al.	UDV-350	8.963.620	308	310	320
Venuti et al.	UDV-343	9.011.802	160	160	172
Venuti et al.	UDV-345	9.057.903	220	220	216
Venuti et al.	UDV-340	9.145.458	178	178	176
Venuti et al.	UDV-360	9.910.299	208	208	184

3.4.4 Correlation between downy mildew resistance and leaf hair density

In principle, the leaf hair density has a negative effect on *P. viticola* infection reduction due to its hydrophobic properties. Hence, correlation between the individual trait data sets was carried out before performing the correlation analysis between downy mildew resistance and leaf hair density. The phenotypic leaf hair correlation between the years 2020, 2021, and 2022 ranged between r 0.78 to 0.92. Whereas, the correlation between the downy mildew resistance ranged between r = 0.72 to 0.86. The influence of leaf hair density on genetic resistance was determined by correlating three years of manually evaluated leaf hair phenotypic data (Figure 18) with downy mildew resistance phenotypic data for each year (Figure 19). The results show a weak negative correlation coefficient (r) ranging between - 0.08 to - 0.12 (Annex I, Table 1). However, no significant correlation was identified in all the three years, except for the fact that leaf hair density and downy mildew resistance were significantly inversely linked, leading to no association or influence of leaf hair on downy mildew disease severity. In addition, the correlation between highly significant LOD-max marker for the trait leaf hair 'chr_5_1449735' and downy mildew resistance marker 'chr_14_6974992' yielded a non-significant correlation.

3.5 Aniline blue staining

All the leaf discs from susceptible 'Morio Muskat' and resistant COxGT2 were inoculated with *P. viticola*. To observe the intracellular development of the mycelium network, aniline blue stained leaf discs were prepared and evaluated at three different days post inoculation (dpi), day_1 (24 h), day_3 (72 h) and day_5 (120 h). Out of six independent staining experiments conducted, a single representative picture for each genotype is presented in Figure 26. In terms of the development of hyphae and germ tubes, there were no discernible changes between the susceptible and resistant genotypes on day one (Figure 26A and 26D). However, on day_3, a substantial amount of differences is observed between the susceptible and resistant genotypes. A moderate amount of dense network can be observed in the susceptible genotype in contrast to the resistant genotype with limited growth (Figure 26B and 26E). The day_5 results provide a clear picture and conclusive differences between both the genotypes (Figure 26C and 26F). In contrast to the resistant genotype, which showed limited fungal development, the susceptible genotype displayed extreme mycelial proliferation that nearly entirely covered the leaf disc. These results indicated

that the restriction of the growth and development of the pathogen were initiated in a time frame of 24 – 72 h.

3.6 Comparison of different resistances: *Rpv8, Rpv12,* and *Rpv32*

To evaluate the proliferation of the pathogen *P. viticola* and to compare the degree of resistance conferred by different genotypes, growth and sporulation were observed on day 5 in susceptible cultivars i. e. 'Müller Thurgau' and 'Morio Muskat' (both *V. vinifera*), and grapevine cultivars carrying *Rpv8* (*V. amurensis*), *Rpv12* ('Kunbarat') and *Rpv32* (COxGT2 and *V. coignetiae*). Since the resistance locus was located in close vicinity to the *Rpv8* and *Rpv12* locus, both originated from *V. amurensis*, it was decided to include them in the experimental setup. The production of sporangia was manually counted on six leaf discs of each genotype and resistance was evaluated by the number of sporangia that formed on 5 dpi. The results of each genotype were statistically compared using multiple pairwise comparisons (Kruskal-Wallis and Conover-Iman test). In general, no differences were observed between the susceptible genotypes as expected for *V. vinifera*. However, the results demonstrated significant and reliable differences between the susceptible (~ 40,000 sporangia/mL) and all the resistant (~ 2,000 - 5,700 sporangia/mL) genotypes (Figure 27). In particular, the number of sporangia quantified on the *Rpv32* carrier COxGT2 was significantly lower than on the susceptible 'Morio Muskat'. In addition, COxGT2 showed highly significant differences in sporangia count in contrast to the *Rpv12* carrier genotype 'Kunbarat'. Furthermore, no major observable differences were found between COxGT2 and the *Rpv8* carrier *V. amurensis*.

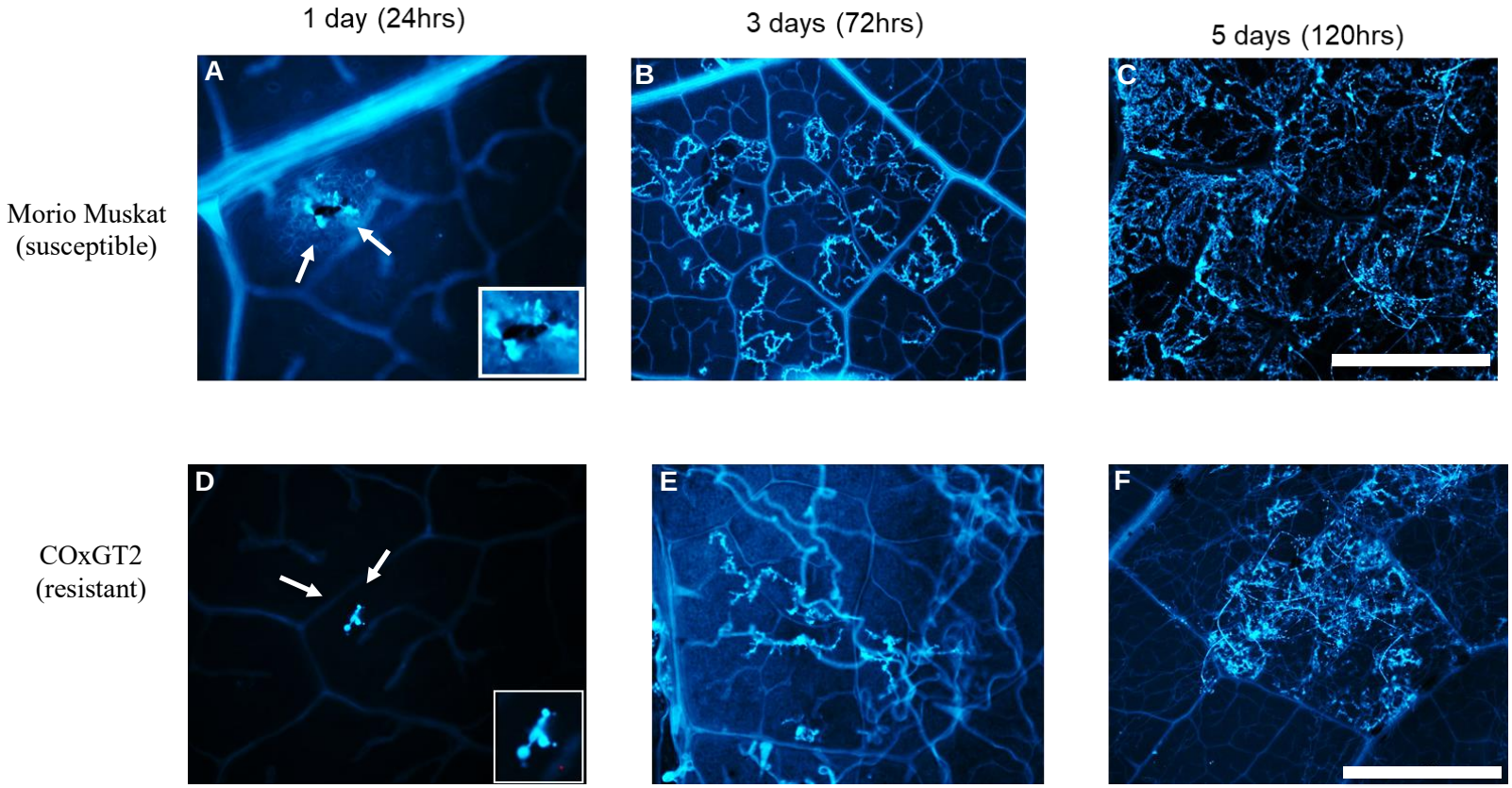

Figure 26 Comparison of intracellular *Plasmopara viticola* development in susceptible 'Morio Muskat' and resistant COxGT2 at three different days post inoculation (dpi). Day1: A and D; Day3: B and E; Day5: C and F. Arrow marks indicating the obscure growth of small mycelial structure. The best representative picture from the three biological replicates and six separate experiments are represented by the images. Scale bars represent 1000 µm. The zoomed in version of the images A and D can be seen on the right bottom corner of their respective picture.

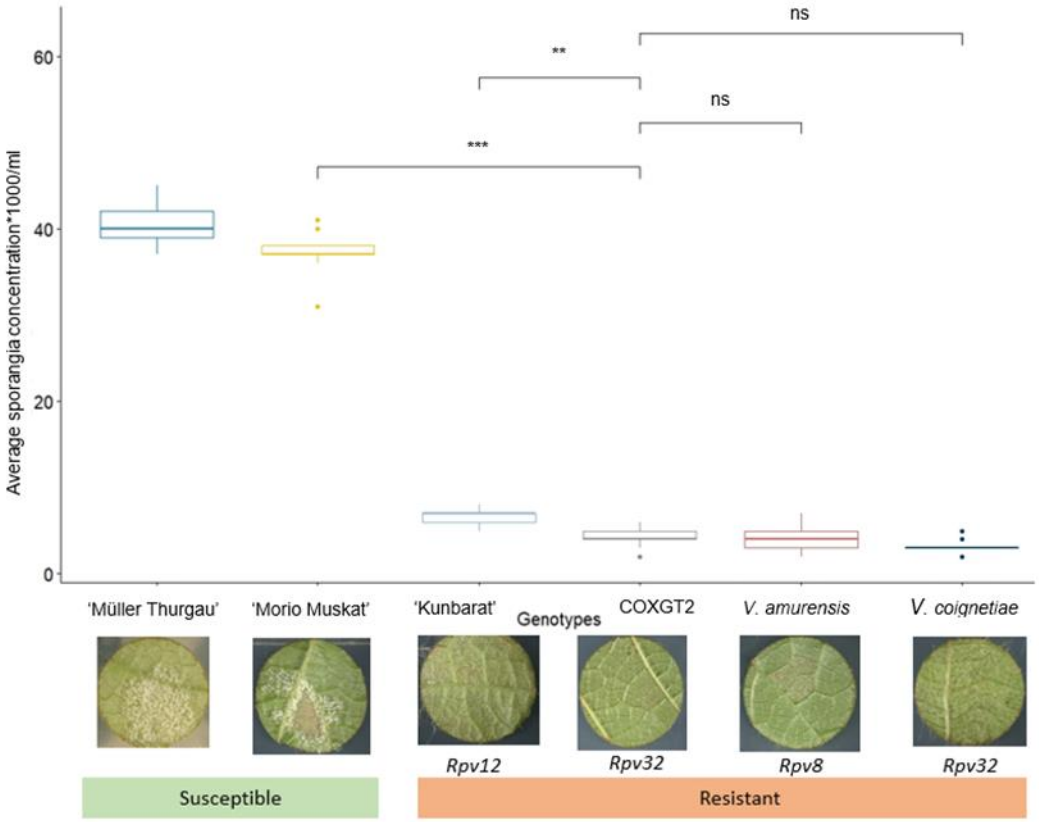

Figure 27 *Plasmopara viticola* proliferation in susceptible ('Müller Thurgau' and 'Morio Muskat') and resistant (COxGT2, 'Kunbarat', *V. amurensis*, and *V. coignetiae*) genotypes evaluated on 5 days post inoculation (dpi). Representative pictures are shown above. X-axis: All the genotypes used in the experiment and their individual resistance loci are indicated below the image. Y-axis: indicating the average sporangia concentration per ml. Whiskers box plot indicating multiple pairwise comparisons using Kruskal -Wallis and Conover-Iman test ($p < 0.05$). Error bars show standard deviation. ns: non-significant. *Rpv*: Resistance to *Plasmopara viticola.*

4 Discussion

4.1 New resistance locus in 'Morio Muskat' x COxGT2 population

In unexploited East Asian wild *Vitis* species *V. coignetiae,* naturally existing resistance was identified in order not only to minimize but also to long-term replacement of fungicides. The ultimate goal is to aid the grapevine breeding community and create PIWI (ger. *pilzwiderstandsfähige Rebsorte* (fungus resistant cultivar), Pioneer wine/vine) cultivars that are durable in resistance, sustainable and environmentally friendly. The below section provides detailed information about the new resistance locus *Rpv32*. In addition, staining studies conducted between the susceptible and the resistant donor to compare the intracellular mycelial growth at different time points provides a conclusive picture of the resistance. Furthermore, quantitative analysis of *P. viticola* involving control susceptible and resistance carrying genotypes (*Rpv8, Rpv12* and *Rpv32*) speak about the strength of the resistance loci. Moreover, this section gives detailed information on the development and validation of two artificial intelligence-based low-cost, high-throughput and objective quantification systems for grapevine downy mildew and leaf hair.

4.1.1 SCNN: An artificial intelligence based downy mildew quantification system

A significant effort is made to breed new grapevine varieties resistant to pathogens, causing severe yield losses in temperate climates. These initiatives attempted to combine excellent wine quality present in the cultivated *Vitis vinifera L. sp. sativa* with resistance traits observed in American/Asian *Vitis* species (Töpfer & Trapp, 2022). A combined approach, including phenotyping and genotyping, is one promising strategy for combating these severe diseases. One of the most significant issues with conventional plant breeding is the genotype-to-phenotype gap (Houle et al., 2010; Großkinsky et al., 2015). The demand for high-throughput phenotyping techniques, however, arises when breeding programs are compelled to expand their capacity (Cid et al., 2019; Rist et al., 2018; Underhill et al., 2020; Carvalho et al., 2021; Dunlevy et al., 2022; YongJian et al., 2022). Many high-throughput digital phenotyping techniques have been put forth recently, all of which promise to ease the current visual phenotyping bottleneck occurring in modern plant breeding programs (Divilov et al., 2017; Biermann et al., 2019). Previous studies conducted on downy mildew involved phenotypic evaluation utilizing traditional manual scores

(Bellin et al., 2009; Schwander et al., 2012; Höschele et al., 2022). Accurate and reliable measurement of a quantitative variable is essential to unveil the hidden genetics of quantitative research. In favour of this context, phenotyping several individuals by different personnel in different years can inevitably introduce subjectivity, affecting the overall results. Furthermore, it can be tedious and time-consuming to measure the responses of the many different treatments at the appropriate time, which is another major challenge.

There have been reports of several distinct CNN architectures for plant phenotyping, and these have shown ground-breaking performance in image classification (Jiang & Li, 2020). However, the type of CNN architecture used determines the amount of time and computational power needed. This work aimed to develop a low-cost-effective model for evaluating disease severity on grapevine leaf discs with a limited amount of image data and computational resources. CNN1 demonstrates that detecting leaf disc image slices is a relatively simple task for the neural network. Based on the training of CNN1, the accuracy of its validation was 98 %, and the validation loss was below 10 %. Due to the sophistication of the distinguishing feature itself (Leaf with sporangiospores vs leaf without sporangiophores), CNN2 had a high validation loss. However, adjustments in terms of additional layers, the validation loss of 15 % and validation accuracy of 95 % were achieved (Figure 13). In general, several CNN models are deployed in plant phenotyping, proving to be an excellent model with validation accuracy of above 80 % (Lee et al., 2015; Pound et al., 2017; Sardogan et al., 2018; Ferenitnos et al., 2018; Kattenborn et al., 2019; Zhang et al., 2020).

Before the model is deployed in a real-world application, it is essential to evaluate its performance. To test this, 30 leaf disc images were selected, three leaf discs for each OIV class. The 30 leaf disc images selected compromised of two different genetic backgrounds i. e., 15 images for each background. In total, three experts independently classified 15,180 image slices into three categories: background, leaf disc with sporangiophores, and leaf disc without sporangiophores (Figure 9). Irrespective of the different genetic backgrounds, a promising characteristic of a trained SCNN is their transferability. Under ideal circumstances, the SCNNs should have learnt different features allowing the classification of new unperceived images. The median ratio of true positives for the images from the trained and unrelated genetic backgrounds was approximately 96 % and 93 %, respectively. These results suggest that there is only a little accuracy loss in the transferability. The plausible reason for the decrease in accuracy might be due to poor image

quality, such as pixel resolution, saturation, and exposure time. If the network is trained on images with very comprehensive information, it can identify and categorize even the smallest feature in the images. It's interesting to see that the last two photos of class_1 in Figure 14, 'Cabernet Dorsa' x Couderc 13, are clearly subjective among the three experts. Additionally, about 6 slices of the background for image classes 5 and 7 were incorrectly classified as a leaf. This is plausible, but in the context of 506 slices, the error contributed is less than 0.5 %. Moreover, use of agar as the background and spore suspension in LDA, it is possible that any accidental droplets of suspension will cause the image slices to be misclassified. In order to optimize transferability and improve the two SCNNs already existing performance, in addition, we suggest adjusting a diverse training set made up of many distinct genetic backgrounds to compensate for the observed discrepancy. Finally, the model's architecture does not decide the excellent accuracy but rather the quality of the training data (Barbedo, 2016; Litjens et al., 2017).

A correlation analysis between SCNN-based downy mildew evaluations and manual evaluations of the leaf disc [%] on two distinct genetic backgrounds produced a significantly high correlation. A slight decrease in the correlation for the unrelated genetic background can be observed in comparison to the population used in model training. However, in both cases the correlation coefficient value is $r > 90$ (Figure 15B). Furthermore, the correlation analysis between the SCNN-based results versus the OIV 452-1 inverse class yielded significantly high correlation coefficient values for both populations (Figure 15C). Based on the above model performance results, it is evident that the two SCNNs are a suitable objective substitute for the subjective manual scoring methods. Moreover, a high number of images can be evaluated within a fraction of a second.

In summary, the proposed SCNN model showed excellent results for the overall downy mildew quantification task. To improve the model accuracy or train the same model for different pathogen systems, the model can be improved by switching from a binary classification system to a categorical. Furthermore, the model presented in this work can be implemented in different magnitudes of application. For instance, grapevine disease, including black rot, rip rot and anthracnose, which lack laboratory-based high-throughput phenotyping tools (Modesto et al., 2022). Additionally to different pathogen, crop-pathogen and any other morphological traits. Depending on the computational resource available, semantic labelling of the trait can deliberately contribute to improved prediction accuracy. Some of the recent CNN architectures have achieved high prediction accuracy based on the trait segmentation and implication of deep neural networks

(Xie et al., 2020; Yasrab et al., 2020; Liu et al., 2021; Esgario et al., 2021; Chen et al., 2021; Tugrul et al., 2022; Wang et al., 2022). In conclusion, the SCNN is an accurate and efficient tool for the automated analysis of leaf disc image data. The subjective and time-consuming manual scoring can be eliminated by implementing SCNN-based leaf disc analysis. It will guarantee uniform score outcomes in experiments and, importantly, across all the years. In addition, it has the potential to serve as a low-cost and valuable tool in a variety of agronomic disciplines, from fundamental research to plant breeding.

4.1.2 Phenotypic evaluation of downy mildew

Leaf disc assays (LDA) were performed to evaluate the response to *P. viticola* infection. For practical reasons, the degree of infection (1: none, 3: low, 5: medium, 7: high, 9: very high) per leaf disk was determined inversely to the guidelines of the OIV-452 descriptor (OIV, 2nd edition 2001, https://www.oiv.int/). For the 'Morio Muskat' x COxGT2 F1-population (n = 496), three to four independent laboratory-controlled artificial infection assays were carried out in all the years, 2020, 2021 and 2022. In the year 2020, skewness (positive/right side) was observed in the phenotypic data (Figure 18A) of the first two LDA experiments (LDA_01 and LDA_02). In the year 2022, similar skewness was seen due to the results of excessive spraying of sulphur. Sulphur was utilized to protect the greenhouse-grown populations from early powdery mildew infections, which eventually contributed to the indirect adverse effect on the downy mildew resistance assays. Bleyer (2021) published similar observations based on concrete experimentations in 2017 and 2021. The third LDA (LDA_3) in the year 2020, conducted two weeks after sulphur spraying showed negligible effect on the phenotypic data.

The LDA_1 and LDA_2 assays for the year 2021 were conducted at the beginning of the season without application of sulphur. The LDA_3 assay of 2020 and the LDA_3 and LDA_4 of 2021 were sprayed a week before the assays were conducted, clearly demonstrating the breakdown of the test's phenotypic distribution. The population's split based on resistance is a result of the parent plants' diverse genetic makeup. A natural bimodal phenotypic data distribution addressing the slight split in the resistance and susceptible genotypes was observed (Figure 18A and 18B). This splitting of resistance characteristics within a bi-parental cross population has already been reported in the phenotypic analysis. According to previous studies, a bimodal distribution of phenotypic data indicates the presence of a major single dominant locus (Bellin et al., 2009;

Malcarane et al., 2011). In general, based on the phenotypic data of all individuals with a low degree of infection (OIV scores 1 and 3) represent genotypes of the population that have increased resistance to *P. viticola*. In case of susceptible genotypes (OIV score 7 and 9) dense growth of sporangiosphores in the infected area could be observed. Mostly, some of the characteristics of observable resistance mechanisms offer convincing evidence of resistance, for instance: A typical programmed cell death-based plant response to the pathogen infection called hypersensitive response (HR) (Mur et al., 2008; Casagrande et al., 2011; Boubakri et al., 2012; Lam, 2004; Liu et al., 2005). No necrotic spots were observed on the leaf disc of the 'Morio Muskat' x COxGT2 population, which confirms the defence mechanism is different from that observed until now in North American and other Asian *Vitis* species. However, several other induced resistances (IR) involving many molecular and cellular activities, such as the induction of reactive oxygen species (ROS), cell wall strengthening, pathogenesis-related protein expression and callose deposition, can contribute to the resistance mechanisms (Boubakri, 2020).

Interestingly, distinguishable quantitative segregation for the trait leaf hair was seen in the population 'Morio Muskat' x COxGT2 (Figure 10). A medium-dense cover of hair (ribbon trichome) was observed in the resistant donor COxGT2 in comparison to no hair susceptible parent 'Morio Muskat' (refer to section introduction, Figure 3), speculating the assumption of leaf hair as a physical barrier against *P. viticola* infection. Ribbon-shaped leaf hair (trichome), evident on the abaxial surface of the leaves of the grape genus *Vitis*, is beneficial for taxonomy (Ma et al., 2016). Based on previous studies, hairs play a significant physico-chemical role and can affect the wettability of the leaves due to their hydrophobic characteristics (Figure 3) (Kortekamp & Zyprian, 1999; Kortekamp et al., 1998), thus, preventing the *P. viticola* infection. The possibility of switching off leaf hair's hydrophobic properties by applying detergent provides sufficient evidence that leaf hair contributes to some degree of physical resistance (Kortekamp & Zyprian, 1999). Leaf discs were prepared to evaluate the leaf hair density phenotypically. The density of hair evaluation was based on (1: none, 3: low, 5: medium, 7: high, 9: very high); each leaf disc was scored according to the guidelines of OIV-086 descriptor (OIV, 2nd edition 2001, https://www.oiv.int/). The results were consistent across different years (2020, 2021 and 2022) (Figure 19). According to the phenotypic data distribution of all the years, only 12 % of the individuals (OIV score 7 and score 9) contributed to the high leaf hair density scores. Very limited segregation of the trait can be seen across the population. Notably, the phenotypic expression of leaf hair density depends on

the age of the leaves and the environmental factors (Roy et al., 2001). However, because it is very subjective, the leaf hair trait is challenging to evaluate using a manual scale and can affect results in general.

4.1.3 Mapping and QTL analysis

In general, our understanding of the *Rpv* loci must be expanded in order to develop long-term sustainable alternatives for controlling *P. viticola* infection and to preventing high-yield losses. To date, 32 downy mildew resistance loci have been identified in different genetic backgrounds, and some of them are employed in developing new resistant cultivars (Bellin et al., 2009; Blasi et al., 2011; Schwander et al., 2011; Venuti et al., 2012; Di Gaspero et al., 2012). All the details regarding the resistant loci can be found on the Vitis International Variety Catalogue's home page (VIVC; http://www.vivc.de).

In addition to the phenotypic evaluation, the construction of a genetic map employing molecular markers serves as a solid foundation for linkage mapping (Grattapaglia & Sederoff, 1994). A classical QTL approach was implemented to identify the genetic region responsible for the resistance to downy mildew. Two DNA marker-based strategies were implemented in the creation of the genetic map. An initial genetic map was created using SSR (simple sequence repeats) markers due to their easy transferability across related *Vitis* species, including both coding and non-coding regions, codominant and highly polymorphic characteristics (Gupta, 1998; Scott et al., 2000; Doligez et al., 2003; Töpfer et al., 2011a). In addition, it was observed that the SSR marker system is an effective useful genomic tool due to the polymorphism of *V. vinifera*-based SSR alleles showing reproducibility in non-*vinifera* species. Furthermore, SSR markers serve as a potential marker system in MAS utilized successfully in different breeding programs. The second marker technique explicitly used for fine mapping utilized the latest rhAmpSeq markers system. This new generation of amplicon-based SNP markers developed specifically for the core *Vitis* genome has potential to detect many variants within the haplotypes (Zou et al., 2020). In contrast to SSR markers, rhAmpSeq sequencing and genotyping promises a high transferability system for the creating dense genetic maps (Yin et al., 2021; Karn et al., 2021; Reshef et al., 2022). The initial SSR-based framework map, which was created for 351 F1 individuals and consisted of 109 uniformly distributed markers (5.7 loci per linkage group), detected all 19 linkage groups (Figure 20 and Table 3). There were no discrepancies detected in the map's overall marker order. Whereas,

out of 2057 rhAmpSeq markers tested, only 647 markers (31 %) were mapped on an average of 42 loci per linkage group, covering the total map length of 1147 cM (Figure 22 and Table 4). In terms of genome coverage, it is similar to those from maps with similar marker quantities (Schwander et al., 2022; Moreira et al., 2011; Zhang et al., 2009) and within the range of comparable grapevine-specific genetic maps (Di Gaspero et al., 2007; Doligez et al., 2006; Welter et al., 2007). A significant high correlation was produced by the association of collinearity between the genomic location (cM) and the physical positions (Mb) of the rhAmpSeq markers (Figure 21). The reference genomes utilized in deriving rhAmpSeq markers involved mainly North American *Vitis* species and European *V. vinifera* (Zou et al., 2020). This may explain the lower number of functional rhAmpSeq markers and poor marker transferability to East Asian genetic backgrounds like *V. coignetiae* used in this study. However, this study presents the first independent SSR and rhAmpSeq marker-based genetic linkage map for the interspecific cross between *V. vinifera* and wild *V. coignetiae*. The three consecutive years of QTL analysis performed on the 'Morio Muskat' x COxGT2 population yielded a stable and highly significant single downy mildew-associated resistance locus.

This *Rpv* locus, located on the upper part of chromosome 14, explained the phenotypic variation of up to 36 % in all three years of the study, including both independent marker approaches, respectively. In the initial single QTL analysis, mapping methods such as Interval Mapping (IM) and subsequent Multiple QTL Mapping (MQM) involving cofactor represented VMC1E12 as the LODmax marker at 3.8 cM (7136678 bp) (Figure 23, Table 5). In addition, QTL analysis using the rhAmpSeq marker yielded QTL in all independent experiments of all the years. The rhAmpSeq marker chr14_6974992 located at 4.5 cM (6974992 bp) was found to be associated with downy mildew resistance in four experiments (Figure 24, Table 6). In this study, we name the new resistance locus as *Rpv32*. Based on the genetic analysis and field observation, *Rpv32* is the first resistance derived from an unexploited East Asian *Vitis* species that confers strong resistance to *P. viticola*. The resistance trait was introgressed by the cross-breeding between susceptible European *Vinifera* 'Morio Muskat', known for excellent high wine quality, and interspecific cross-derived COxGT2 (*V. coignetiae* x 'Gewürztraminer'). Downy mildew disease resistance QTLs are important for improving resistance in susceptible varieties (Eibach et al., 2007).

In COxGT2 derived population, resistance to downy mildew can be explained by a dominant major locus contributing to the total resistance. Considering the fact that, QTL analysis utilizing two

distinct genetic maps that covered the entire genome produced no additional significant factors that could contribute to the resistance. Resistance loci from unspecified American *Vitis* species have been found in some of the already described loci display varying levels of resistance (Merdinoglu et al., 2003; Wiedemann-Merdinoglu et al., 2006; Welter et al., 2007; Bellin et al., 2009; Fischer et al., 2004; Marguerit et al., 2009; Ochssner et al., 2016). Few *Rpv* loci have also been identified in Asian genetic background, *V. amurensis,* contributing to a high degree of resistance (Blasi et al., 2011; Schwander et al., 2012; Venuti et al., 2013; Lin et al., 2018). A recent study has also identified resistance loci in *V. vinifera* germplasm (Sargolzaei et al., 2020). However, the mode of interaction between *Vitis* species and the pathogen, as well as the co-evolution of the pathogen, are the main determinants of the degree of resistance conferred (Jürges et al., 2009).

Among all the 32 resistance loci identified against downy mildew, three loci are located on chromosome 14 (https://www vivc.de/loci). *Vitis amurensis* accession-derived resistance *Rpv8* and *Rpv12* are located on the upper part of chromosome 14 (Blasi et al., 2011; Venuti et al., 2013). While, *Rpv27* is mapped on the lower part of chromosome 14 (Sargolzaei et al., 2020). *Rpv8* was originally localized close to 'Chr14V015' marker (6641772 bp), and flanked by VVIp05 (3275203 bp) and VVIp22 (18364396 bp) markers (Blasi et al., 2011). In total, this covered approx. a distance of 15.11 Mb. Whereas, *Rpv12*, identified a few years later, was confined between the markers UDV014 (8034665 bp) and UDV370 (10110182 bp) (Venuti et al., 2013). Although *V. amurensis* and *V. coignetiae* differ in their geographical origin (Galet, 1988), the presence of the *Rpv32* marker VMC1E12 (7136678 bp) in close proximity to *Rpv8* and *Rpv12* genomic regions raises concerns. To answer these questions, two approaches were used. Firstly, ampelographic-based characterization clearly showed the difference in shoots, young leaves and mature leaves (Galet, 1988) of *V. amurensis* and *V. coignetiae*. In addition, the genetic analysis performed utilizing SSR marker published by Blasi et al. (2011) and Venuti et al. (2013) on the *Rpv8, Rpv12* and *Rpv32* carrying genotypes showed a substantial amount of reliable difference in the SSR alleles between *Rpv8* and *Rpv32,* and *Rpv12* and *Rpv32* (Table 7). The marker Chr14V015 (Blasi et al., 2011) at the physical position of 6641772 bp and all the markers (Sc81_7.4, Sc81_8.2, UDV-350, UDV-343, UDV-345, UDV-340 and UDV-360) published in Venuti et al. (2013), ranging between the physical positions of 8426630 bp to 9910299 bp showed significant differences in all the allele sizes. However, the presence of the *Rpv32*-associated LODmax marker VMC1E12

position (7136678 bp) is located far above the suggested markers by Venuti et al., 2013. On the contrary, no differences were observed between the allele sizes of *Rpv8* and *Rpv12* carrier, except for a 2 bp difference for the marker UDV350 (8963620 bp). The comparative SSR marker data between *Rpv8* and *Rpv12* are in accordance with Müllner et al. (2022). These results provide strong evidence that there is a genetic basis for distinguishing between the *Rpv8*/*Rpv12* and *Rpv32* based on their ampelographic and genetic differences in the allele sizes. The *V. amurensis* accessions and COxGT2 do not share any common ancestry.

4.1.4 Aniline blue staining

Grapevines susceptible to *P. viticola* are infected through the substomatal space of their leaves or other young green tissue. Under optimal conditions, the pathogen penetrates the stomata utilizing germ tube of the zoospores, followed by dense intracellular mycelial network development (Fröbel & Zyprian, 2019b; Burruano et al., 2000). In this investigation, aniline blue staining demonstrated that zoospores were equally capable of encysting the stomata and developing primary hyphae on susceptible 'Morio Muskat' and resistant carrying genotype COxGT2 after 1 dpi (24 hours) (Figure 26). In general, the results are consistent with the previous studies conducted by Kortekamp et al. (1997) and Eisenmann et al. (2019) showing no significant observable differences between the susceptible and resistant genotypes in the early stages of infection. In resistant grape varieties, defence reactions were triggered as soon as the haustoria were visible (Díez-Navajas et al., 2008). At 3 dpi, leaf discs showed interesting results between the susceptible and the resistant donor. Slightly decreased sporulation was observed on the resistant donor COxGT2, in comparison to the susceptible 'Morio Muskat'. At 5 dpi clear differences were observed, COxGT2 genotype exhibited reduced and stagnated sporulation but not complete suppression of *P. viticola* (Figure 26). A previous study of susceptible and resistant varieties revealed differences in histology after infection with *P. viticola* (Kortekamp et al., 1998; Gindro et al., 2003; Polesani et al., 2010). According to Kortekamp et al. (1998), the resistant varieties 'Orion' (*Rpv3.1*) and 'Phoenix' (*Rpv3.1*) were able to demonstrate restricted hyphal growth on 3dpi. Based on Gindro et al. (2003), 'Solaris' (*Rpv10, Rpv3.3*) exhibited a defence mechanism involving callose and attachment to encysted zoospores. These results suggest that defence mechanisms-mediated resistance rely on the recognition of elicitors from plants or pathogens (Keen & Yoshikawa, 1983; Kortekamp &

Zyprian, 2003; Selim, 2013). In oomycetes, β-1,3- and β-1,6-glucan are already identified as elicitors (Raaymakers & Ackerveken, 2016).

Subsequently, similar staining experiments were conducted, including three additional different resistant carrying genotypes, i. e., 'Muscaris' (*Rpv10*), *Vitis amurensis* (*Rpv8*), *V. amurensis* (*Rpv12)* and *V. coignetiae* (*Rpv32*). The preliminary results indicated successful completion of the life cycle of *P. viticola* on all the genotypes with no differences on 1 dpi. Nevertheless, comparable establishment and initiation of primary hyphae and haustorium were observed in susceptible and all resistant genotypes (Annex II, Figure 1). According to earlier studies, the first interaction of *P. viticola* with the plant cell occurs post-pathogen haustoria formation (Langcake et al., 1980: Unger et al., 2007). Similarly, to the results of Figure 26, observable differences in hyphal growth were seen at 3 dpi. Contrary to the resistant genotypes, a high amount of elongated hyphae and branching within the mesophyll can be seen on the susceptible cultivar. At 5 dpi, the susceptible cultivar showed intercostal field filled with mycelium, whereas resistant genotypes showed loose mycelium in the intercostal field, indicating the presence of resistant mechanism hindering tissue colonization. The pathogen development on susceptible 'Morio Muskat' was seen to produce fan-shaped lobed hyphae on 5 dpi to overcome physical obstacles like conducting tissue, as observed by Fröbel & Zyprian et al. (2019).

Furthermore, based on the preliminary results, *Rpv10* carrier 'Muscaris' and *Rpv32* carrier wild *V. coignetiae* showed a comparably low level of mycelial development between 3dpi to 5 dpi in comparison to COxGT2 (*Rpv32*), *V. amurensis* (*Rpv8*) and *V. amurensis* (*Rpv12*). The mechanism of *Rpv10*-mediated resistance from the Asian wild species *V. amurensis* and *Rpv12* is presently being studied (Zyprian et al., in preparation). Nevertheless, Foria et al. (2020) reported the resistance associated with HR and accumulation of stilbene phytoalexins for *Rpv10* carriers (Alonso-Villaverde et al., 2011). Previous studies conducted using *Rpv10* carrying genotypes showed similar results (Fröbel et al., 2019; Marie Jurascheck et al., 2022). Furthermore, based on recent studies the early (8 hpi) production of hydrogen peroxide in *Rpv12* carrier coincided with the appearance of PCD (Wingerter et al., 2021). No significant differences were observed between the *Rpv8* (*V. amurensis*), *Rpv12* (*V. amurensis*) and *Rpv32* (COxGT2). However, a number of variables, including the leaf's surface and age, influence the LDA. For example, the *Rpv8* carrier plant utilized in this experiment is a wild type, whereas the *Rpv12* carrier is a non-wild type. Another reasonable possibility is that the experiment's leaf material came from a greenhouse (Blasi

et al., 2011) or field (Venuti et al., 2013). Moreover, no differences in *Rpv8* and *Rpv12* mediated resistance were observed. The microscopic differences between *Rpv8* and *Rpv12* mediated resistance are explained in Müllner et al. (2022), where no difference in mycelial growth was identified. In conclusion, additional experiments, including different strains of *P. viticola* and staining methods are needed to conclusively elucidate the distinguishable characteristics between different resistant carriers. The interpretations here are based solely on the spread of the pathogen in the leaf tissue by staining hyphae and cell wall compartments of encysted zoospores.

4.1.5 Growth and sporulation of *P. viticola* on different resistance loci carriers

P. viticola proliferation was measured quantitatively at 5 dpi on the susceptible cultivar 'Müller-Thurgau' and 'Morio Muskat' (negative control), and resistance carrying genotypes, i. e., *V. amurensis* (*Rpv8*) *V. amurensis* (*Rpv12)* and *V. coignetiae (Rpv32*) and COxGT2 (*Rpv32*) leaf discs to report the degree of resistance conferred by each genotype (Figure 27). Previous investigations have reported on the degree of resistance imparted by *Rpv12* carriers (Bellin et al., 2009; Venuti et al., 2013; Possamai et al., 2020; Bove & Rossi, 2020; Wingerter et al., 2021; Panineau et al., 2022) in comparison to different resistance carrying loci. A comparable level of *P. viticola* resistance between *Rpv10* and *Rpv12* was reported by Bovi & Rossi in 2020. Whereas, Possamai et al. (2020) stated that stronger resistance was mediated by *Rpv12* carrier in comparison to *Rpv10* mediated *P. viticola* resistance. In addition, Wingerter et al. (2021) demonstrated significant differences between *Rpv10* and *Rpv12* resistance based on two different isolates of *P. viticola*. The different techniques employed to measure the degree of resistance and the lack of reference protocols could be the reasons explaining these contradictory results. However, the absence of the *Rpv10* carrying genotype in our experimental setup makes it difficult to draw conclusions based on the previously found results. Nevertheless, our preliminary results based on the microscopic studies are in accordance with the previous studies conducted by Wingerter et al. (2021). It was discovered that, in contrast to cultivars that are susceptible, sporulation is much lower on *Rpv32* resistant carriers, indicating strong resistance. Interestingly, highly significant differences were observed between the *Rpv12* (*V. amurensis*) and *Rpv32* (COxGT2) mediated resistance carriers, with low sporulation on COxGT2. However, no significant difference is seen between *Rpv8* and *Rpv32* (COxGT2). In addition, prominent necrotic lesions were observed on *Rpv8* and *Rpv12* carrying genotypes as described by Possamai et al. (2020), with no difference in

sporulation. This adds intrigue to the study and recommends that additional research is necessary to determine the differences between *Rpv8, Rpv12*, and *Rpv32*. Moreover, it is worth noting that no significant difference in sporulation on COxGT2 and wild *V. coignetiae* (parent of COxGT2) indicates a loss of resistance intensity in the next generation. Complicated biological conditions with uncharacterized strains can complicate research because the pathogen's evolution is a factor in the breakdown of resistance (Panineau et al., 2022). Further experiments in upcoming years, including different resistant carriers, could provide more detailed insights and concrete results.

4.1.6 Downy mildew vs. leaf hair: A weak negative correlation

A quantitative segregation for leaf hair (trichome) density on the abaxial surface of the leaf was shown in 'Morio Muskat' x COxGT2, the same population where the *Rpv32* was identified. A trichome is a distinctive feature of different organ surfaces and is essential for taxonomy in the grape genus *Vitis*. The diversity and anatomy of trichomes have been studied previously, providing preliminary insights into the distribution and density of trichomes (Yong-hua et al., 1994; Werker, 2000; Chitwood et al., 2014). Recent research provides opportunities for better ampelographic identification of grapevine (*Vitis vinifera L.*) cultivars via understanding of the microanatomy of leaf trichrome (Gago et al., 2016). A systematic study of *Vitis* trichome morphology, structure and ontology has been presented in great detail (Ma et al., 2016). In the population Gf.2018-063, segregation for ribbon trichomes was observed which are flat, twisted and with varying density (Figure 10). In North America, East Asia, and Europe, both subgenera of *Vitis* have ribbon trichrome (Moore, 1991; Ma et al., 2016). Due to their diverse morphological, phytochemical and mechanical properties, trichomes have a variety of functions in plant physiology and ecology (Levin, 1973; Kortekamp & Zyprian, 1999; Wagner et al., 2004).

Earlier versions of the hypothesis came from Kortekamp and Zyprian (1999) and Divilov et al. (2018) that illustrated the effect of leaf hair on downy mildew disease resistance. The QTL on chromosome 5 (7.6 cM) identified in this study has been overlapping with a previously reported QTL region by Kono et al. (2018) in a population of *V. vinifera* 'Muscat of Alexandria' × *V. labruscana* 'Campbell Early'. They found a major QTL for leaf trichome (ribbon) density on the upper end of LG 5 at 2.8 cM, named Leaf Hairs 1 (LH1) and provided concrete evidence on leaf hair as a structural defence against downy mildew. In addition, QTL on LG 5 was also identified by Barba et al. (2019) for the trait hair on leaf blade, showing the influence on predatory

mite abundance. This QTL has been validated in different genetic backgrounds by Teh et al. (2017) and found to overlap with the QTL identified by Barba et al. (2019). Furthermore, on LG 5, loci identified as *Rpv10* and *Rpv11* had small effects on downy mildew resistance (Fischer et al., 2004; Schwander et al., 2012). However, leaf hair is not a qualitative resistance and disease progression cannot be completely stopped. Nevertheless, the disease incidence and severity were found to be less in hairy genotypes than in non-hairy indicating quantitative resistance characteristics supporting durability (Kou et al., 2010). Irrespective of population, the ultimate outcome of our research is in contrary to the study conducted by Kono et al. (2018). The leaf hair QTL on chromosome 5 was consistent in all three years of the experiment (Figure 25). However, a weak correlation (ranging between R = -0.08 to -0.12) was found between the downy mildew resistance and leaf hair density. Only 10 % of the 496 F1 individuals showed high densities of abaxial leaf hair (OIV score 7 and 9), reflecting limited segregation. *Vitis labrusca* species generally show an extremely high density of abaxial leaf hair covering the whole leaf except the veins (Gerrath et al., 2015). According to Cadle-Davidson (2008), 'Concord', a hybrid between 'Catawba' and *V. labrusca*, showed consistent and moderate foliar resistance due to the high density of leaf hair. Based on the results with the population utilized, Kono et al. (2018) concluded that the presence of thick and dense hair contributes to durable resistance. Additionally, environmental influences may impact the leaf hair density depending on whether the study was conducted on field plants or greenhouse plants. However, it is unclear how genetic mechanisms improve leaf hair density—nevertheless, the first candidate gene contributing to the trait leaf hair was proposed by Barba et al. (2019). The recent studies conducted by Yin et al. (2021) validated the function of transcription factor WER (regulates the hairless cell fate), NAC transcription factor 29, EF-hand protein, and MYB140. Furthermore, it was found that the homozygous deletion at the end of the transcription factor WER caused the dense trichome phenotype. Additionally, they discovered that a heterozygous deletion at the exact location in a different genotype resulted in a less dense trichome phenotype (Yin et al., 2021).

However, the resolution of the phenotypic evaluation and variability in the phenotypic score caused due to age of the leaves might have contributed to the poor phenotypic association with downy mildew. Although there was no strong correlation between trichome density and downy mildew resistance, further detailed analysis is required, mainly focusing on generating leaf hair phenotypic data and a more suitable population showing high segregation for leaf hair density.

Instead of only quantifying leaf hair, a different new approach is required to provide phenotypic measurements that highlight wettability. Since leaf hair represents a physical barrier, it is not sufficient to quantify only leaf hair, but also its wettability in a new phenotyping approach. An ultimate goal should be to eludidate whether or not physical resistance imparted by leaf hair can be utilized in breeding programs to complement systems like gene for gene resistance.

5 Conclusion and future perspective

In this study, the East Asian species *Vitis coignetiae* was investigated for the very first time to identify downy mildew resistance. The bi-parental F1 population Gf.2018-063 was utilized in linkage mapping and phenotypic studies across three years. Two independent marker technologies, i. e., SSR and the latest rhAmpSeq haplotype markers, have been implemented to create a genetic map and identify the resistance locus responsible for downy mildew resistance. At the same time, the rhAmpSeq-based genetic map shows a higher marker density than the SSR-based genetic map. The QTL analysis performed based on the linkage mapping and phenotypic data of all three years in two to three independent experiments showed a strong and stable QTL on the upper arm of chromosome 14. A novel resistance locus identified in this study was named *Rpv32* (Resistance to *P. viticola*) (Malagol et al., 2023, in preparation). The *Rpv32*-associated markers identified in this study can be used in marker-assisted selection, and developing pyramided cultivars, eventually contributing to the reduction of fungicides in viticulture. Based on the reference genome PN40024, the genomic area responsible for resistance to downy mildew can be screened for putative candidate genes. However, the available reference genome PN40024 is susceptible to downy mildew, thus, making the study intricate. Nevertheless, sequencing the resistance donor and functionally characterizing the genes can be carried out. As the grapevine genome is highly heterozygous, the trio-binning method exploits heterozygosity and can effectively identify the resistance genes. The advantage of trio binning over other methods is that it offers simplifying haplotype assembly by resolving allelic variation prior to assembly, thus, improving diploid genome assembly and will facilitate studies of haplotype variation and inheritance (Koren et al., 2018; Yen et al., 2020; Sichel et al., 2022). Furthermore, an alternate option could be RNA-Seq analysis of resistant and susceptible genotypes to identify the differentially expressed genes mediating *Rpv32* resistance.

The preliminary results of pathogen proliferation between the *Rpv12* and *Rpv32* carrier genotypes showed significant differences. In comparison, no differences were observed between *Rpv8* and *Rpv32*. Additional experiments are required to conclusively demonstrate the strength of *Rpv32* resistance in contrast to other *P. viticola* resistance-carrying genotypes (*Rpv8, Rpv12, Rpv10,* and *Rpv3*). To expand upon the current work, analyzing resistance mechanisms with different staining methods to gain detailed insights on *Rpv32* mediated defence mechanisms to *P. viticola*. Furthermore, adding different isolates of *P. viticola* in addition to different resistance-carrying

genotypes to the current experimental set-up can shed information on minimizing the danger of new isolates breaking the resistance.

This study investigated the intriguing question of leaf hair as a physical barrier against the downy mildew pathogen. The existence of quantitative segregation of the trait leaf hair (ribbon trichome) in the Gf.2018-063 population resulted in the identification of a locus on the upper end of chromosome 5 (previously mentioned by Kono et al., 2018). However, a very weak and negligible association was found between the leaf hair density and the downy mildew disease severity/incidence. Although the current work was performed on a population exhibiting limited segregation for the trait leaf hair, in order to answer the questions and utilize the trait for breeding purposes, it is necessary to study populations showing high segregation. In addition, it is necessary to use more precise and accurate phenotyping tools to measure the trait.

This study also includes developing two independent low-cost artificial intelligence-based CNN models used for the automated analysis of grapevine leaf disc image data: The SCNN model for the high-throughput downy mildew disease severity quantification (Zendler et al., 2021) and a ResNet-based model for leaf hair quantification (Malagol et al., 2023, in preparation). Both the models were tested, validated and cross-validated using three independent experts and yielded a significant correlation coefficient ($r > 90$) with manual scoring. Implementing these AI-based pipelines eliminates the need for subjective manual scoring, reduces staffing, and provides consistency across all experiments over the years. For future work, it would be better to switch from binary to categorical classification using the most recent deep convolutional architectures (Ex: YOLO, RCNN, AX-RetinaNet etc.). Semantic labelling and segmentation are preferable alternatives for improving prediction accuracy. However, this can result in a large amount of computing resources, high image quality, and intense model training. Additionally, the SCNN pipeline for DM quantification is publicly available on the GitHub repository and can be retrained, adapted to the specific plant-pathogen system and different traits (https://www.github.com/Daniel-Ze/Leaf-disc-scoring). These pipelines can serve as a valuable and efficient tool in a wide range of studies, from basic plant research to breeding.

References

Alleweldt, G., & Possingham, J. V. (1988). Progress in grapevine breeding. *Theoretical and Applied Genetics, 75*(5), 669-673.

Adam-Blondon, A. F., Martinez-Zapater, J. M., & Kole, C. (Eds.). (2016). *Genetics, genomics, and breeding of grapes*. CRC Press.

Agarwal, M., Shrivastava, N., & Padh, H. (2008). *Advances in molecular marker techniques and their applications in plant sciences. Plant cell reports, 27*(4), 617-631.

Alahakoon, D., Fennell, A., Helget, Z., Bates, T., Karn, A., Manns, D., ... & Londo, J. P. (2022). Berry Anthocyanin, Acid, and Volatile Trait Analyses in a Grapevine-Interspecific F2 Population Using an Integrated GBS and rhAmpSeq Genetic Map. *Plants, 11*(5), 696.

Aleynova, O. A., Suprun, A. R., Ananev, A. A., Nityagovsky, N. N., Ogneva, Z. V., Dubrovina, A. S., & Kiselev, K. V. (2022). Effect of Calmodulin-like Gene (CML) Overexpression on Stilbene Biosynthesis in Cell Cultures of Vitis amurensis Rupr. *Plants, 11*(2), 171.

Ali, S., Ganai, B. A., Kamili, A. N., Bhat, A. A., Mir, Z. A., Bhat, J. A., ... & Grover, A. (2018). Pathogenesis-related proteins and peptides as promising tools for engineering plants with multiple stress tolerance. *Microbiological Research, 212*, 29-37.

Alonso-Villaverde, V., Voinesco, F., Viret, O., Spring, J. L., & Gindro, K. (2011). The effectiveness of stilbenes in resistant Vitaceae: ultrastructural and biochemical events during Plasmopara viticola infection process. *Plant Physiology and Biochemistry, 49*(3), 265-274.

Andrade-Sanchez, P., Gore, M. A., Heun, J. T., Thorp, K. R., Carmo-Silva, A. E., French, A. N., ... & White, J. W. (2013). Development and evaluation of a field-based high-throughput phenotyping platform. *Functional Plant Biology, 41*(1), 68-79.

Ausubel, F. M. (2005). Are innate immune signaling pathways in plants and animals conserved? *Nature immunology, 6*(10), 973-979.

Arroyo-García, R., Ruiz-Garcia, L., Bolling, L., Ocete, R., López, M. A., Arnold, C., ... & Martinez-Zapater, J. M. (2006). Multiple origins of cultivated grapevine (Vitis vinifera L. ssp. sativa) based on chloroplast DNA polymorphisms. *Molecular ecology, 15*(12), 3707-3714.

Ballabio, C., Panagos, P., Lugato, E., Huang, J. H., Orgiazzi, A., Jones, A., ... & Montanarella, L. (2018). Copper distribution in European topsoils: An assessment based on LUCAS soil survey. *Science of The Total Environment, 636*, 282-298.

Barba, P., Loughner, R., Wentworth, K., Nyrop, J. P., Loeb, G. M., & Reisch, B. I. (2019). A QTL associated with leaf trichome traits has a major influence on the abundance of the predatory mite Typhlodromus pyri in a hybrid grapevine population. *Horticulture research, 6*.

Barbara Richter (2022). PIWIS IM PORTRÄT. PIWIS Anbaueignung, Rebsortenmerkmale und Geschmacksprofile ausgewählter weißer PIWI-Rebsorten.

Barbedo, J. G. A. (2016). A review on the main challenges in automatic plant disease identification based on visible range images. *Biosystems engineering*, *144*, 52-60.

Basler, R., & Scherz, P. (2011). PIWI Rebsorten. Pilzwiderstandsfähige Rebsorte, 8.

Beakes, G. W. (1987). Oomycete phylogeny: ultrastructural perspectives. *Evolutionary biology of the fungi*, 405-421.

Beakes, G. W. (1989). Oomycete fungi: their phylogeny and relationship to chromophyte algae. In *The chromophyte algae: problems and perspectives* (pp. 325-342). Oxford: Clarendon Press.

Bebber, D. P., Holmes, T., Smith, D., & Gurr, S. J. (2014). Economic and physical determinants of the global distributions of crop pests and pathogens. *New Phytologist*, *202*(3), 901-910.

Bellin, D., Peressotti, E., Merdinoglu, D., Wiedemann-Merdinoglu, S., Adam-Blondon, A. F., Cipriani, G., ... & Di Gaspero, G. (2009). Resistance to Plasmopara viticola in grapevine 'Bianca'is controlled by a major dominant gene causing localised necrosis at the infection site. *Theoretical and Applied Genetics*, *120*(1), 163-176.

Bendel, N., Kicherer, A., Backhaus, A., Klück, H. C., Seiffert, U., Fischer, M., ... & Töpfer, R. (2020). Evaluating the suitability of hyper-and multispectral imaging to detect foliar symptoms of the grapevine trunk disease Esca in vineyards. *Plant methods*, *16*(1), 1-18.

Bent, A. F., & Mackey, D. (2007). Elicitors, effectors, and R genes: the new paradigm and a lifetime supply of questions. *Annu. Rev. Phytopathol.*, *45*, 399-436.

Bent, A. F., Kunkel, B. N., Dahlbeck, D., Brown, K. L., Schmidt, R., Giraudat, J., ... & Staskawicz, B. J. (1994). RPS2 of Arabidopsis thaliana: a leucine-rich repeat class of plant disease resistance genes. *Science*, *265*(5180), 1856-1860.

Bentham, A. R., De la Concepcion, J. C., Mukhi, N., Zdrzałek, R., Draeger, M., Gorenkin, D., ... & Banfield, M. J. (2020). A molecular roadmap to the plant immune system. *Journal of Biological Chemistry*, *295*(44), 14916-14935.

Bereswill, R., Golla, B., Streloke, M., & Schulz, R. (2012). Entry and toxicity of organic pesticides and copper in vineyard streams: Erosion rills jeopardise the efficiency of riparian buffer strips. *Agriculture, Ecosystems & Environment*, *146*(1), 81-92.

Berkeley, M. C. (1847). The Gardeners' Chronicle. 47, 779.

Bhattarai, G., Fennell, A., Londo, J. P., Coleman, C., & Kovacs, L. G. (2021). A novel grape downy mildew resistance locus from Vitis rupestris. *American Journal of Enology and Viticulture*, *72*(1), 12-20.

Bianchi, D., Brancadoro, L., & De Lorenzis, G. (2020). Genetic diversity and population structure in a Vitis spp. core collection investigated by SNP markers. *Diversity*, *12*(3), 103.

Bierman, A., LaPlumm, T., Cadle-Davidson, L., Gadoury, D., Martinez, D., Sapkota, S., & Rea, M. (2019). A high-throughput phenotyping system using machine vision to quantify severity of grapevine powdery mildew. Plant Phenomics, 2019.

Bigeard, J., Colcombet, J., & Hirt, H. (2015). Signaling mechanisms in pattern-triggered immunity (PTI). *Molecular plant, 8*(4), 521-539.

Blasi, P., Blanc, S., Wiedemann-Merdinoglu, S., Prado, E., Rühl, E. H., Mestre, P., & Merdinoglu, D. (2011). Construction of a reference linkage map of Vitis amurensis and genetic mapping of Rpv8, a locus conferring resistance to grapevine downy mildew. *Theoretical and applied genetics, 123*(1), 43-53.

Bleyer, G. (2021). WBI. *Planzenschutz gegen Pernospora.*

Bock, C. H., Poole, G. H., Parker, P. E., and Gottwald, T. R. (2010). Plant disease severity estimated visually, by digital photography and image analysis, and by hyperspectral imaging. *Crit. Rev. Plant Sci. 29*, 59–107.

Boller, T., & Felix, G. (2009). A renaissance of elicitors: perception of Microbe–associated molecular patterns and danger signals by pattern-recognition. *Ann. Rev. Plant Biol., 60*, 379-406.

Boubakri, H. (2020). Induced resistance to biotic stress in plants by natural compounds: Possible mechanisms. *In Priming-Mediated Stress and Cross-Stress Tolerance in Crop Plants* (pp. 79-99). Academic Press.

Boubakri, H., Wahab, M. A., Chong, J., Bertsch, C., Mliki, A., & Soustre-Gacougnolle, I. (2012). Thiamine induced resistance to Plasmopara viticola in grapevine and elicited host–defense responses, including HR like-cell death. *Plant Physiology and Biochemistry, 57*, 120-133.

Boutrot, F., & Zipfel, C. (2017). Function, discovery, and exploitation of plant pattern recognition receptors for broad-spectrum disease resistance. *Annual review of phytopathology, 55*, 257-286.

Bouquet, A., & Torregrosa, L. (2003). Micropropagation of the grapevine (*Vitis* spp.). *Micropropagation of woody trees and fruits*, 319-352.

Bove, F., & Rossi, V. (2020). Components of partial resistance to *Plasmopara viticola* enable complete phenotypic characterization of grapevine varieties. *Scientific reports, 10*(1), 1-12.

Brader, G., Compant, S., Vescio, K., Mitter, B., Trognitz, F., Ma, L. J., & Sessitsch, A. (2017). Ecology and genomic insights into plant-pathogenic and plant-nonpathogenic endophytes. *Annual Review of Phytopathology, 55*(1).

Brilli, M., Asquini, E., Moser, M., Bianchedi, P. L., Perazzolli, M., & Si-Ammour, A. (2018). A multi-omics study of the grapevine-downy mildew (*Plasmopara viticola*) pathosystem unveils a complex protein coding-and noncoding-based arms race during infection. *Scientific Reports, 8*(1), 1-12.

Brown, J. K., & Hovmøller, M. S. (2002). Aerial dispersal of pathogens on the global and continental scales and its impact on plant disease. *Science, 297*(5581), 537-541.

Buck, K. (2022). An Investigation of Factors Affecting the Rooting Ability of Hardwood Muscadine Cuttings and Genetic Diversity of Wild and Cultivated Muscadine Grapes (Vitis rotundifolia Michx.) (*Doctoral dissertation, University of Arkansas*).

Buonassisi, D. (2017). A comparative study of plant-pathogen interaction in different genotypes and organs of grapevine (*Vitis* spp.), based on optimized and new screening methods for resistance to downy mildew (*Plasmopara viticola*-Berk. & Curt.). *Euphytica, 213* (103).

Burruano, S. (2000). The life-cycle of *Plasmopara viticola*, cause of downy mildew of vine. *Mycologist, 14*(4), 179-182.

Caffi, T., Gilardi, G., Monchiero, M., & Rossi, V. (2013). Production and release of asexual sporangia in Plasmopara viticola. *Phytopathology, 103*(1), 64-73.

Caffi, T., Rossi, V., Cossu, A., & Fronteddu, F. (2007). Empirical vs. mechanistic models for primary infections of Plasmopara viticola. *EPPO bulletin, 37*(2), 261-271.

Calonnec, A., Cartolaro, P., Poupot, C., Dubourdieu, D., & Darriet, P. (2004). Effects of Uncinula necator on the yield and quality of grapes (*Vitis vinifera*) and wine. *Plant pathology, 53*(4), 434-445.

Canziani, A., Paszke, A., & Culurciello, E. (2016). An analysis of deep neural network models for practical applications. *arXiv preprint arXiv:1605.07678.*

Carausu, E. M., Checherita, L. E., Stamatin, O., & Albu, A. (2016). Study of serum and saliva biochemical levels for copper, zinc and cooper-zinc imbalance in patients with oral cancer and oral potentially malignant disorders and their prostetical and dsss (disfunctional syndrome of stomatognathic system) treatment. *Revista de Chimie, 67*(9), 1832-1836.

Carvalho, L. C., Gonçalves, E. F., Marques da Silva, J., & Costa, J. M. (2021). Potential phenotyping methodologies to assess inter-and intravarietal variability and to select grapevine genotypes tolerant to abiotic stress. *Frontiers in Plant Science, 12*, 718202.

Casagrande, K., Falginella, L., Castellarin, S. D., Testolin, R., & Di Gaspero, G. (2011). Defence responses in *Rpv3*-dependent resistance to grapevine downy mildew. *Planta, 234*(6), 1097-1109.

Chakraborty, S., Tiedemann, A. V., & Teng, P. S. (2000). Climate change: potential impact on plant diseases. *Environmental pollution, 108*(3), 317-326.

Chang, X., & Nick, P. (2012). Defence signalling triggered by Flg22 and Harpin is integrated into a different stilbene output in *Vitis* cells. *PLoS One, 7*(7), e40446.

Chang, X., Seo, M., Takebayashi, Y., Kamiya, Y., Riemann, M., & Nick, P. (2017). Jasmonates are induced by the PAMP flg22 but not the cell death-inducing elicitor Harpin in Vitis rupestris. *Protoplasma, 254(1)*, 271-283.

Chen, S., Zhang, K., Zhao, Y., Sun, Y., Ban, W., Chen, Y., ... & Yang, T. (2021). An approach for rice bacterial leaf streak disease segmentation and disease severity estimation. *Agriculture, 11(5)*, 420.

Chen, Y., Wu, W., Yang, B., Xu, F., Tian, S., Lu, J., & Fu, P. (2022). Grapevine VaRPP13 protein enhances oomycetes resistance by activating SA signal pathway. *Plant Cell Reports, 41*(12), 2341-2350.

Cheng, D. W., Jiang, J. F., Fan, X. C., Zhang, Y., Zhang, G. H., & Liu, C. H. (2013). Diversity analysis of Chinese wild grape species. Journal of Plant Genetic Resources, 14(6), 996-1012.Cheng, D. W., Lin, H., Takahashi, Y., Walker, M. A., Civerolo, E. L., & Stenger, D. C. (2010). Transcriptional regulation of the grape cytochrome P450 monooxygenase gene CYP736B expression in response to Xylella fastidiosa infection. BMC Plant *Biology*, *10*(1), 1-14.

Chepsergon, J., Motaung, T. E., & Moleleki, L. N. (2021). "Core" RxLR effectors in phytopathogenic oomycetes: A promising way to breeding for durable resistance in plants?. *Virulence, 12*(1), 1921-1935.

Chinchilla, D., Zipfel, C., Robatzek, S., Kemmerling, B., Nürnberger, T., Jones, J. D., ... & Boller, T. (2007). A flagellin-induced complex of the receptor FLS2 and BAK1 initiates plant defence. *Nature, 448*(7152), 497-500.

Chisholm, S. T., Coaker, G., Day, B., & Staskawicz, B. J. (2006). Host-microbe interactions: shaping the evolution of the plant immune response. *Cell, 124*(4), 803-814.

Chitwood, D. H., Ranjan, A., Martinez, C. C., Headland, L. R., Thiem, T., Kumar, R., ... & Sinha, N. R. (2014). A modern ampelography: a genetic basis for leaf shape and venation patterning in grape. *Plant physiology, 164*(1), 259-272.

Chojnacka, K. (2010). Fermentation products. *Chemical engineering and chemical process technology, 5*, 189-200.

Cid, P., García, M., Pinolef, A., & Barba, P. (2018, July). Phenotyping tools for genetic improvement of table grapes in Chile. *In XII International Conference on Grapevine Breeding and Genetics 1248* (pp. 267-274).

Ciubotaru, R. M., Franceschi, P., Zulini, L., Stefanini, M., Škrab, D., Rossarolla, M. D., ... & Chitarrini, G. (2021). Mono-locus and pyramided resistant grapevine cultivars reveal early putative biomarkers upon artificial inoculation with Plasmopara viticola. *Frontiers in Plant Science, 12*, 693887.

Coakley, S. M., Scherm, H., & Chakraborty, S. (1999). Climate change and plant disease management. *Annual review of phytopathology, 37*(1), 399-426.

Collard, B. C., & Mackill, D. J. (2008). Marker-assisted selection: an approach for precision plant breeding in the twenty-first century. Philosophical Transactions of the Royal Society B: *Biological Sciences, 363*(1491), 557-572.

Collard, B. C., Jahufer, M. Z. Z., Brouwer, J. B., & Pang, E. C. K. (2005). An introduction to markers, quantitative trait loci (QTL) mapping and marker-assisted selection for crop improvement: the basic concepts. *Euphytica, 142*(1), 169-196.

Couto, D., & Zipfel, C. (2016). Regulation of pattern recognition receptor signalling in plants. *Nature Reviews Immunology, 16*(9), 537-552.

Crossa, J., Pérez-Rodríguez, P., Cuevas, J., Montesinos-López, O., Jarquín, D., De Los Campos, G., ... & Varshney, R. K. (2017). Genomic selection in plant breeding: methods, models, and perspectives. *Trends in plant science, 22*(11), 961-975.

Dangl, J. L., & Jones, J. D. (2001). Plant pathogens and integrated defence responses to infection. *Nature, 411*(6839), 826-833.

Dalbó, M. A., Ye, G. N., Weeden, N. F., Steinkellner, H., Sefc, K. M., & Reisch, B. I. (2000). A gene controlling sex in grapevines placed on a molecular marker-based genetic map. *Genome, 43*(2), 333-340.

De Lorenzis, G., Mercati, F., Bergamini, C., Cardone, M. F., Lupini, A., Mauceri, A., ... & Brancadoro, L. (2019). SNP genotyping elucidates the genetic diversity of Magna Graecia grapevine germplasm and its historical origin and dissemination. *BMC plant biology, 19*(1), 1-15.

Delmas, C. E., Mazet, I. D., Jolivet, J., Delière, L., & Delmotte, F. (2014). Simultaneous quantification of sporangia and zoospores in a biotrophic oomycete with an automatic particle analyzer: Disentangling dispersal and infection potentials. *Journal of microbiological methods, 107*, 169-175.

Delmotte, F., Chen, W. J., RICHARD-CERVERA, S., Greif, C., Papura, D., Giresse, X., ... & CORIO-COSTET, M. F. (2006). Microsatellite DNA markers for Plasmopara viticola, the causal agent of downy mildew of grapes. *Molecular Ecology Notes, 6*(2), 379-381.

Delmotte, F., Mestre, P., Schneider, C., Kassemeyer, H. H., Kozma, P., Richart-Cervera, S., ... & Delière, L. (2014). Rapid and multiregional adaptation to host partial resistance in a plant pathogenic oomycete: evidence from European populations of Plasmopara viticola, the causal agent of grapevine downy mildew. *Infection, Genetics and Evolution, 27*, 500-508.

Delrot, S., Grimplet, J., Carbonell-Bejerano, P., Schwandner, A., Bert, P. F., Bavaresco, L., ... & Vezzulli, S. (2020). Genetic and genomic approaches for adaptation of grapevine to climate change. *Genomic designing of climate-smart fruit crops*, 157-270.

DeStatis. (2016). Land- und Forstwirtschaft, Fischerei. *Grunderhebung der Rebflächen. Statistisches Bundesamt*, Wiesbaden.

De Lorenzis, G., Mercati, F., Bergamini, C., Cardone, M. F., Lupini, A., Mauceri, A., ... & Brancadoro, L. (2019). SNP genotyping elucidates the genetic diversity of Magna Graecia grapevine germplasm and its historical origin and dissemination. *BMC plant biology, 19*, 1-15.

Di Gaspero, G., Copetti, D., Coleman, C., Castellarin, S. D., Eibach, R., Kozma, P., ... & Testolin, R. (2012). Selective sweep at the Rpv3 locus during grapevine breeding for downy mildew resistance. *Theoretical and Applied Genetics, 124*(2), 277-286.

Dick, M. W. (2001). Straminipilous Fungi Kluwer Academic Publishers. The Netherlands.

Diez-Navajas, A. M., Wiedemann-Merdinoglu, S., Greif, C., & Merdinoglu, D. (2008). Nonhost versus host resistance to the grapevine downy mildew, Plasmopara viticola, studied at the tissue level. *Phytopathology, 98*(7), 776-780.

Divilov, K., Barba, P., Cadle-Davidson, L., & Reisch, B. I. (2018). Single and multiple phenotype QTL analyses of downy mildew resistance in interspecific grapevines. *Theoretical and Applied Genetics, 131*, 1133-1143.

Dodds, P. N., & Rathjen, J. P. (2010). Plant immunity: towards an integrated view of plant–pathogen interactions. *Nature Reviews Genetics, 11*(8), 539-548.

Doligez, A., Adam-Blondon, A. F., Cipriani, G., Di Gaspero, G., Laucou, V., Merdinoglu, D., ... & This, P. (2006). An integrated SSR map of grapevine based on five mapping populations. *Theoretical and applied genetics, 113*(3), 369-382.

Douglas, E., & Halpin, C. (2009). Gene stacking. *Molecular Techniques in Crop Improvement*: *2nd Edition*, 613-629.

D'Onofrio, C., Tumino, G., Gardiman, M., Crespan, M., Bignami, C., De Palma, L., ... & Terzi, V. (2021). Parentage atlas of Italian grapevine varieties as inferred from SNP genotyping. *Frontiers in Plant Science, 11*, 605934.

Dumitriu, G. D., Teodosiu, C., & Cotea, V. V. (2021). *Management of pesticides from vineyard to wines: Focus on wine safety and pesticides removal by emerging technologies* (pp. 1-27). London, UK: IntechOpen.

Dunlevy, J. D., Blackmore, D. H., Betts, A., Jewell, N., Brien, C., Berger, B., ... & Walker, A. R. (2022). Investigating the effects of elevated temperature on salinity tolerance traits in grapevine rootstocks using high-throughput phenotyping. *Australian Journal of Grape and Wine Research, 28*(2), 276-291.

Eibach, R., Zyprian, E., Welter, L., & Topfer, R. (2007). The use of molecular markers for pyramiding resistance genes in grapevine breeding. *VITIS-GEILWEILERHOF-*, *46*(3), 120.

Eibach, R., & Töpfer, R. (2015). Traditional grapevine breeding techniques. *In Grapevine breeding programs for the wine industry* (pp. 3-22). Woodhead Publishing.

Eisenmann, B., Czemmel, S., Ziegler, T., Buchholz, G., Kortekamp, A., Trapp, O., ... & Bogs, J. (2019). Rpv3–1 mediated resistance to grapevine downy mildew is associated with specific host transcriptional responses and the accumulation of stilbenes. *BMC plant biology, 19*(1), 1-17.

Erbs, G., Silipo, A., Aslam, S., De Castro, C., Liparoti, V., Flagiello, A., ... & Cooper, R. M. (2008). Peptidoglycan and muropeptides from pathogens Agrobacterium and Xanthomonas elicit plant innate immunity: structure and activity. *Chemistry & biology, 15*(5), 438-448.

Esgario, J. G., de Castro, P. B., Tassis, L. M., & Krohling, R. A. (2022). An app to assist farmers in the identification of diseases and pests of coffee leaves using deep learning. *Information Processing in Agriculture, 9*(1), 38-47.

Esmaeel, Q., Miotto, L., Rondeau, M., Leclère, V., Clément, C., Jacquard, C., ... & Barka, E. A. (2018). Paraburkholderia phytofirmans PsJN-plants interaction: from perception to the induced mechanisms. *Frontiers in Microbiology, 9*, 2093.

Ezzat, A., Szabó, Z., & Nyéki, J. (2014). Induce the plant resistance to pathogen infection. *International Journal of Horticultural Science, 20*(1-2), 89-93.

Fawke, S., Doumane, M., & Schornack, S. (2015). Oomycete interactions with plants: infection strategies and resistance principles. *Microbiology and Molecular Biology Reviews, 79*(3), 263-280.

Feechan, A., Anderson, C., Torregrosa, L., Jermakow, A., Mestre, P., Wiedemann-Merdinoglu, S., ... & Dry, I. B. (2013). Genetic dissection of a TIR-NB-LRR locus from the wild North A merican grapevine species Muscadinia rotundifolia identifies paralogous genes conferring resistance to major fungal and oomycete pathogens in cultivated grapevine. *The Plant Journal, 76*(4), 661-674.

Felix, G., Regenass, M., & Boller, T. (1993). Specific perception of subnanomolar concentrations of chitin fragments by tomato cells: induction of extracellular alkalinization, changes in protein phosphorylation, and establishment of a refractory state. *The Plant Journal, 4*(2), 307-316.

Felix, G., Duran, J. D., Volko, S., & Boller, T. (1999). Plants have a sensitive perception system for the most conserved domain of bacterial flagellin. *The Plant Journal, 18*(3), 265-276.

Ferentinos, K. P. (2018). Deep learning models for plant disease detection and diagnosis. *Computers and electronics in agriculture, 145*, 311-318.

Ferris, H., Zheng, L., & Walker, M. A. (2012). Resistance of grape rootstocks to plant-parasitic nematodes. *Journal of nematology, 44*(4), 377.

Finger, R., Zachmann, L., & McCallum, C. (2022). Short supply chains and the adoption of fungus-resistant grapevine varieties. *Applied Economic Perspectives and Policy*.

Fischer, B. M., Salakhutdinov, I., Akkurt, M., Eibach, R., Edwards, K. J., Toepfer, R., & Zyprian, E. M. (2004). Quantitative trait locus analysis of fungal disease resistance factors on a molecular map of grapevine. *Theoretical and Applied Genetics, 108*(3), 501-515.

Flor, H. H. (1971). Current status of the gene-for-gene concept. *Annual review of phytopathology, 9*(1), 275-296.

Florea, A., Sipos, A., & Stoisor, M. C. (2022). Applying AI Tools for Modeling, Predicting and Managing the White Wine Fermentation Process. *Fermentation, 8*(4), 137.

Fontaine, M. C., Labbé, F., Dussert, Y., Delière, L., Richart-Cervera, S., Giraud, T., & Delmotte, F. (2021). Europe as a bridgehead in the worldwide invasion history of grapevine downy mildew, Plasmopara viticola. *Current Biology, 31*(10), 2155-2166.

Foria, S., Copetti, D., Eisenmann, B., Magris, G., Vidotto, M., Scalabrin, S., ... & Morgante, M. (2020). Gene duplication and transposition of mobile elements drive evolution of the Rpv3 resistance locus in grapevine. *The Plant Journal, 101*(3), 529-542.

Fraiwan, M., Faouri, E., & Khasawneh, N. (2022). Classification of Corn Diseases from Leaf Images Using Deep Transfer Learning. *Plants, 11*(20), 2668.

Fröbel, S. (2019a). *Studien zum Resistenzlokus Rpv10 gegen den Falschen Mehltau (Plasmopara viticola) der Weinrebe (Vitis vinifera)*. Julius Kühn-Institut, Bundesforschungsinstitut für Kulturpflanzen.

Fröbel, S., & Zyprian, E. (2019b). Colonization of different grapevine tissues by Plasmopara viticola—a histological study. *Frontiers in plant science, 10*, 951.

Fu, P., Wu, W., Lai, G., Li, R., Peng, Y., Yang, B., et al. (2020). Identifying Plasmopara viticola resistance Loci in grapevine (Vitis amurensis) via genotyping-by-sequencing-based QTL mapping. *Plant Physiol. Biochem. 154*, 75–84.

Furbank, R. T., and Tester, M. (2011). Phenomics—technologies to relieve the phenotyping bottleneck. *Trends Plant Sci. 16*, 635–644.

Furiosi, M., Rossi, V., Legler, S., & Caffi, T. (2022). Study on fungicides' use in viticulture: present and future scenarios to control powdery and downy mildew. *In BIO Web of Conferences* (Vol. 50, p. 03006). EDP Sciences.

Gago, P., Conejero, G., Martínez, M. C., Boso, S., This, P., & Verdeil, J. L. (2016). Microanatomy of leaf trichomes: opportunities for improved ampelographic discrimination of grapevine (Vitis vinifera L.) cultivars. *Australian journal of grape and wine research, 22*(3), 494-503.

Galet, P. (1988). Cépages et vignobles de France. *Les vignes américaines*. 2ème Ed. Imprimerie Charles Dehan. Montpellier. Francia.

Garcia-Garcia, A., Orts-Escolano, S., Oprea, S., Villena-Martinez, V., Martinez-Gonzalez, P., & Garcia-Rodriguez, J. (2018). A survey on deep learning techniques for image and video semantic segmentation. *Applied Soft Computing, 70*, 41-65.

Gerrath, J., Posluszny, U., & Melville, L. (2015). *Taming the wild grape: Botany and horticulture in the Vitaceae*. Springer.

Gessler, C., Pertot, I., & Perazzolli, M. (2011). Plasmopara viticola: a review of knowledge on downy mildew of grapevine and effective disease management. *Phytopathologia Mediterranea, 50*(1), 3-44.

Gindro, K., Spring, J. L., Pezet, R., Richter, H., & Viret, O. (2006). Histological and biochemical criteria for objective and early selection of grapevine cultivars resistant to Plasmopara viticola. VITIS-GEILWEILERHOF-, 45(4), 191.

Głowacki, S., Macioszek, V., & Kononowicz, A. (2011). R proteins as fundamentals of plant innate immunity. *Cellular and Molecular Biology Letters, 16*(1), 1-24.

Godfrey, D., Able, A. J., & Dry, I. B. (2007). Induction of a grapevine germin-like protein (VvGLP3) gene is closely linked to the site of Erysiphe necator infection: a possible role in defense?. *Molecular Plant-Microbe Interactions, 20*(9), 1112-1125.

Gómez-Gómez, L. (2004). Plant perception systems for pathogen recognition and defence. *Molecular immunology, 41*(11), 1055-1062.

Gómez-Gómez, L., & Boller, T. (2002). Flagellin perception: a paradigm for innate immunity. *Trends in plant science, 7*(6), 251-256.

Gómez-Zeledón, J., Kaiser, M., & Spring, O. (2017). Exploring host-pathogen combinations for compatible and incompatible reactions in grapevine downy mildew. *European Journal of Plant Pathology, 149*(1), 1-10.

Gómez-Zeledón, J., Zipper, R., & Spring, O. (2013). Assessment of phenotypic diversity of Plasmopara viticola on Vitis genotypes with different resistance. *Crop Protection, 54*, 221-228.

Gong, P., Kang, J., Sadeghnezhad, E., Bao, R., Ge, M., Zhuge, Y., ... & Fang, J. (2022). Transcriptional Profiling of Resistant and Susceptible Cultivars of Grapevine (*Vitis L.*) Reveals Hypersensitive Responses to Plasmopara viticola. *Frontiers in microbiology, 13*.

Granett, J., Walker, M. A., Kocsis, L., & Omer, A. D. (2001). Biology and management of grape phylloxera. *Annual review of entomology, 46*, 387.

Grant, M. R., Godiard, L., Straube, E., Ashfield, T., Lewald, J., Sattler, A., ... & Dangl, J. L. (1995). Structure of the Arabidopsis RPM1 gene enabling dual specificity disease resistance. *Science, 269*(5225), 843-846.

Grassi, F., & Arroyo-Garcia, R. (2020). Origins and Domestication of the Grape. *Frontiers in Plant Science, 11*, 1176.

Grattapaglia, D., & Sederoff, R. (1994). Genetic linkage maps of Eucalyptus grandis and Eucalyptus urophylla using a pseudo-testcross: mapping strategy and RAPD markers. *Genetics, 137*(4), 1121-1137.

Gindro, K., Pezet, R., & Viret, O. (2003). Histological study of the responses of two Vitis vinifera cultivars (resistant and susceptible) to Plasmopara viticola infections. *Plant Physiology and Biochemistry, 41*(9), 846-853.

Großkinsky, D. K., Svensgaard, J., Christensen, S., & Roitsch, T. (2015). Plant phenomics and the need for physiological phenotyping across scales to narrow the genotype-to-phenotype knowledge gap. *Journal of experimental botany, 66*(18), 5429-5440.

Grover, A., & Sharma, P. C. (2016). Development and use of molecular markers: past and present. *Critical reviews in biotechnology, 36*(2), 290-302.

Guan, P., Schmidt, F., Riemann, M., Fischer, J., Thines, E., & Nick, P. (2020). Hunting modulators of plant defence: the grapevine trunk disease fungus Eutypa lata secretes an amplifier for plant basal immunity. *Journal of experimental botany*, *71*(12), 3710-3724.

Gupta, P. K., Balyan, H. S., Sharma, P. C., & Ramesh, B. (1996). Microsatellites in plants: a new class of molecular markers. *Current science*, 45-54.

Gust, A. A., Biswas, R., Lenz, H. D., Rauhut, T., Ranf, S., Kemmerling, B., ... & Nürnberger, T. (2007). Bacteria-derived peptidoglycans constitute pathogen-associated molecular patterns triggering innate immunity in Arabidopsis. *Journal of Biological Chemistry*, *282*(44), 32338-32348.

Han, X., & Tsuda, K. (2022). Evolutionary footprint of plant immunity. Current Opinion in Plant *Biology*, *67*, 102209.

Hatsugai, N., Yamada, K., Goto-Yamada, S., & Hara-Nishimura, I. (2015). Vacuolar processing enzyme in plant programmed cell death. *Frontiers in plant science*, *6*, 234.

Héloir, M. C., Adrian, M., Brulé, D., Claverie, J., Cordelier, S., Daire, X., ... & Poinssot, B. (2019). Recognition of elicitors in grapevine: From MAMP and DAMP perception to induced resistance. *Frontiers in plant science*, *10*, 1117.

Höschele, T. (2021). Identifikation und genetische Kartierung neuer Resistenzen gegen *Plasmopara viticola* aus asiatischen und amerikanischen Wildarten (Doctoral dissertation, Karlsruher Institut für Technologie (KIT)).

Houle, D., Govindaraju, D. R., & Omholt, S. (2010). Phenomics: the next challenge. *Nature reviews genetics*, *11*(12), 855-866.

Huang, Z., Qin, A., Lu, J., Menon, A., & Gao, J. (2020, November). Grape Leaf Disease Detection and Classification Using Machine Learning. *In 2020 International Conferences on Internet of Things (iThings) and* IEEE *Green Computing and Communications (GreenCom) and* IEEE *Cyber, Physical and Social Computing (CPSCom) and* IEEE *Smart Data (SmartData) and* IEEE *Congress on Cybermatics (Cybermatics)* (pp. 870-877). IEEE.

Hulme, P. E. (2009). Trade, transport and trouble: managing invasive species pathways in an era of globalization. *Journal of applied ecology*, *46*(1), 10-18.

Ingle, R. A., Carstens, M., & Denby, K. J. (2006). PAMP recognition and the plant–pathogen arms race. *Bioessays*, *28*(9), 880-889.

Inohara, N., Chamaillard, M., McDonald, C., & Nunez, G. (2005). NOD-LRR proteins: role in host-microbial interactions and inflammatory disease. *Annu. Rev. Biochem.*, *74*, 355-383.

Imazio, S., Labra, M., Grassi, F., Scienza, A., & Failla, O. (2006). Chloroplast microsatellites to investigate the origin of grapevine. *Genetic Resources and Crop Evolution*, *53*, 1003-1011.

Jiang, Y., & Li, C. (2020). Convolutional neural networks for image-based high-throughput plant phenotyping: a review. *Plant Phenomics, 2020*.

Jaillon O, Aury J-M, Noel B. (2007). The grapevine genome sequence suggests ancestral hexaploidization in major angiosperm phyla. *Nature, 449*,463–467.

Jaillon, O., Aury, J. M., Noel, B., Policriti, A., Clepet, C., Casagrande, A., ... & Wincker, P. (2007). French-Italian Public Consortium for Grapevine Genome Characterization The grapevine genome sequence suggests ancestral hexaploidization in major angiosperm phyla. *Nature, 449*(7161), 463-467.

Jermini, M., Blaise, P., & Gessler, C. (2010). Quantitative effect of leaf damage caused by downy mildew (Plasmopara viticola) on growth and yield quality of grapevine 'Merlot' *(Vitis vinifera). Vitis, 49*(2), 77-85.

Jermini, M., Gessler, C., & Blaise, P. (1997). Preliminary investigations on the impact of Plasmopara viticola on yield quantity and quality of Vitis vinifera. *Wein-Wissenschaft, 52*(3-4), 154-155.

Jiang, R. H., & Tyler, B. M. (2012). Mechanisms and evolution of virulence in oomycetes. *Annual review of phytopathology, 50*, 295-318.

Jiang, P., Ergu, D., Liu, F., Cai, Y., & Ma, B. (2022). A Review of Yolo algorithm developments. *Procedia Computer Science, 199*, 1066-1073.

Jones, J. D., & Dangl, J. L. (2006). The plant immune system. *nature, 444*(7117), 323-329.

Judelson, H. S., & Ah-Fong, A. M. (2019). Exchanges at the plant-oomycete interface that influence disease. *Plant Physiology, 179*(4), 1198-1211.

Jürges, G., Kassemeyer, H. H., Dürrenberger, M., Düggelin, M., & Nick, P. (2009). The mode of interaction between Vitis and Plasmopara viticola Berk. & Curt. Ex de Bary depends on the host species. *Plant Biology, 11*(6), 886-898.

Kanyuka, K., & Rudd, J. J. (2019). Cell surface immune receptors: the guardians of the plant's extracellular spaces. *Current opinion in plant biology, 50*, 1-8.

Karimi, B., Masson, V., Guilland, C. (2021). Ecotoxicity of copper input and accumulation for soil biodiversity in vineyards. *Environ Chem Lett 19*, 2013–2030

Karling, J. S. (1981). Predominantly holocarpic and eucarpic simple biflagellate phycomycetes.

Karn, A., Diaz-Garcia, L., Reshef, N., Zou, C., Manns, D. C., Cadle-Davidson, L., ... & Sacks, G. L. (2021). The Genetic Basis of Anthocyanin Acylation in North American Grapes (Vitis spp.). *Genes, 12*(12), 1962.

Karn, A., Zou, C., Brooks, S., Fresnedo-Ramírez, J., Gabler, F., Sun, Q., ... & Cadle-Davidson, L. (2021). Discovery of the REN11 locus from Vitis aestivalis for stable resistance to grapevine powdery mildew in a family segregating for several unstable and tissue-specific quantitative resistance loci. *Frontiers in Plant Science, 12*, 733899.

Kassemeyer, H. (2017). Fungi of grapes. In: König, H., Unden, G. & Fröhlich, J. (eds) Biology of microorganisms on grapes, in must and in wine. *Springer, Cham. Chapter 4*, 103-132.

Kato, J., & Svensson, C. I. (2015). Role of extracellular damage-associated molecular pattern molecules (DAMPs) as mediators of persistent pain. *Progress in Molecular Biology and Translational Science, 131*, 251-279.

Kattenborn, T., Eichel, J., & Fassnacht, F. E. (2019). Convolutional Neural Networks enable efficient, accurate and fine-grained segmentation of plant species and communities from high-resolution UAV imagery. *Scientific reports*, *9*(1), 1-9.

Kearsey, M. J. (1998). The principles of QTL analysis (a minimal mathematics approach). *Journal of experimental botany, 49*(327), 1619-1623.

Keen, N. T., & Yoshikawa, M. (1983). β-1, 3-Endoglucanase from soybean releases elicitor-active carbohydrates from fungus cell walls. *Plant Physiology, 71*(3), 460-465.

Keller M. (2015a). Botany and anatomy: 1-57. In: The science of grapevines. 2nd ed. *Oxford: Elsevier* LTD. pp. 522.

Keller, H., Boyer, L., & Abad, P. (2016). Disease susceptibility in the Zig-Zag model of host–microbe interactions: only a consequence of immune suppression?.*Molecular plant pathology, 17*(4), 475.

Kiefer, B., Riemann, M., Büche, C., Kassemeyer, H. H., & Nick, P. (2002). The host guides morphogenesis and stomatal targeting in the grapevine pathogen *Plasmopara viticola. Planta, 215*(3), 387-393.

Kim, S. G., Kim, S. T., Wang, Y., Yu, S., Choi, I. S., Kim, Y. C., ... & Kang, K. Y. (2011). The RNase activity of rice probenazole-induced protein1 (PBZ1) plays a key role in cell death in plants. *Molecules and cells, 31*(1), 25-31.

Koblet, W., Candolfi-Vasconcelos, M. C., Zweifel, W., & Howell, G. S. (1994). Influence of leaf removal, rootstock, and training system on yield and fruit composition of Pinot noir grapevines. *American Journal of Enology and Viticulture, 45*(2), 181-187.

Kocsis, L., Granett, J., Walker, M. A., Lin, H., & Omer, A. D. (1999). Grape phylloxera populations adapted to *Vitis berlandieri x V. riparia rootstocks*. *American Journal of Enology and Viticulture, 50*(1), 101-106.

Kole, C. (2011). *Genetics, Genomics, and Breeding of Grapes.*CRC press.

Koledenkova, K., Esmaeel, Q., Jacquard, C., Nowak, J., Clément, C., & Barka, E. A. (2022). Plasmopara viticola the causal agent of downy mildew of grapevine: from its taxonomy to disease management. *Frontiers in Microbiology, 13*.

Kono, A., Ban, Y., Mitani, N., Fujii, H., Sato, S., Suzaki, K., ... & Sato, A. (2018). Development of SSR markers linked to QTL reducing leaf hair density and grapevine downy mildew resistance in Vitis vinifera. *Molecular Breeding, 38*(11), 1-19.

Koren, S., Rhie, A., Walenz, B. P., Dilthey, A. T., Bickhart, D. M., Kingan, S. B., ... & Phillippy, A. M. (2018). De novo assembly of haplotype-resolved genomes with trio binning. *nature biotechnology, 36*(12), 1174-1182.

Kortekamp, A. (2005). Growth, occurrence and development of septa in Plasmopara viticola and other members of the Peronosporaceae using light-and epifluorescence-microscopy. *Mycological research, 109*(5), 640-648.

Kortekamp, A., Wind, R., & Zyprian, E. (1998). Investigation of the interaction of Plasmopara viticola with susceptible and resistant grapevine cultivars/Untersuchungen zur Interaktion von Plasmopara viticola mit anfälligen und resistenten Rebsorten. *Zeitschrift für Pflanzenkrankheiten und Pflanzenschutz/Journal of Plant Diseases and Protection*, 475-488.

Kortekamp, A., Wind, R. & Zyprian, E. (1999). The role of hairs on the wettability of grapevine (*Vitis spp.*) leaves. *Vitis 38* (3), 101-105.

Kortekamp, A., & Zyprian, E. (1999). Leaf hairs as a basic protective barrier against downy mildew of grape. *Journal of Phytopathology, 147*(7-8), 453-459

Kortekamp, A., & Zyprian, E. (2003). Characterization ofPlasmopara-Resistance in grapevine usingin vitroplants. *Journal of plant physiology, 160*(11), 1393-1400.

Kosambi, DD. (1944). The estimation of map distances from recombination values. *Ann Eugenics 12*:172–175

Kou, Y., & Wang, S. (2010). Broad-spectrum and durability: understanding of quantitative disease resistance. *Current opinion in plant biology, 13*(2), 181-185.

Kourelis, J., & Van Der Hoorn, R. A. (2018). Defended to the nines: 25 years of resistance gene cloning identifies nine mechanisms for R protein function. *The Plant Cell, 30*(2), 285-299.

Kühne, S., Roßberg, D., Röhrig, P., Von Mehring, F., Weihrauch, F., Kanthak, S., ... & Gitzel, J. (2017). The use of copper pesticides in Germany and the search for minimization and replacement strategies. *Organic Farming, 3*(1), 66-75.

Lafon, R., & Clerjeau, M. (1988). Downy mildew. Compendium of grape diseases, 11-13.

Lam, E. (2004). Controlled cell death, plant survival and development. *Nature reviews Molecular cell biology, 5*(4), 305-315.

Lan, X., Liu, Y., Song, S., Yin, L., Xiang, J., Qu, J., & Lu, J. (2019). Plasmopara viticola effector PvRXLR131 suppresses plant immunity by targeting plant receptor-like kinase inhibitor BKI1. *Molecular plant pathology, 20*(6), 765-783.

Langcake, P., & Lovell, P. A. (1980). Light and electron microscopical studies of the infection of Vitis spp. by Plasmopara viticola, the downy mildew pathogen. *Vitis, 19*(4), 321-337.

Lau, E. (2014). High-throughput phenotyping of rice growth traits. *Nature Reviews Genetics, 15*(12), 778-778.

Laucou, V., Launay, A., Bacilieri, R., Lacombe, T., Adam-Blondon, A. F., Berard, A., ... & Boursiquot, J. M. (2018). Extended diversity analysis of cultivated grapevine *Vitis vinifera* with 10K genome-wide SNPs. *PloS one, 13*(2), e0192540.

LeCun, Y., & Bengio, Y. (1995). Convolutional networks for images, speech, and time series. *The handbook of brain theory and neural networks, 3361*(10), 1995.

Lee, S. H., Chan, C. S., Wilkin, P., & Remagnino, P. (2015, September). Deep-plant: Plant identification with convolutional neural networks. *In 2015* IEEE *international conference on image processing (ICIP)* (pp. 452-456). IEEE.

Levin, D. A. (1973). The role of trichomes in plant defense. *The quarterly review of biology, 48*(1, Part 1), 3-15.

Li, B., Fan, X., Zhang, Y., Liu, C., & Jiang, J. (2021). Genetic Diversity and Population Structure Analysis of Chinese Wild Grape Using Simple Sequence Repeat Markers. *Journal of the American Society for Horticultural Science, 146*(3), 158-168.

Li, X., Dong, S., & Su, X. (2018). Copper and other heavy metals in grapes: a pilot study tracing influential factors and evaluating potential risks in China. *Scientific Reports, 8*(1), 17407.

Li, Y. B., Han, L. B., Wang, H. Y., Zhang, J., Sun, S. T., Feng, D. Q., ... & Xia, G. X. (2016). The thioredoxin GbNRX1 plays a crucial role in homeostasis of apoplastic reactive oxygen species in response to Verticillium dahliae infection in cotton. *Plant Physiology, 170*(4), 2392-2406.

Li, Z., Yue, H., & Xing, D. (2012). MAP Kinase 6-mediated activation of vacuolar processing enzyme modulates heat shock-induced programmed cell death in Arabidopsis. *New Phytologist, 195*(1), 85-96.

Li, F., Liu, W., & Zhou, X. (2019). Pivoting plant immunity from theory to the field. *Science China Life Sciences, 62*, 1539-1542.

Lijavetzky, D., Cabezas, J. A., Ibáñez, A., Rodríguez, V., & Martínez-Zapater, J. M. (2007). High throughput SNP discovery and genotyping in grapevine (*Vitis vinifera L.*) by combining a re-sequencing approach and SNPlex technology. *BMC genomics, 8*(1), 1-11.

Lin, H., Leng, H., Guo, Y., Kondo, S., Zhao, Y., Shi, G., & Guo, X. (2019). QTLs and candidate genes for downy mildew resistance conferred by interspecific grape (*V. vinifera L.*× *V. amurensis Rupr.*) crossing. *Scientia Horticulturae, 244*, 200-207.

Litjens, G., Kooi, T., Bejnordi, B. E., Setio, A. A. A., Ciompi, F., Ghafoorian, M., ... & Sánchez, C. I. (2017). A survey on deep learning in medical image analysis. *Medical image analysis, 42*, 60-88.

Liu, B., Zhang, Y., He, D., & Li, Y. (2017). Identification of apple leaf diseases based on deep convolutional neural networks. *Symmetry, 10*(1), 11.

Liu, C., Fan, X., Jiang, J., Guo, D., Sun, H., Zhang, Y., & Feng, J. (2012). Genetic diversity of Chinese wild grape species by SSR and SRAP markers. *Biotechnology & Biotechnological Equipment, 26*(2), 2899-2903.

Liu, Y., Schiff, M., & Czymmek, K. Tallo czy, Z., Levine, B., and Dinesh-Kumar, SP (2005). Autophagy regulates programmed cell death during the plant innate immune response. *Cell, 121*, 567-577.

Liu, Y., Su, J., Shen, L., Lu, N., Fang, Y., Liu, F., ... & Su, B. (2021). Development of a mobile application for identification of grapevine (*Vitis vinifera L.*) cultivars via deep learning. *International journal of agricultural and biological engineering, 14*(5), 172-179

Lu, J., Tan, L., & Jiang, H. (2021). Review on convolutional neural network (CNN) applied to plant leaf disease classification. *Agriculture, 11*(8), 707.

Lu, Y., & Tsuda, K. (2021). Intimate association of PRR-and NLR-mediated signaling in plant immunity. *Molecular Plant-Microbe Interactions, 34*(1), 3-14.

Luderer, R., & Joosten, M. H. (2001). Avirulence proteins of plant pathogens: determinants of victory and defeat. *Molecular Plant Pathology, 2*(6), 355-364.

Lauguico, S. C., Concepcion, R. S., Alejandrino, J. D., Tobias, R. R., Macasaet, D. D., & Dadios, E. P. (2020). A comparative analysis of machine learning algorithms modeled from machine vision-based lettuce growth stage classification in smart aquaponics. *Int. J. Environ. Sci. Dev, 11*(9), 442-449.

Ma, Z. Y., Wen, J., Ickert-Bond, S. M., Chen, L. Q., & Liu, X. Q. (2016). Morphology, structure, and ontogeny of trichomes of the grape genus (Vitis, Vitaceae). *Frontiers in Plant Science, 7*, 704.

Mahesh, B. (2020). Machine learning algorithms-a review. *International Journal of Science and Research (IJSR). [Internet], 9*, 381-386.

Mahlein, A. K., Kuska, M. T., Thomas, S., Wahabzada, M., Behmann, J., Rascher, U., & Kersting, K. (2019). Quantitative and qualitative phenotyping of disease resistance of crops by hyperspectral sensors: seamless interlocking of phytopathology, sensors, and machine learning is needed!. *Current opinion in plant biology, 50*, 156-162.

Malacarne, G., Vrhovsek, U., Zulini, L., Cestaro, A., Stefanini, M., Mattivi, F., ... & Moser, C. (2011). Resistance to Plasmopara viticolain a grapevine segregating population is associated with stilbenoid accumulation and with specific host transcriptional responses. *BMC plant biology, 11*(1), 1-13.

Marguerit, E., Boury, C., Manicki, A., Donnart, M., Butterlin, G., Némorin, A., ... & Decroocq, S. (2009). Genetic dissection of sex determinism, inflorescence morphology and downy mildew resistance in grapevine. *Theoretical and Applied Genetics, 118(7)*, 1261-1278.

Marie Juraschek, L., Matera, C., Steiner, U., & Oerke, E. C. (2022). Pathogenesis of Plasmopara viticola depending on resistance mediated by Rpv3_1, and Rpv10 and Rpv3_3, and by the vitality of leaf tissue. *Phytopathology®, 112*(7), 1486-1499.

Marinho, M.d., Diogo, B.S., Lage, O.M. (2020). Ecotoxicological evaluation of fungicides used in viticulture in non-target organisms. *Environ Sci Pollut Res 27*, 43958–43969

Marone Fassolo, E., Lecchi, B., Marcianò, D., Maddalena, G., & Toffolatti, S. L. (2022). Pathogen Adaptation to American (Rpv3-1) and Eurasian (Rpv29) Grapevine Loci Conferring Resistance to Downy Mildew. *Plants, 11*(19), 2619.

Maul, E. (2021). *Vitis international variety catalogue*: www.vivc.de. Date accessed: accessed, (01/2021)

McGeoch, M. A., Butchart, S. H., Spear, D., Marais, E., Kleynhans, E. J., Symes, A., ... & Hoffmann, M. (2010). Global indicators of biological invasion: species numbers, biodiversity impact and policy responses. *Diversity and Distributions, 16*(1), 95-108.

McGovern, P. E. (2003). Ancient Wine: The Search for the origins of viniculture. *Princeton Univ Press, Princeton*. 363 ff. ISBN 0-691-07080-6.

McHale, L., Tan, X., Koehl, P., & Michelmore, R. W. (2006). Plant NBS-LRR proteins: adaptable guards. *Genome biology, 7*(4), 1-11.

McKinney, M. L., & Lockwood, J. L. (1999). Biotic homogenization: a few winners replacing many losers in the next mass extinction. *Trends in ecology & evolution, 14*(11), 450-453.

Meénard, R., Alban, S., de Ruffray, P., Jamois, F., Franz, G., Fritig, B., ... & Kauffmann, S. (2004). β-1, 3 glucan sulfate, but not β-1, 3 glucan, induces the salicylic acid signaling pathway in tobacco and Arabidopsis. *The Plant Cell, 16*(11), 3020-3032.

Mendgen, K., & Hahn, M. (2002). Plant infection and the establishment of fungal biotrophy. *Trends in plant science, 7*(8), 352-356.

Mercati, F., De Lorenzis, G., Brancadoro, L., Lupini, A., Abenavoli, M. R., Barbagallo, M. G., ... & Sunseri, F. (2016). High-throughput 18K SNP array to assess genetic variability of the main grapevine cultivars from Sicily. *Tree Genetics & Genomes, 12*(3), 1-15.

Meyerson, L. A., & Mooney, H. A. (2007). Invasive alien species in an era of globalization. *Frontiers in Ecology and the Environment, 5*(4), 199-208.

Mindrinos, M., Katagiri, F., Yu, G. L., & Ausubel, F. M. (1994). The A. thaliana disease resistance gene RPS2 encodes a protein containing a nucleotide-binding site and leucine-rich repeats. *Cell, 78*(6), 1089-1099.

Modesto, L. R., Welter, L. J., Steiner, D. R. M., Stefen, D., Dias, A. H., Dalbo, M. A., ... & da Silva, A. L. (2022). Phenotyping strategies for Elsinöe ampelina symptoms in grapevine (Vitis spp.). *Journal of Phytopathology, 170*(10), 746-752.

Mohimont, L., Alin, F., Rondeau, M., Gaveau, N., & Steffenel, L. A. (2022). Computer Vision and Deep Learning for Precision Viticulture. *Agronomy, 12*(10), 2463.

Moore, M. O. (1991). Classification and systematics of eastern North American Vitis L.(Vitaceae) north of Mexico. *Sida, contributions to botany*, 339-367.

Moreira, F. M., Madini, A., Marino, R., Zulini, L., Stefanini, M., Velasco, R., ... & Grando, M. S. (2011). Genetic linkage maps of two interspecific grape crosses (*Vitis spp*.) used to localize quantitative trait loci for downy mildew resistance. *Tree Genetics & Genomes*, *7*(1), 153-167.

Moriondo, M., Orlandini, S., Giuntoli, A., & Bindi, M. (2005). The effect of downy and powdery mildew on grapevine (Vitis vinifera L.) leaf gas exchange. *Journal of Phytopathology*, *153*(6), 350-357.

Mullins, M. G., Bouquet, A., & Williams, L. E. (1992). *Biology of the grapevine.* Cambridge University Press.

Müllner, S. (2021). *Zytologische und molekulare Studien zum Resistenzlocus Rpv12 gegen den Falschen Mehltau der Rebe (Plasmopara viticola)* (Doctoral dissertation, Dissertation, Karlsruhe, Karlsruher Institut für Technologie (KIT), 2021).

Mur, L. A., Kenton, P., Lloyd, A. J., Ougham, H., & Prats, E. (2008). The hypersensitive response; the centenary is upon us but how much do we know?. *Journal of experimental Botany*, *59*(3), 501-520.

Mutka, A. M., & Bart, R. S. (2015). Image-based phenotyping of plant disease symptoms. *Frontiers in plant science*, *5*, 734.

Myles, S., Boyko, A. R., Owens, C. L., Brown, P. J., Grassi, F., Aradhya, M. K., ... & Buckler, E. S. (2011). Genetic structure and domestication history of the grape. *Proceedings of the National Academy of Sciences*, *108*(9), 3530-3535.

Nadeem, M. A., Nawaz, M. A., Shahid, M. Q., Doğan, Y., Comertpay, G., Yıldız, M., ... & Baloch, F. S. (2018). DNA molecular markers in plant breeding: current status and recent advancements in genomic selection and genome editing. *Biotechnology & Biotechnological Equipment*, *32*(2), 261-285.

Nasiri, A., Taheri-Garavand, A., Fanourakis, D., Zhang, Y. D., & Nikoloudakis, N. (2021). Automated grapevine cultivar identification via leaf imaging and deep convolutional neural networks: a proof-of-concept study employing primary iranian varieties. *Plants*, *10*(8), 1628.

Núñez, D. R., & Walker, M. J. (1989). A review of palaeobotanical findings of early Vitis in the Mediterranean and of the origins of cultivated grape-vines, with special reference to new pointers to prehistoric exploitation in the western Mediterranean. *Review of Palaeobotany and Palynology*, *61*(3-4), 205-237.

Negus, K. L., Chen, L. L., Fresnedo-Ramírez, J., Scott, H. A., Sacks, G. L., Cadle-Davidson, L., & Hwang, C. F. (2021). Identification of QTLs for berry acid and tannin in a Vitis aestivalis-derived 'Norton'-based population. *Fruit Research*, *1*(1), 1-11.

Niazian, M., & Niedbała, G. (2020). Machine learning for plant breeding and biotechnology. *Agriculture, 10*(10), 436.

Nicholas, P., Magarey, P., & Wachtel, M. (1994). *Grape Production Series number 1: Diseases and pests.*

Nishad, R., Ahmed, T., Rahman, V. J., & Kareem, A. (2020). Modulation of plant defense system in response to microbial interactions. *Frontiers in Microbiology, 11*, 1298.

Nürnberger, T., & Kemmerling, B. (2009). Pathogen-associated molecular patterns (PAMP) and PAMP-triggered immunity. *Annu. Plant Rev, 34*, 16-47.

Ochssner, I., Hausmann, L., & Töpfer, R. (2016). Rpv14, a new genetic source for Plasmopara viticola resistance conferred by *Vitis cinerea*. *Vitis, 55*(2), 79-81.

Oerke, E. C., Herzog, K., & Toepfer, R. (2016). Hyperspectral phenotyping of the reaction of grapevine genotypes to Plasmopara viticola. *Journal of Experimental Botany, 67*(18), 5529-5543.

OIV. (2009). OIV descriptor list for grape varieties and Vitis species. *Organisation Internationale de la Vigne et du Vin*, Paris, France.

OIV. (2020). OIV descriptor list for grape varieties and Vitis species. *Organisation Internationale de la Vigne et du Vin*, Paris, France.

OIV. (2021). OIV descriptor list for grape varieties and Vitis species. *Organisation Internationale de la Vigne et du Vin*, Paris, France.

OIV. (2022). OIV descriptor list for grape varieties and Vitis species. *Organisation Internationale de la Vigne et du Vin*, Paris, France.

Okamoto, G., Ueki, K., Ichi, T., Aoki, H., Fujiwara, M., & Hirano, K. (2002). Juice constituents and skin pigments in Vitis coignetiae Pulliat grapevines. *Vitis, 41*(3), 161-162.

Olien, W. C. (1990). The muscadine grape: botany, viticulture, history, and current industry. *HortScience, 25*(7), 732-739.

Ollat, N., & Gaudillere, J. P. (1998). The effect of limiting leaf area during stage I of berry growth on development and composition of berries of Vitis vinifera L. cv. Cabernet Sauvignon. *American journal of enology and viticulture, 49*(3), 251-258.

Olson, J., Zou, C., Karn, A., Reisch, B., Cadle-Davidson, L., Sun, Q., & Clark, M. (2022). Genetic Analyses for Leaf Variegation in Hybrid Grape Populations (Vitis spp.) Reveals Two Loci, Lvar1 and Lvar2. *HortScience, 57*(11), 1416-1423.

Oort, A. J. P. (1944). Onderzoekingen over stuifbrand. *Tijdschrift over plantenziekten, 50*(4), 73-106.

Ordish, G. (1972). *The great wine blight*.

Paris, F., Krzyżaniak, Y., Gauvrit, C., Jamois, F., Domergue, F., Joubès, J., ... & Trouvelot, S. (2016). An ethoxylated surfactant enhances the penetration of the sulfated laminarin through leaf cuticle and stomata, leading to increased induced resistance against grapevine

downy mildew. Physiologia plantarum, 156(3), 338-350mildew. *Physiol. Plant. 156*, 338–350

Paineau, M., Mazet, I. D., Wiedemann-Merdinoglu, S., Fabre, F., & Delmotte, F. (2022). The Characterization of Pathotypes in Grapevine Downy Mildew Provides Insights into the Breakdown of Rpv3, Rpv10, and Rpv12 Factors in Grapevines. *Phytopathology®, 112*(11), 2329-2340.

Park, E. W., Seem, R. C., Gadoury, D. M., & Pearson, R. C. (1997). DMCAST: a prediction model for grape downy mildew development. *Wein-Wissenschaft, 52*(3-4), 182-189.

Park, M., Vera, D., Kambrianda, D., Gajjar, P., Cadle-Davidson, L., Tsolova, V., & El-Sharkawy, I. (2022). Chromosome-level genome sequence assembly and genome-wide association study of Muscadinia rotundifolia reveal the genetics of 12 berry-related traits. *Horticulture research*, 9.

Patel, Z. M., Mahapatra, R., & Jampala, S. S. M. (2020). Role of fungal elicitors in plant defense mechanism. *In Molecular Aspects of Plant Beneficial Microbes in Agriculture* (pp. 143-158). Academic Press.

Paterson, A. H., Lander, E. S., Hewitt, J. D., Peterson, S., Lincoln, S. E., & Tanksley, S. D. (1988). Resolution of quantitative traits into Mendelian factors by using a complete linkage map of restriction fragment length polymorphisms. *Nature, 335*(6192), 721-726.

Pedneault, K., & Provost, C. (2016). Fungus resistant grape varieties as a suitable alternative for organic wine production: Benefits, limits, and challenges. *Scientia Horticulturae, 208*, 57-77.

Pei, M. S., Liu, H. N., Wei, T. L., Yu, Y. H., & Guo, D. L. (2021). Detection and characterization of genome-wide genetic variation associated with the early-ripening phenotype of grape mutants. *Scientia Horticulturae, 285*, 110195.

Peressotti, E., Wiedemann-Merdinoglu, S., Delmotte, F., Bellin, D., Di Gaspero, G., Testolin, R., ... & Mestre, P. (2010). Breakdown of resistance to grapevine downy mildew upon limited deployment of a resistant variety. *BMC Plant Biology, 10*(1), 1-11.

Polesani, M., Bortesi, L., Ferrarini, A., Zamboni, A., Fasoli, M., Zadra, C., ... & Polverari, A. (2010). General and species-specific transcriptional responses to downy mildew infection in a susceptible (*Vitis vinifera*) and a resistant (*V. riparia*) grapevine species. *BMC genomics, 11*(1), 1-16.

Possamai, T., & Wiedemann-Merdinoglu, S. (2022). Phenotyping for QTL identification: A case study of resistance to Plasmopara viticola and Erysiphe necator in grapevine. *Frontiers in plant science, 13*, 930954.

Possamai, T., Migliaro, D., Gardiman, M., Velasco, R., and De Nardi, B. (2020). Rpv mediated defense responses in grapevine offspring resistant to Plasmopara viticola. *Plants, 9*, 1–10.

Pound, M. P., Atkinson, J. A., Townsend, A. J., Wilson, M. H., Griffiths, M., Jackson, A. S., ... & French, A. P. (2017). Deep machine learning provides state-of-the-art performance in image-based plant phenotyping. *Gigascience*, *6*(10), gix083.

Pruitt, R. N., Locci, F., Wanke, F., Zhang, L., Saile, S. C., Joe, A., ... & Nürnberger, T. (2021). The EDS1–PAD4–ADR1 node mediates Arabidopsis pattern-triggered immunity. *Nature*, *598*(7881), 495-499.

Qi, Y., Tsuda, K., Glazebrook, J., & Katagiri, F. (2011). Physical association of pattern-triggered immunity (PTI) and effector-triggered immunity (ETI) immune receptors in Arabidopsis. *Molecular plant pathology*, *12*(7), 702-708.

Qiao, F., Chang, X. L., & Nick, P. (2010). The cytoskeleton enhances gene expression in the response to the Harpin elicitor in grapevine. *Journal of Experimental Botany*, *61*(14), 4021-4031.

Raaymakers, T. M., & Van den Ackerveken, G. (2016). Extracellular recognition of oomycetes during biotrophic infection of plants. *Frontiers in Plant Science*, *7*, 906.

Rawat, W., & Wang, Z. (2017). Deep convolutional neural networks for image classification: A comprehensive review. *Neural computation*, *29*(9), 2352-2449.

Ren, A., Jiang, D., Kang, M., Wu, J., Xiao, F., Hou, P., & Fu, X. (2022). Evaluation of an intelligent artificial climate chamber for high-throughput crop phenotyping in wheat. *Plant Methods*, *18*(1), 1-15.

Ren, H. & Wen, J. (2007). *VITIS* Linnaeus, p. 210–222. In: H. Peng (ed.). *Flora of China (English edition)*. Science Press, Beijing, China

Reshef, N., Karn, A., Manns, D. C., Mansfield, A. K., Cadle-Davidson, L., Reisch, B., & Sacks, G. L. (2022). Stable QTL for malate levels in ripe fruit and their transferability across *Vitis* species. *Horticulture research*, 9.

Riaz, S., Dangl, G. S., Edwards, K. J., & Meredith, C. P. (2004). A microsatellite marker-based framework linkage map of Vitis vinifera L. *Theoretical and Applied Genetics*, *108*, 864-872.

Riaz, S., Krivanek, A. F., Xu, K., & Walker, M. A. (2006). Refined mapping of the Pierce's disease resistance locus, PdR1, and Sex on an extended genetic map of *Vitis rupestris*× *V. arizonica*. *Theoretical and Applied Genetics*, *113*(7), 1317-1329.

Richter, B. (2022). *Piwis im porträt*: PIWIS Anbaueignung, Rebsortenmerkmale und Geschmacksprofile, ausgewählter weißer PIWI-Rebsorten. D*er Deutsche Weinbau 10/2022*. https://piwi-international.org/

Rist, F., Herzog, K., Mack, J., Richter, R., Steinhage, V., & Töpfer, R. (2018). High-precision phenotyping of grape bunch architecture using fast 3D sensor and automation. *Sensors*, *18*(3), 763.

Rist, F., Schwander, F., Richter, R., Mack, J., Schwandner, A., Hausmann, L., ... & Herzog, K. (2022). Relieving the Phenotyping Bottleneck for Grape Bunch Architecture in Grapevine Breeding Research: Implementation of a 3D-Based Phenotyping Approach for Quantitative Trait Locus Mapping. *Horticulturae, 8*(10), 907.

Rivas, S. (2012). Nuclear dynamics during plant innate immunity. *Plant physiology, 158*(1), 87-94.

Robinson, S. M., & Bostock, R. M. (2015). β-glucans and eicosapolyenoic acids as MAMPs in plant–oomycete interactions: past and present. *Frontiers in plant science, 5*, 797.

Romero, M., Luo, Y., Su, B., & Fuentes, S. (2018). Vineyard water status estimation using multispectral imagery from an UAV platform and machine learning algorithms for irrigation scheduling management. *Computers and electronics in agriculture, 147*, 109-117.

Rousseau, J., Chanfreau, S., & Bontemps, É. (2013). *Les Cépages Résistants and Maladies Cryptogamiques*. Groupe ICV: Bordeaux, France, 228.

Rouzet, J., & Jacquin, D. (2003). Development of overwintering oospores of Plasmopara viticola and severity of primary foci in relation to climate. *EPPO Bulletin, 33*(3), 437-442.

Roy, B. A., Stanton, M. L., & Eppley, S. M. (1999). Effects of environmental stress on leaf hair density and consequences for selection. *Journal of Evolutionary Biology*, *12*(6), 1089-1103.

Ruyters, S., Salaets, P., Oorts, K., & Smolders, E. (2013). Copper toxicity in soils under established vineyards in Europe: a survey. *Science of the Total Environment, 443*, 470-477.

Saleem, M. H., Potgieter, J., & Arif, K. M. (2019). Plant disease detection and classification by deep learning. *Plants, 8(11),* 468.

Salinari, F., Giosue, S., Rossi, V., Tubiello, F. N., Rosenzweig, C., & Gullino, M. L. (2007). Downy mildew outbreaks on grapevine under climate change: elaboration and application of an empirical-statistical model. *EPPO bulletin, 37*(2), 317-326.

Sapkota, S., Chen, L. L., Schreiner, K., Ge, H., & Hwang, C. F. (2015). A phenotypic study of Botrytis bunch rot resistance in *Vitis aestivalis*-derived 'Norton' grape. *Tropical Plant Pathology, 40*, 279-282.

Sapkota, S., Chen, L. L., Yang, S., Hyma, K. E., Cadle-Davidson, L., & Hwang, C. F. (2019). Construction of a high-density linkage map and QTL detection of downy mildew resistance in Vitis aestivalis-derived 'Norton'. *Theoretical and applied genetics, 132*, 137-147.

Sardogan, M., Tuncer, A., & Ozen, Y. (2018, September). Plant leaf disease detection and classification based on CNN with LVQ algorithm. In *2018 3rd international conference on computer science and engineering* (UBMK) (pp. 382-385). IEEE.

Sargolzaei, M., Maddalena, G., Bitsadze, N., Maghradze, D., Bianco, P. A., Failla, O., ... & De Lorenzis, G. (2020). Rpv29, Rpv30 and Rpv31: three novel genomic loci associated with resistance to Plasmopara viticola in Vitis vinifera. *Frontiers in plant science, 11*, 562432.

Schneider, C., Onimus, C., Prado, E., Dumas, V., Wiedemann-Merdinoglu, S., Dorne, M. A., ... & Merdinoglu, D. (2018, July). INRA-ResDur: the French grapevine breeding programme for durable resistance to downy and powdery mildew. *In XII International Conference on Grapevine Breeding and Genetics 1248* (pp. 207-214).

Schramowski, P., Stammer, W., Teso, S., Brugger, A., Herbert, F., Shao, X., ... & Kersting, K. (2020). Making deep neural networks right for the right scientific reasons by interacting with their explanations. *Nature Machine Intelligence, 2*(8), 476-486.

Schwander, F., Eibach, R., Fechter, I., Hausmann, L., Zyprian, E., & Töpfer, R. (2012). Rpv10: a new locus from the Asian Vitis gene pool for pyramiding downy mildew resistance loci in grapevine. *Theoretical and Applied Genetics, 124*(1), 163-176.

Scott, K. D., Eggler, P., Seaton, G., Rossetto, M., Ablett, E. M., Lee, L. S., & Henry, R. J. (2000). Analysis of SSRs derived from grape ESTs. *Theoretical and applied genetics, 100*(5), 723-726.

Selim, M. (2013). Elicitation of grapevine defense responses against Plasmopara viticola, the causal agent of downy mildew (Dissertation). University of Giessen.

Sewak, M., Karim, M. R., & Pujari, P. (2018). Practical convolutional neural networks: implement advanced deep learning models using Python. Packt Publishing Ltd.

Shao, Z. Q., Xue, J. Y., Wang, Q., Wang, B., & Chen, J. Q. (2019). Revisiting the origin of plant NBS-LRR genes. *Trends in plant science, 24*(1), 9-12.

Sichel, V., SARAH, G., Girollet, N., Laucou, V., Roux, C., BERT, P., ... & Lacombe, T. (2022). Chimeras in Merlot grapevine revealed by phased assembly.

Singh, A., Ganapathysubramanian, B., Singh, A. K., & Sarkar, S. (2016). Machine learning for high-throughput stress phenotyping in plants. *Trends in plant science, 21*(2), 110-124.

Singh, D., Wang, X., Kumar, U., Gao, L., Noor, M., Imtiaz, M., ... & Poland, J. (2019). High-throughput phenotyping enabled genetic dissection of crop lodging in wheat. *Frontiers in plant science, 10*, 394.

Singpho, N. L., & Sharma, J. G. (2021, June). Importance of Cytochrome P450 gene family from metabolite biosynthesis to stress tolerance: A review. *In IOP Conference Series: Earth and Environmental Science* (Vol. 775, No. 1, p. 012012). IOP Publishing.

Smit, S. J., Vivier, M. A., & Young, P. R. (2020). Comparative (within species) genomics of the Vitis vinifera L. terpene synthase family to explore the impact of genotypic variation using phased diploid genomes. *Frontiers in genetics, 11*, 421.

Song, S., Fu, P., & Lu, J. (2018). Downy mildew resistant QTLs in Vitis amurensis "Shuang Hong" grapevine. *Abstract Book GBG, 131*.

Sosa-Zuniga, V., Vidal Valenzuela, Á., Barba, P., Espinoza Cancino, C., Romero-Romero, J. L., & Arce-Johnson, P. (2022). Powdery mildew resistance genes in vines: An opportunity to achieve a more sustainable viticulture. *Pathogens*, *11*(6), 703.

Spring,L., & Dupraz, Ph.(2021).Die Rebenzüchtung bei Agroscope,Agroscope.

Stassen, J. H., & Van den Ackerveken, G. (2011). How do oomycete effectors interfere with plant life? *Current opinion in plant biology*, *14*(4), 407-414.

Staudt, G., & Kassemeyer, H. H. (1995). Evaluation of downy mildew resistance in various accessions of wild *Vitis* species. *Vitis*, *34(4)*, 225-228.

Steenland, K., & Boffetta, P. (2000). Lead and cancer in humans: where are we now?. *American journal of industrial medicine*, *38*(3), 295-299.

Takken, F. L., & Joosten, M. H. (2000). Plant resistance genes: their structure, function and evolution. *European Journal of Plant Pathology*, *106*(8), 699-713.

Tamm, L., Schärer, H. J., & Speiser, B. (2018a). Kupfer: Wo stehen wir heute?. *Ökologie & Landbau*, (02/18), 15-17.

Tamm, L., Speiser, B., & Niggli, U. (2018b). Reduktion von Pflanzenschutzmitteln in der Schweiz: Beitrag des Biolandbaus. *Agrarforschung Schweiz*, *9*(2), 52-59.

Tanksley, S. D. (1993). Mapping polygenes. Annual review of genetics, 27(1), 205-233.

Tardieu, F., Cabrera-Bosquet, L., Pridmore, T., & Bennett, M. (2017). Plant phenomics, from sensors to knowledge. *Current Biology*, *27*(15), R770-R783

Team, R. C. (2013). R: A language and environment for statistical computing. R Foundation for Statistical Computing, Vienna, Austria. http://www. R-project. org/.

Teh, S. L., Fresnedo-Ramírez, J., Clark, M. D., Gadoury, D. M., Sun, Q., Cadle-Davidson, L., & Luby, J. J. (2017). Genetic dissection of powdery mildew resistance in interspecific half-sib grapevine families using SNP-based maps. *Molecular Breeding*, *37*, 1-16.

This, P., Lacombe, T., & Thomas, M. R. (2006). Historical origins and genetic diversity of wine grapes. *TRENDS in Genetics*, *22*(9), 511-519.

Thomma, B. P., Nürnberger, T., & Joosten, M. H. (2011). Of PAMPs and effectors: the blurred PTI-ETI dichotomy. *The plant cell*, *23*(1), 4-15.

Töpfer, R., Hausmann, L., Harst, M., Maul, E., Zyprian, E., & Eibach, R. (2011). New horizons for grapevine breeding. *Fruit, vegetable and cereal science and biotechnology*, *5*(1), 79-100.

Töpfer, R., Maul, E., & Eibach, R. (2011a). Geschichte und Entwicklung der Rebenzüchtung auf dem Geilweilerhof. Ges. für Geschichte des Weines.

Töpfer, R., Trapp, O. (2022). A cool climate perspective on grapevine breeding: climate change and sustainability are driving forces for changing varieties in a traditional market. *Theor Appl Genet 135*, 3947–3960

Trouvelot, S., Varnier, A. L., Allegre, M., Mercier, L., Baillieul, F., Arnould, C., ... & Daire, X. (2008). A β-1, 3 glucan sulfate induces resistance in grapevine against Plasmopara viticola through priming of defense responses, including HR-like cell death. *Molecular plant-microbe interactions, 21*(2), 232-243.

Tsuda, K., & Katagiri, F. (2010). Comparing signaling mechanisms engaged in pattern-triggered and effector-triggered immunity. *Current opinion in plant biology, 13*(4), 459-465.

Tugrul, B., Elfatimi, E., & Eryigit, R. (2022). Convolutional neural networks in detection of plant leaf diseases: *A review. Agriculture, 12*(8), 1192.

Underhill, A., Hirsch, C., & Clark, M. (2020). Image-based phenotyping identifies quantitative trait loci for cluster compactness in grape. *Journal of the American Society for Horticultural Science, 145*(6), 363-373.

Unger, S., Büche, C., Boso, S., & Kassemeyer, H. H. (2007). The course of colonization of two different Vitis genotypes by Plasmopara viticola indicates compatible and incompatible host-pathogen interactions. *Phytopathology, 97*(7), 780-786.

van der Heijden, G., Song, Y., Horgan, G., Polder, G., Dieleman, A., Bink, M., ... & Glasbey, C. (2012). SPICY: towards automated phenotyping of large pepper plants in the greenhouse. *Functional Plant Biology, 39*(11), 870-877.

van der Hoorn, R. A., & Kamoun, S. (2008). From guard to decoy: a new model for perception of plant pathogen effectors. *The Plant Cell, 20*(8), 2009-2017.

van Dijk, A. D. J., Kootstra, G., Kruijer, W., & de Ridder, D. (2021). Machine learning in plant science and plant breeding. *Iscience, 24*(1), 101890.

van Es, S. W., van der Auweraert, E. B., Silveira, S. R., Angenent, G. C., van Dijk, A. D., & Immink, R. G. (2019). Comprehensive phenotyping reveals interactions and functions of Arabidopsis thaliana TCP genes in yield determination. *The Plant Journal, 99*(2), 316-328.

Van Heerden, C. J., Burger, P., Vermeulen, A., and Prins, R. (2014). Detection of downy and powdery mildew resistance QTL in a 'Regent' × 'RedGlobe' population. *Euphytica 200,* 281–295.

Van Ooijen, J. W. (2004). MapQTL® 5, Software for the mapping of quantitative trait loci in experimental populations. Kyazma BV, Wageningen, 63.

Vavilov, N. I. (1930). Wild progenitors of the fruit trees of Turkistan and the Caucasus and the problem of the origin of fruit trees. Report. and Proc. *9th Int. Hort. Congr.*, 271-86.

Velasco, R., Zharkikh, A., Troggio, M., Cartwright, D. A., Cestaro, A., Pruss, D., ... & Viola, R. (2007). A high quality draft consensus sequence of the genome of a heterozygous grapevine variety. *PloS one, 2*(12), e1326.

Velasquez-Camacho, L., Otero, M., Basile, B., Pijuan, J., & Corrado, G. (2022). Current Trends and Perspectives on Predictive Models for Mildew Diseases in Vineyards. *Microorganisms, 11*(1), 73.

Velt, A., Frommer, B., Blanc, S., Holtgräwe, D., Duchêne, È., Dumas, V., ... & Rustenholz, C. (2022). An improved reference of the grapevine genome supports reasserting the origin of the PN40024 highly-homozygous genotype. *bioRxiv, 2022-12*

Venuti, S., Copetti, D., Foria, S., Falginella, L., Hoffmann, S., Bellin, D., ... & Di Gaspero, G. (2013). Historical introgression of the downy mildew resistance gene Rpv12 from the Asian species Vitis amurensis into grapevine varieties. *Plos one, 8*(4), e61228.

Vervalle, J. A., Costantini, L., Lorenzi, S., Pindo, M., Mora, R., Bolognesi, G., ... & Bellin, D. (2022). A high-density integrated map for grapevine based on three mapping populations genotyped by the Vitis18K SNP chip. *Theoretical and Applied Genetics, 135*(12), 4371-4390.

Véstias, M. P. (2019). A survey of convolutional neural networks on edge with reconfigurable computing. *Algorithms, 12*(8), 154.

Vezzulli, S., Vecchione, A., Stefanini, M., & Zulini, L. (2018). Downy mildew resistance evaluation in 28 grapevine hybrids promising for breeding programs in Trentino region (Italy). *European journal of plant pathology, 150*(2), 485-495.

Vezzulli, S., Gramaje, D., Tello, J., Gambino, G., Bettinelli, P., Pirrello, C., ... & Reisch, B. I. (2022). Genomic designing for biotic stress resistant grapevine. *In Genomic designing for biotic stress resistant fruit crops* (pp. 87-255). Cham: Springer International Publishing.

Vieira, M. L. C., Santini, L., Diniz, A. L., & Munhoz, C. D. F. (2016). Microsatellite markers: what they mean and why they are so useful. Genetics and molecular biology, 39, 312-328.

Virlet, N., Sabermanesh, K., Sadeghi-Tehran, P., & Hawkesford, M. J. (2016). Field Scanalyzer: An automated robotic field phenotyping platform for detailed crop monitoring. *Functional Plant Biology, 44*(1), 143-153.

Wagner, G. J., Wang, E., & Shepherd, R. (2004). New approaches for studying and exploiting an old protuberance, the plant trichome. *Annals of botany, 93*(1), 3.

Walker, C. A., & van West, P. (2007). Zoospore development in the oomycetes. *Fungal biology reviews, 21*(1), 10-18.

Walker, M. A., Lider, L. A., Goheen, A. C., & Olmo, H. P. (1991). VR 039-16 grape rootstock. *HortScience, 26*(9), 1224-1225.

Wan, D., Li, R., Zou, B., Zhang, X., Cong, J., Wang, R., ... & Li, G. (2012). Calmodulin-binding protein CBP60g is a positive regulator of both disease resistance and drought tolerance in Arabidopsis. *Plant cell reports, 31*(7), 1269-1281.

Wan, W. L., Fröhlich, K., Pruitt, R. N., Nürnberger, T., & Zhang, L. (2019). Plant cell surface immune receptor complex signaling. *Current opinion in plant biology, 50*, 18-28.

Wan, Y., Schwaninger, H. R., Baldo, A. M., Labate, J. A., Zhong, G. Y., & Simon, C. J. (2013). A phylogenetic analysis of the grape genus (*Vitis L.*) reveals broad reticulation and

concurrent diversification during neogene and quaternary climate change. *BMC evolutionary biology, 13*(1), 1-20.

Wan, Y., Schwaninger, H., Li, D., Simon, C. J., Wang, Y., & Zhang, C. (2008). A review of taxonomic research on Chinese wild grapes. *Vitis, 47*(2), 81-88.

Wang, F., Rao, Y., Luo, Q., Jin, X., Jiang, Z., Zhang, W., & Li, S. (2022). Practical cucumber leaf disease recognition using improved Swin Transformer and small sample size. *Computers and Electronics in Agriculture, 199*, 107163.

Wang, Y., Hao, X., Lu, Q., Wang, L., Qian, W., Li, N., ... & Yang, Y. (2018). Transcriptional analysis and histochemistry reveal that hypersensitive cell death and H2O2 have crucial roles in the resistance of tea plant (Camellia sinensis (L.) O. Kuntze) to anthracnose. *Horticulture research, 5*.

Wang, Z., & Gou, X. (2021). The First Line of Defense: Receptor-like Protein Kinase-Mediated Stomatal Immunity. *International Journal of Molecular Sciences, 23*(1), 343.

Warren, R. F., Henk, A., Mowery, P., Holub, E., & Innes, R. W. (1998). A mutation within the leucine-rich repeat domain of the Arabidopsis disease resistance gene RPS5 partially suppresses multiple bacterial and downy mildew resistance genes. *The Plant Cell, 10*(9), 1439-1452.

Weaver, R. J. (1976). *Grape growing*. John Wiley & Sons.

Welter, L. J., Göktürk-Baydar, N., Akkurt, M., Maul, E., Eibach, R., Töpfer, R., & Zyprian, E. M. (2007). Genetic mapping and localization of quantitative trait loci affecting fungal disease resistance and leaf morphology in grapevine (*Vitis vinifera L*). *Molecular Breeding, 20*(4), 359-374.

Werker, E. (2000). Trichome diversity and development. *Advances in botanical research,31*, 1-35.

Wiedeman-Merdinoglu, S., Coste, P., Dumas, V., Haetty, S., Butterlin, G., Greif, C., & Merdinoglu, D. (2002, August). Genetic analysis of downy mildew resistance derived from Muscadinia rotundifolia. *In VIII International Conference on Grape Genetics and Breeding 603* (pp. 451-456).

Wiedemann-Merdinoglu, S., Prado, E., Coste, P., Dumas, V., Butterlin, G., Bouquet, A., & Merdinoglu, D. (2006, July). Genetic analysis of resistance to downy mildew from Muscadinia rotundifolia. *In 9th international conference on grape genetics and breeding* (Vol. 2, No. 06.07, p. 2006).

Wilcox, W. F., Gubler, W. D., & Uyemoto, J. K. (Eds.). (2015). Compendium of grape diseases, disorders, and pests (pp. 39-45). Tomball, TX: APS Press, *The American Phytopathological Society*.

Wingerter, C., Eisenmann, B., Weber, P., Dry, I., & Bogs, J. (2021). Grapevine Rpv3-, Rpv10-and Rpv12-mediated defense responses against Plasmopara viticola and the impact of their deployment on fungicide use in viticulture. *BMC Plant Biology, 21*(1), 1-17.

Xie, X., Ma, Y., Liu, B., He, J., Li, S., & Wang, H. (2020). A deep-learning-based real-time detector for grape leaf diseases using improved convolutional neural networks. *Frontiers in plant science, 11*, 751.

Xiang, J., Li, X., Wu, J., Yin, L., Zhang, Y., & Lu, J. (2016). Studying the mechanism of Plasmopara viticola RxLR effectors on suppressing plant immunity. *Frontiers in Microbiology, 7*, 709.

Xing, Z., Liu, Y., Cai, W., Huang, X., Wu, S., & Lei, Z. (2017). Efficiency of trichome-based plant defense in Phaseolus vulgaris depends on insect behavior, plant ontogeny, and structure. *Frontiers in Plant Science, 8*, 2006.

Yang, B., & Xu, Y. (2021). Applications of deep-learning approaches in horticultural research: a review. *Horticulture Research, 8*.

Yang, X., & Guo, T. (2017). Machine learning in plant disease research. March, 31, 1.

Yasrab, R., Pound, M. P., French, A. P., & Pridmore, T. P. (2020). RootNet: a convolutional neural networks for complex plant root phenotyping from high-definition datasets. *bioRxiv, 2020-05*

Yen, E. C., McCarthy, S. A., Galarza, J. A., Generalovic, T. N., Pelan, S., Nguyen, P., ... & Jiggins, C. D. (2020). A haplotype-resolved, de novo genome assembly for the wood tiger moth (Arctia plantaginis) through trio binning. *GigaScience, 9*(8), giaa088.

Yin, L., An, Y., Qu, J., Li, X., Zhang, Y., Dry, I., ... & Lu, J. (2017). Genome sequence of Plasmopara viticola and insight into the pathogenic mechanism. *Scientific Reports, 7*(1), 1-12.

Yin, L., Karn, A., Cadle-Davidson, L., Zou, C., Underhill, A., Atkins, P., ... & Clark, M. (2021). Fine mapping of leaf trichome density revealed a 747-kb region on chromosome 1 in cold-hardy hybrid wine grape populations. *Frontiers in plant science, 12*, 587640.

Yong-hua, H., Chao-luan, L., & Ya-ling, C. (1994). Comparative anatomy of vegetative organs in the genus Vitis L. and its systematic significance. *Journal of Systematics and Evolution, 32*(2), 154.

Yongjian, W. A. N. G., Junhua, K. O. N. G., Peige, F. A. N., Zhenchang, L. I. A. N. G., Xiuliang, J. I. N., Buchun, L. I. U., & Zhanwu, D. A. I. (2022). Grape Phenome High-throughput Acquisition and Analysis Methods: A Review. *Acta Horticulturae Sinica, 49*(8), 1815.

Zänker, K. S. (2008). General introduction to innate immunity: Dr. Jekyl/Mr. Hyde quality of the innate immune system. *Trends in Innate Immunity, 15*, 12-20.

Zendler, D. (2018). Die *Erysiphe necator* Resistenzen *Ren3* und *Ren9* aus 'Regent'–Eingrenzung, Analyse von Kandidatengenen und differentielle Genregulation (Doctoral dissertation,

Dissertation, Karlsruhe, Deutschland, KIT-Fakultät für Chemie und Biowissenschaften des Karlsruher Instituts für Technologie (KIT), 2018).

Zendler, D., Malagol, N., Schwandner, A., Töpfer, R., Hausmann, L., & Zyprian, E. (2021). High-throughput phenotyping of leaf discs infected with grapevine downy mildew using shallow convolutional neural networks. *Agronomy, 11(9),* 1768.

Zhang, J., Hausmann, L., Eibach, R., Welter, L. J., Töpfer, R., & Zyprian, E. M. (2009). A framework map from grapevine V3125 (Vitis vinifera 'Schiava grossa'×'Riesling') × rootstock cultivar 'Börner'(Vitis riparia× Vitis cinerea) to localize genetic determinants of phylloxera root resistance. *Theoretical and applied genetics, 119*(6), 1039-1051.

Zhang, L., Xu, Z., Xu, D., Ma, J., Chen, Y., & Fu, Z. (2020). Growth monitoring of greenhouse lettuce based on a convolutional neural network. *Horticulture research, 7*.

Zhang, S., Zhang, A., Wu, X., Zhu, Z., Yang, Z., Zhu, Y., & Zha, D. (2019). Transcriptome analysis revealed expression of genes related to anthocyanin biosynthesis in eggplant (Solanum melongena L.) under high-temperature stress. *BMC plant biology, 19*(1), 1-13.

Zhou, J. M., & Zhang, Y. (2020). Plant immunity: danger perception and signaling. *Cell, 181*(5), 978-989.

Zhou, Y., Massonnet, M., Sanjak, J. S., Cantu, D. & Gaut, B. S. (2017). Evolutionary genomics of grape (*Vitis vinifera ssp. vinifera*), domestication. *Proc Natl Acad Sci U S A, 114*, 11715–11720.

Zhou, Z. H. (2021). *Machine learning*. Springer Nature.

Zini, E., Dolzani, C., Stefanini, M., Gratl, V., Bettinelli, P., Nicolini, D., ... & Vezzulli, S. (2019). R-loci arrangement versus downy and powdery mildew resistance level: a *Vitis* hybrid survey. *International journal of molecular sciences, 20*(14), 3526.

Zohary, D. (2003). The domestication of the grapevine *Vitis vinifera L*. in the Near East. *In The origins and ancient history of wine* (pp. 44-51). Routledge.

Zohary, D., Hopf, M. (1994). Domestication of plants in the Old World: *the origin and spread of cultivated plants in West Asia, Europe, and the Nile Valley*. 2nd ed. (Oxford: New York: Clarendon Press).

Zou, C., Karn, A., Reisch, B., Nguyen, A., Sun, Y., Bao, Y., ... & Cadle-Davidson, L. (2020). Haplotyping the Vitis collinear core genome with rhAmpSeq improves marker transferability in a diverse genus. *Nature communications, 11*(1), 1-11.

Zyprian, E., Ochßner, I., Schwander, F., Šimon, S., Hausmann, L., Bonow-Rex, M., ... & Töpfer, R. (2016). Quantitative trait loci affecting pathogen resistance and ripening of grapevines. *Molecular Genetics and Genomics, 291*(4), 1573-1594.

Zyprian, E., Eibach, R., Trapp, O., Schwander, F., & Toepfer, R. (2018). Grapevine breeding under climate change: applicability of a molecular marker linked to veraison. *Vitis, 57*(3), 119-123.

Annex I

Table 1 Phenotypic and genotypic correlation of Downy mildew and leaf hair correlation data for the year 2020, 2021 and 2022.

	Downy mildew vs. Leaf hair correlation data (r_s)	
Year	**Phenotypic**	**Genotypic (marker)**
2020	-0.08	
2021	-0.10	0.10
2022	-0.12	

Annex II

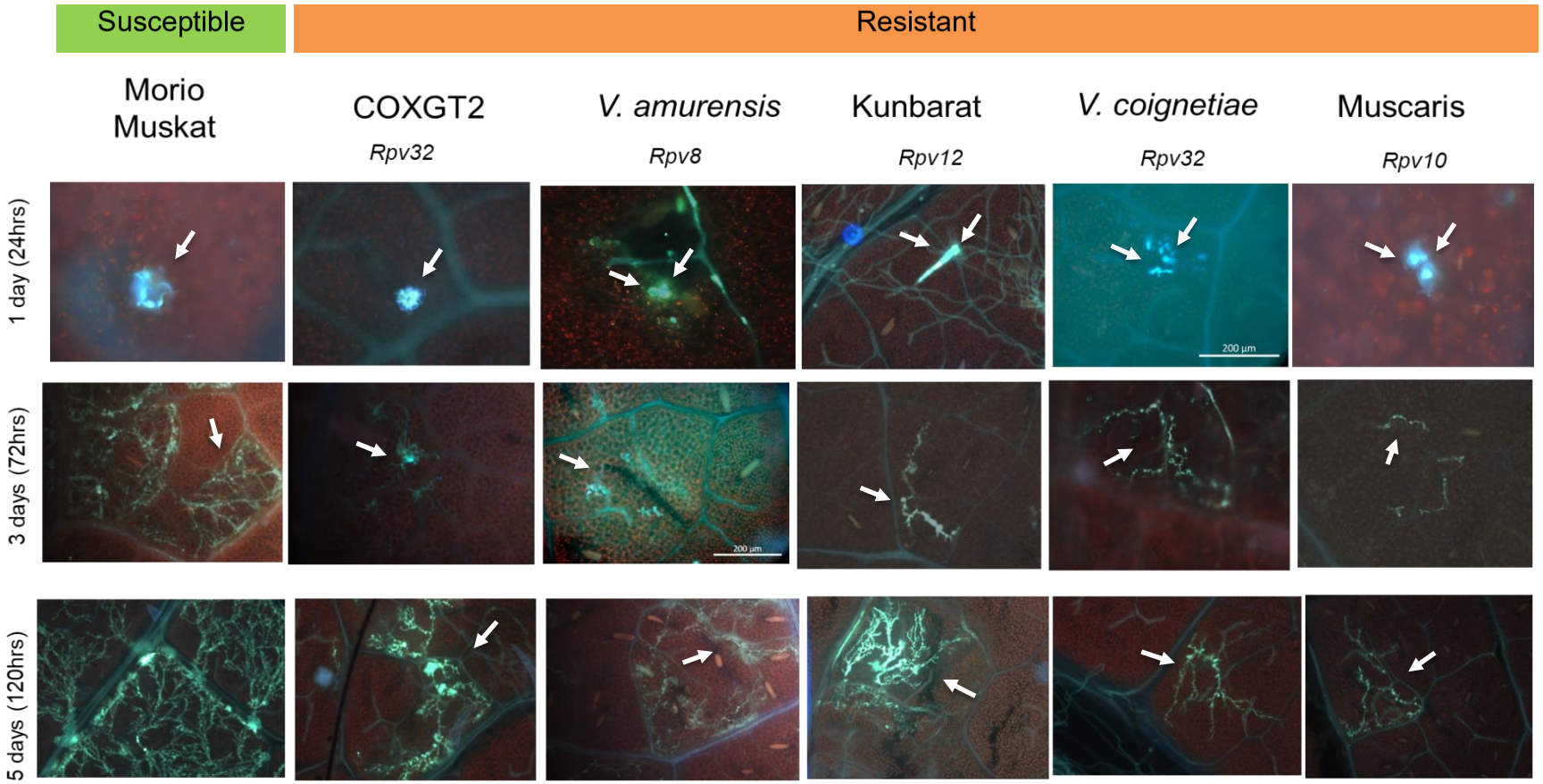

Figure 1 Comparison of intracellular *P. viticola* development on the leaf discs of susceptible ('Morio Muskat') and resistant carrying genotypes (COXGT2: *Rpv32*; *Vitis amurensis*: *Rpv8*; 'Kunbarat': *Rpv12; Vitis coignetiae*: *Rpv32*; 'Muscaris': *Rpv10*) at three different time points. White arrow indicating *P. viticola* mycelial network. Row 1: 1 day post inoculation; Row 2: 3 days post inoculation; Row 3: 5 days post inoculation. Scale bars correspond to 200 µm.

Annex III

ResNet model development: Training and performance evaluation

A slightly different approach was utilized in producing labelled input images for the training of the Residual Network-based CNN model for leaf hair quantification. Leaf disc images were divided into four equal halves, 70% for the training and 30% for testing, followed by slicing into 506 equal segments, and were manually classified into respective classes as background, leaf with hair and leaf without hair (Annex III, Figure 1). All the image slices were manually classified into three classes, background (water agar), leaf without hair, and leaf with hair using a python script 'image_sorter2'.

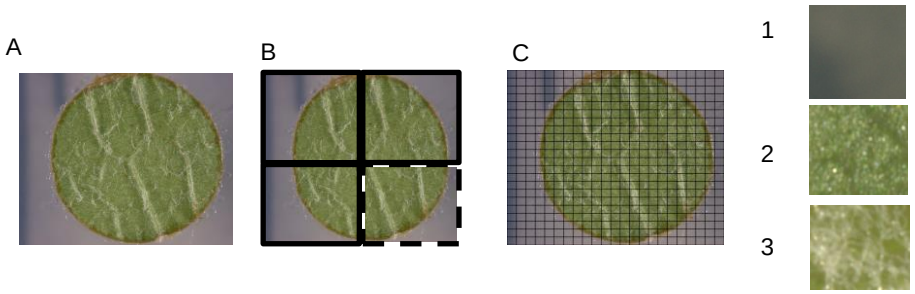

Figure 1 Leaf disc images. (A) divided into four equal halves (B), ¾ images for training (with bold borders) and ¼ (dotted border) for testing the model followed by 506 slices (C) of the leaf disc to produce individual input slices (1: Background, 2: Leaf without hair 3: leaf with hair).

In both the CNNs employed in classification workflow, a residual neural network with a structure resembling 'Xception network' was selected. The CNN1 was trained to classify between 'background' and 'leaf' with 10089 images from the training set and validated with 4323 images per class. Whereas, the CNN2 was trained to classify between 'leaf with hair' and 'leaf without hair', trained using 1872 slices and tested with 4369 slices. All the CNN calculations were performed on the GPU. All CNNs were trained using Jupyter Notebooks on Google Colaboratory Instances running Ubuntu 18.04.5 LTS, a 2-core Xeon CPU at 2.20 GHz, 13.3GB RAM, and an Nvidia Tesla K80 GPU with 12GB Memory. Each slice for CNN1 was loaded in the shape of 112 x 112 with RGB channels and followed by rescaling to scale the RGB values lying between 0 and 255 down to 0 and 1 and applied two blocks consisting of a 2D Convolution layer, a Batch

Normalization Layer, followed by an Activation Layer using ReLU. Block one compromises a 32-layer convolution, whereas block with 64-layer convolution. The residual was retained until further usage after the initial two blocks. Furthermore, four blocks with separable 2D convolutions in sizes 128, 256, 512, and 728 were added. Each block consists of a 2D Max Pooling Layer, a final 2D Convolution layer with the previous block residual as input, an Activation Layer (ReLU), a Separable 2D Convolution layer, a Batch Normalization Layer, another Activation Layer (ReLU), a Separable 2D Convolution layer, another Batch Normalization Layer, and a final 2D Convolution layer. The current values were updated with the previous outcome and reused in the following block. The Separable 2D Convolution Layer of size 1024, the Batch Normalization Layer, and the Activation Layer (ReLU) is added after the first four blocks, and the outcome was passed through a Global 2D Average Pooling Layer before being transmitted through a Dropout layer with a rate of 0.5. A deeply Connected Dense Layer with one unit in a combination of sigmoid activation was used as the output layer for CNN1 and similar architecture with a dropout rate of 0.2 were utilized for CNN2 (Annex III, Figure 2). Finally, Adam optimizer with a learning rate of 0.001 and loss calculation was done using binary_crossentropy. Both CNN's were trained for 30 epochs each (Annex IV, Figure 1). All datasets for Downy mildew quantification (https://www.github.com/Daniel-Ze/Leaf-disc-scoring) and leaf hair quantification (https://github.com/1708nagarjun/ResNet-CNN-Leaf-hair) are available as open source on the given GitHub Repository.

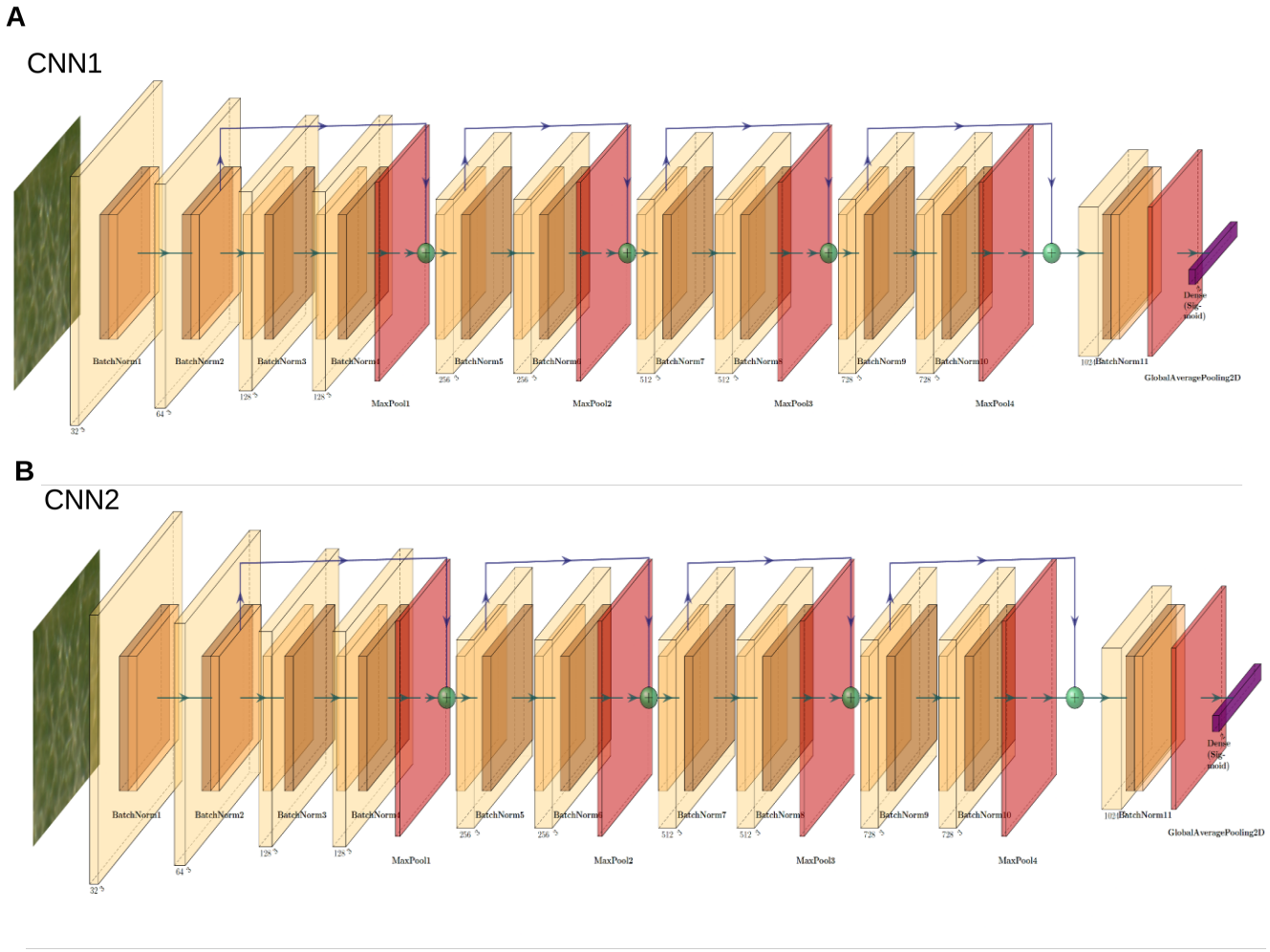

Figure 2 Above diagram is a detailed representation of two ResNet CNNs architecture compromising of different layers. Each convolution layer consists of: Batch normalization (BatchNorm), global average pooling (A 2-D global average pooling), activation layer (ReLU = rectified linear unit activation function). The fully connected layers (“Dense”) also have the ReLU activation. The Sigmoid activation function necessary for the CNNs' binary output is present in the last "Dense" "1" layer. Each "Dense" layer's number of nodes are indicated. Each red blocks indicate the residual blocks incorporated between the layers. For both the CNNs the Adam optimizer with a learning rate of 0.001 and loss calculation was done with binary_crossentrop

Annex IV

ResNet based CNN performance evaluation

Training results

The first ResNet CNN1 "background" vs. "leaf disc" considering a small margin of validation loss after 30 epochs, yielded an overall final validation accuracy of 98%. In contrast, the second ResNet CNN2, "leaf with no hair" vs. "leaf with hair" resulted in overall validation accuracy of 94.51% and a validation loss of 13%. Due to the input slices simpler feature sets than CNN2, CNN1 has a greater model validation accuracy than CNN2 (Annex IV, Figure 1). As a consequence, the CNN2 model has a little lower validation accuracy as a result of its more thorough feature complexities extraction. Although no overfitting nor under fitting of the models was found, this suggests the existence of a possible image classifier model. In general, the model has achieved satisfying overall validation accuracy.

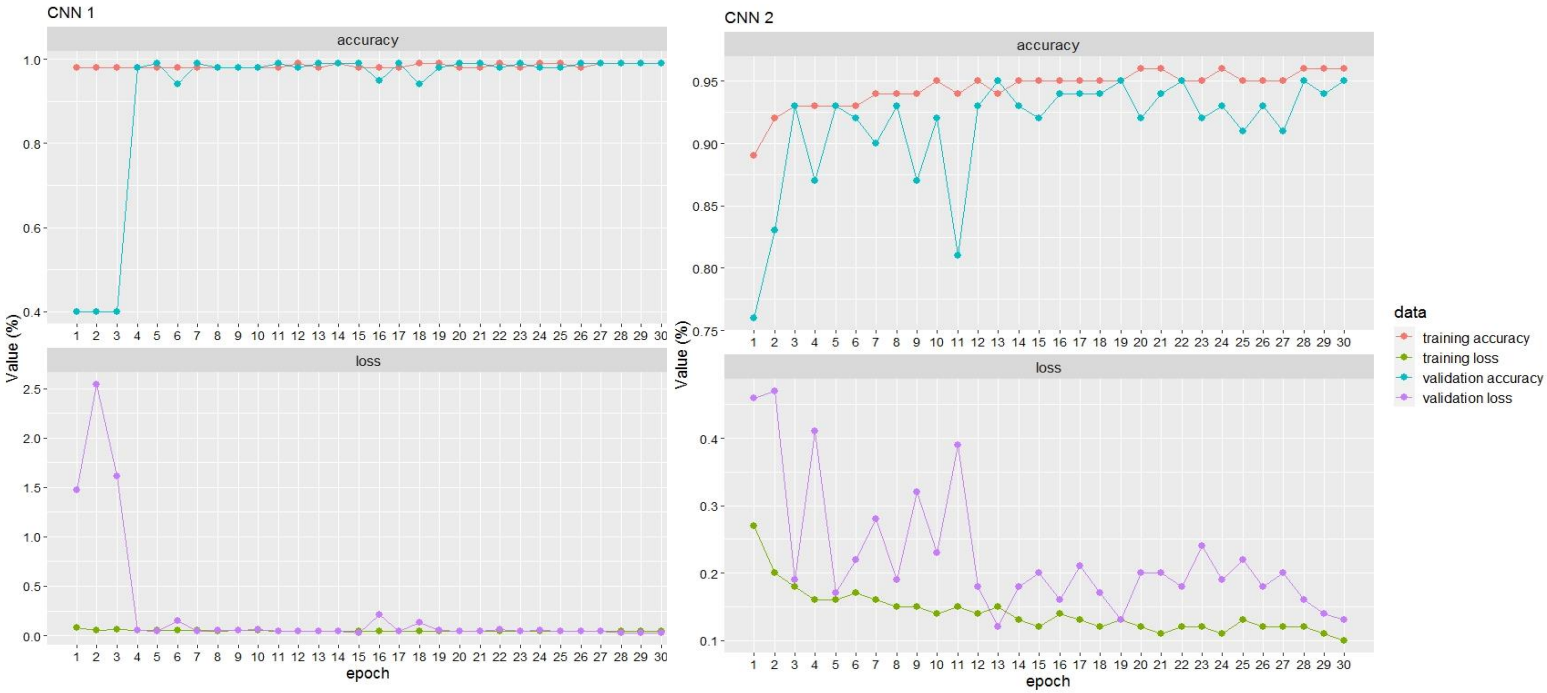

Figure 1 Training and validation accuracy, training and validation loss performances of CNN1 “background" and "leaf disc" and CNN2 "leaf with no hair" and "leaf with hair" after 30 epochs. X-axis: indicating the number of epochs and Y-axis: indicating the value (%).

Performance validation

In order to evaluate the model performance, three different model validation approaches were performed.

Expert validation

After the completion of training and testing the model, the model was employed in quantifying 20 leaf disc images (4 images per OIV class) (Annex IV, Figure 2). By categorizing the slices and manually rating the leaf discs, two experts independently evaluated the identical set of images to produce the ground truth. The expert-generated independent ground truth data are very similar between slices and manual ratings (Annex IV, Table 1). The ResNet CNN values (%) for all the leaf disc images (four for each OIV 086 class) are in excellent agreement with the ground truth data produced by two experts. Additionally, both the expert's slice (%) and ResNet CNN (%) results looked to be quite close, proving the accuracy and sensitivity of working at the slice level. However, there are some discrepancies. For instance, Image 1 of class 9 (Annex IV, Figure 2) is poorly quantified by ResNet CNN and expert 1 due to poor image characteristics, uneven illumination, and image quality. The validation showed a strong connection between expert evaluation and predictions made by the ResNet CNN model (Annex IV, Figure 3). With extremely significant R-square values of 0.98 and 0.92 and RMSE (Root Mean Square Error) values of 8.20 and 14.18, respectively, the correlation between expert slice categorization (%) for both experts and ResNet CNN (Annex IV, Figure 3A). While in contrast the correlation between manual rating (%) and ResNet CNN (%) for experts was considerably less significant, with R values of 0.86 and 0.87 with RMSE of 21.43 and 20.37, respectively (Annex IV, Figure 3B). In summary, it was determined for both experts, the correlation at the slice level categorization was more thorough, accurate, and superior to manual rating correlation. The need for an objective classification approach was demonstrated by the significant subjectivity between the Manual (%) ratings and slice (%) level categorization in both experts. Our findings also suggest that manual rating is preferable for qualitative traits. The discs covered between 70% - 90% of the leaf hair, the correlation coefficient varied most in the case of manual evaluation, impacting the total correlation. The correctness and effectiveness of the model are amply demonstrated by the classification correlation of ResNet CNN (%) and expert slice (%) for both experts (i.e., R=0.98 and R=0.92,

respectively). To precisely define statistically separating characteristics like leaf hair, it is imperative to apply objective machine vision.

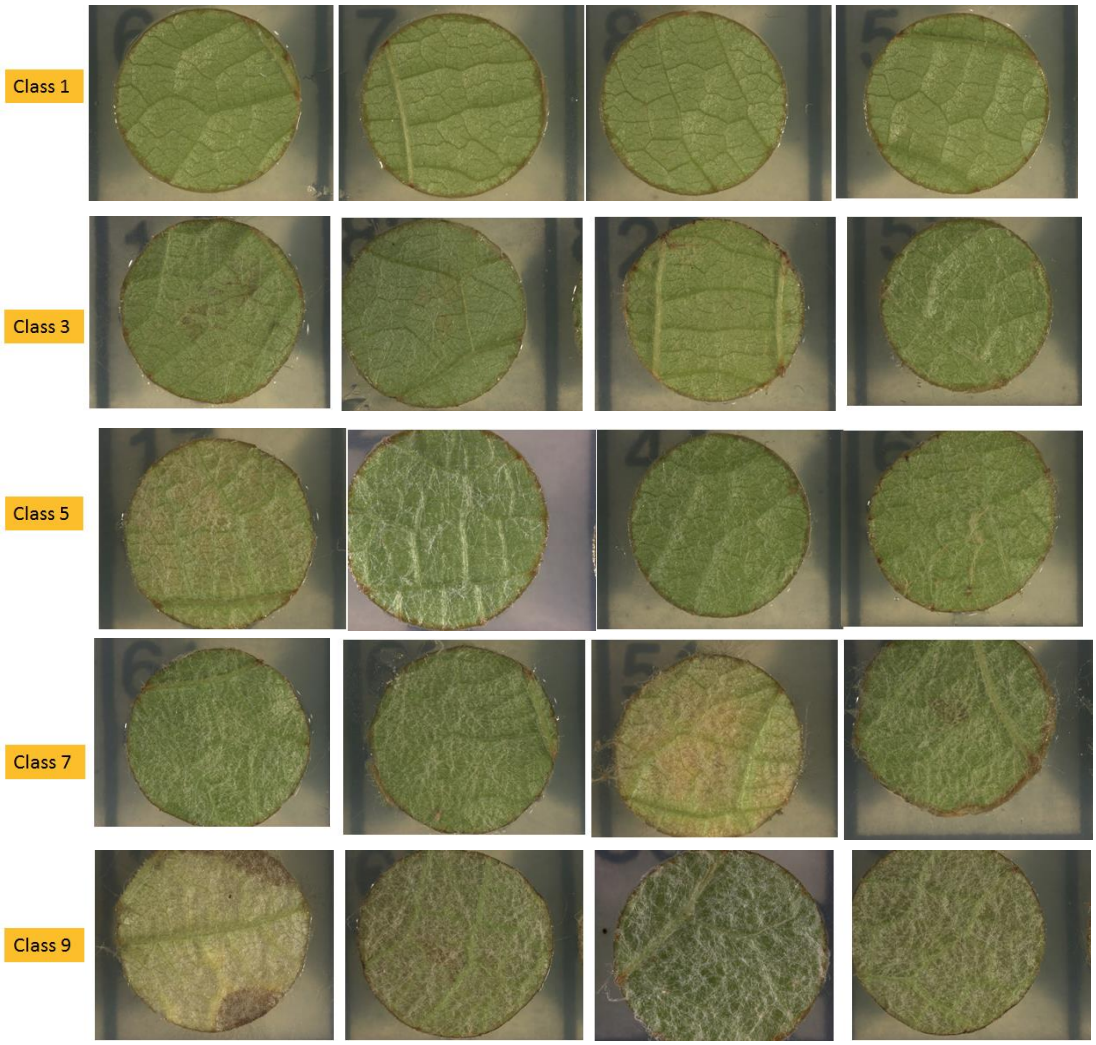

Figure 2 Leaf disc images used four per OIV-086 class for model validation (Validation 1; between ResNet CNN and two experts).

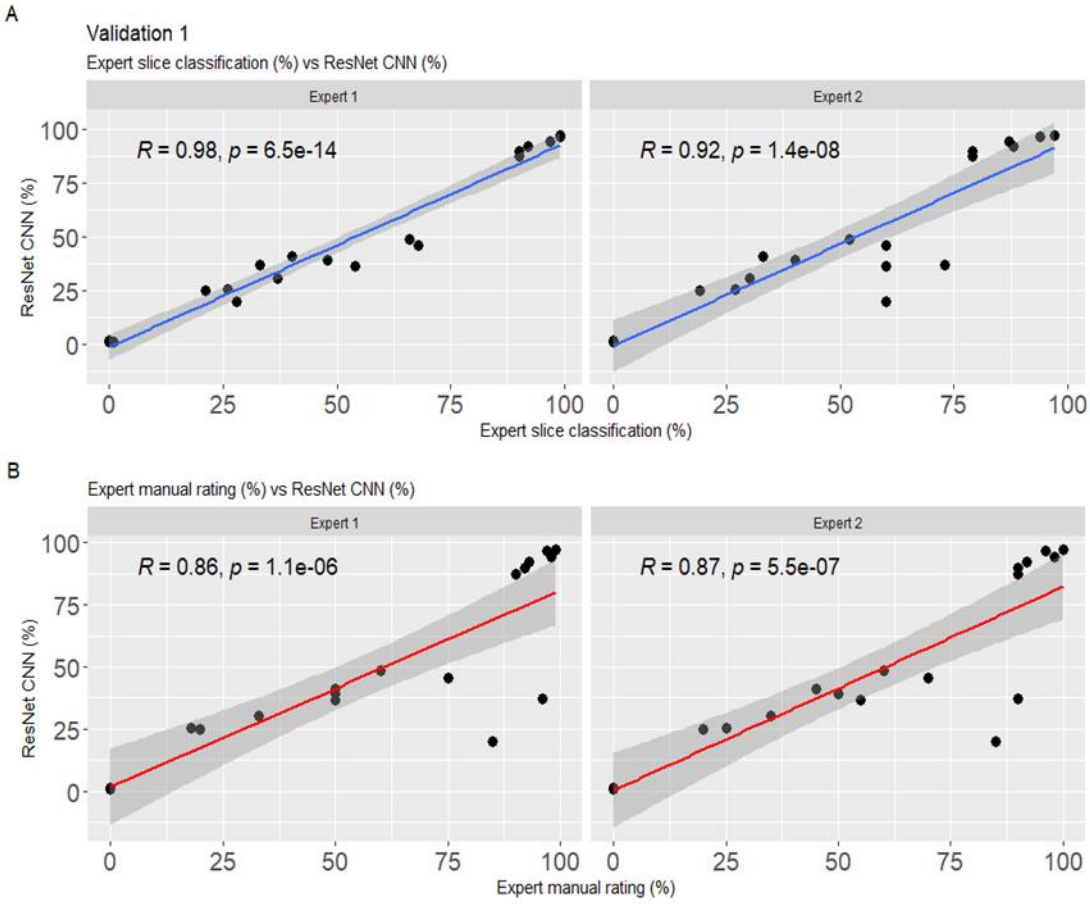

Figure 3 Validation 1: A) Correlation results between two experts slice (%) classification vs. ResNet CNN (%) evaluation and B) experts manual (%) rating vs. ResNet CNN (%) evaluation of leaf discs. ($p<0.05$).

Expert vs. non-expert validation

ResNet CNN model was employed to identify and assess the leaf hair density of three hairy genotypes (‘Pinot Meunier‘, ‘Tigvoasa‘, and *V. thunbergii*) and three non-hairy genotypes (‘Riesling‘, ‘Regent‘, and ‘Cabernet Sauvignon‘) (Annex IV, Table 2). In addition, absolute accuracy error (absolute error) was estimated for each of the subsequent individual leaf discs. A panel consisting of two experts and two non-experts and considered ResNet CNN (%) to be true values and evaluator values as the estimated values (Annex IV, Table 3, Figure 4). For the evaluated genotypes, absolute error variance was determined to be extremely low and negligible between two experts on both the slice (%) and manual (%) assessments (Annex IV, Figure 4A; B1 and B2). Experts showed improved precision, accuracy, and repeatability in the evaluations that were conducted. The absolute error on slice (%) categorization for both non-experts varied from 15% to

30%, strongly suggesting an overestimation bias. Furthermore, both non-experts underestimated the density of the leaf hair when grading it manually (%), with absolute errors ranging between -20% and -50% (Annex IV, Figure 4A; B3 and B4). Surprisingly, the three hairy genotypes were underrated, demonstrating that manual evaluation made by non-experts might include considerable bias. These results strongly suggest the necessity for an objective and accurate method to measure leaf hair density.

Audience validation

A panel compromising of 16 audience members evaluated the leaf disc images varying in hair density presented on a projector. In general, our results suggest the evaluations often overestimate the non-hairy genotypes and underestimate the hairy genotypes in the absence of a ResNet CNN classifier (Annex IV, Figure 5, Table 4). For completely non-hairy genotypes, the overall

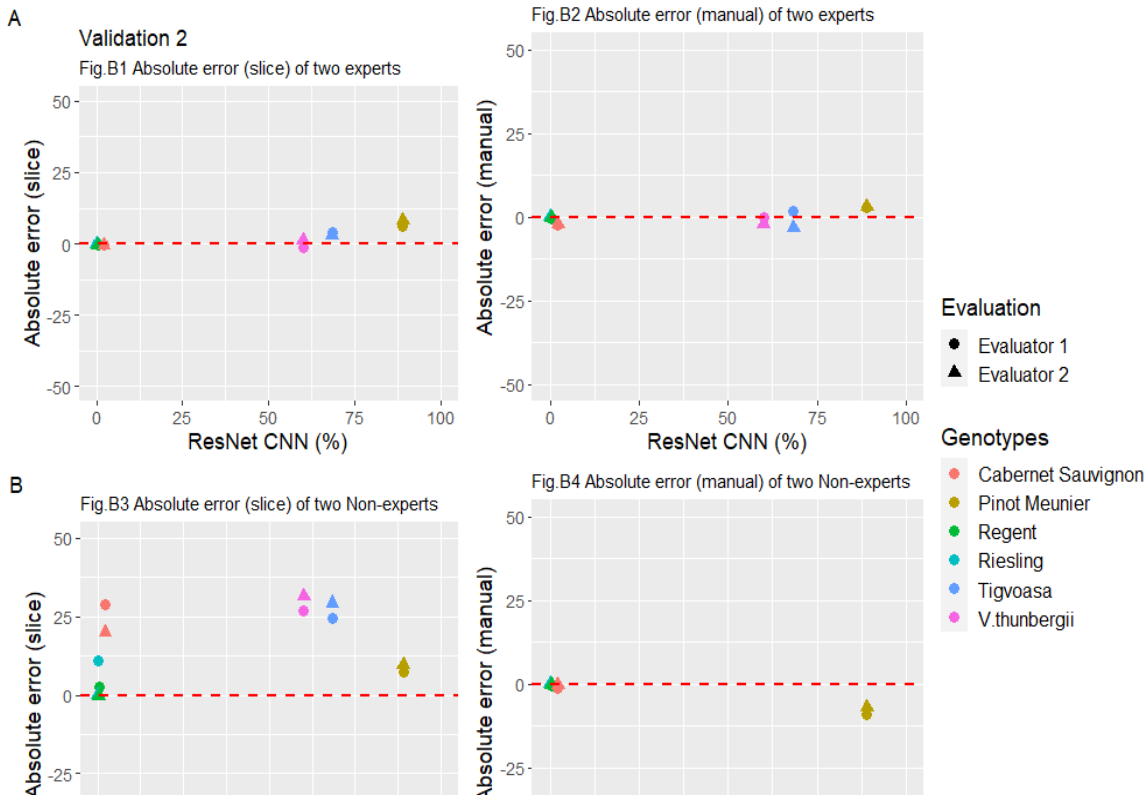

Figure 4 Validation 2: Absolute errors (actual value - estimated value) estimation. A) Comparison between two experts for (B1) slice% and (B2) manual% rating vs. B) Two non-experts for (B3) slice% and (B4) manual% rating, respectively. The red dotted ("0") line represents the no error line. Filled circles represent evaluator 1 and filled triangles represent evaluator 2. Each color indicates a single genotype.

significant bias in terms of absolute error was found to range from 0% to 30%, whereas, for hairy genotypes, it ranged between -5% to -60% (Annex IV, Table 5). Additionally, the results indicate it was difficult to rank the intermediate genotypes, *V. thunbergii* and Tigvoasa.

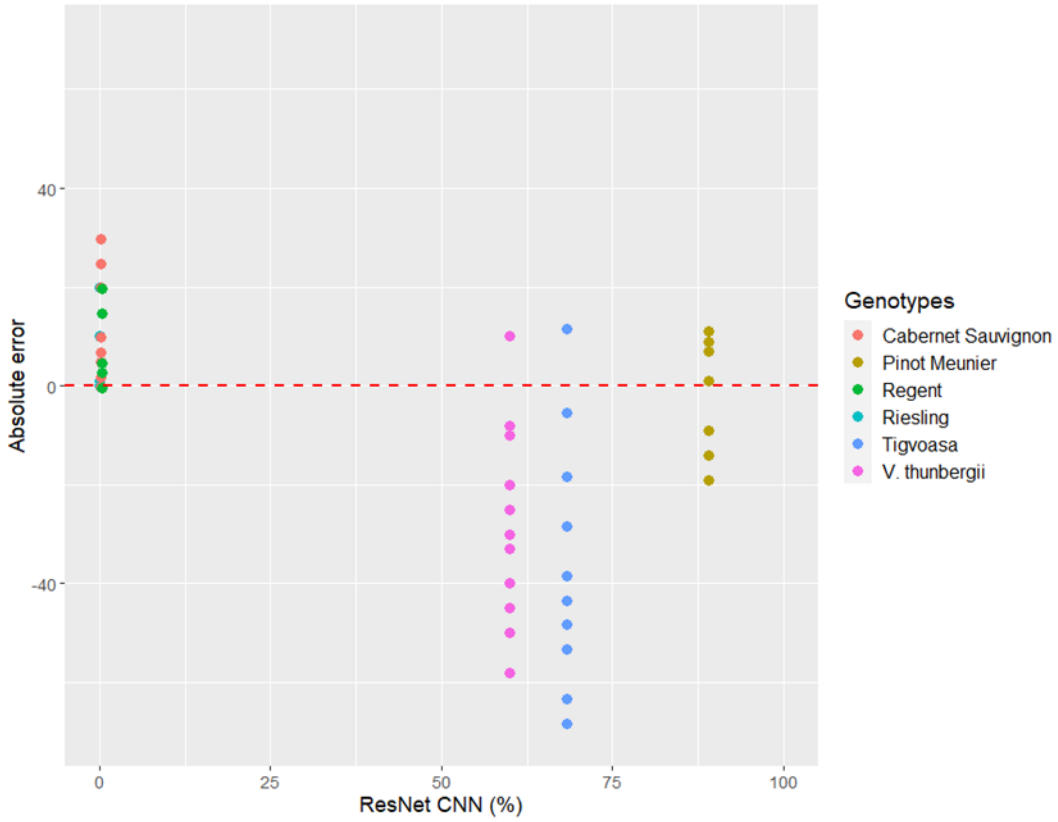

Figure 5 Validation 3: Absolute errors (actual value - estimated value) estimation of manual rating for a panel of 16 novice evaluators.

Table 1 Validation 1: Summary of ResNet CNN (%) and experts evaluation of leaf discs, four each OIV 086 class. Slice%: Slice classification ("background"/"Leaf with hair"/"Leaf without hair"). Manual%: Manual rating of leaf discs (0-100%).

	ResNet CNN (%)	**1**	**0.7**	**1.4**	**0.7**
	Expert 1 (Slice %)	0	0	0	1
Class 1	Expert 2 (Slice%)	0	0	0	0
	Expert 1 (Manual %)	0	0	0	0
	Expert 2 (Manual %)	1	0	0	0
	ResNet CNN (%)	**25.4**	**24.7**	**30.5**	**48.6**
	Expert 1 (Slice %)	26	21	37	66
Class 3	Expert 2 (Slice%)	18	20	33	60
	Expert 1 (Manual %)	27	19	30	52
	Expert 2 (Manual %)	25	20	35	60

	ResNet CNN (%)	**45.8**	**41**	**39.2**	**36.5**
	Expert 1 (Slice %)	68	40	48	54
	Expert 2 (Slice%)	75	50	50	50
	Expert 1 (Manual %)	60	33	40	60
	Expert 2 (Manual %)	70	45	50	55
Class 7	ResNet CNN (%)	**87.2**	**89.8**	**20**	**92.2**
	Expert 1 (Slice %)	90	90	28	92
	Expert 2 (Slice%)	90	92	85	93
	Expert 1 (Manual %)	79	79	60	88
	Expert 2 (Manual %)	90	90	85	92
	ResNet CNN (%)	**37**	**94.1**	**96.7**	**97.1**
	Expert 1 (Slice %)	33	97	99	99

Class 9	Expert 2 (Slice%)	96	98	97	99
	Expert 1 (Manual %)	73	87	94	97
	Expert 2 (Manual %)	90	98	96	100

Table 2 Validation 2: Summary of ResNet CNN (%) vs panel of two expert and non-expert evaluation of six genotype leaf discs. Slice%: Slice classification ("background"/"Leaf with hair"/"Leaf without hair"). Manual%: Manual rating of leaf discs (0-100%).

		Hairy genotypes			Non hairy genotypes		
		V. thunbergii	**'Tigvoasa'**	**'Pinot Meunier'**	**'Riesling'**	**'Regent'**	**'Cabernet Sauvignon'**
	ResNet CNN (%)	60.0	68,4	89	0	0.4	2.2
Evaluator 1	Expert 1 (slice %)	58.9	72.2	95	0	0	1.8
Evaluator 2	Expert 2 (Slice %)	61	71.2	97	0	0	1.5
Evaluator 1	Expert 1 (Manual %)	60	70	92	0	0	0
Evaluator 2	Expert 2 (Manual %)	58	65	92	0	0	0
Evaluator 1	Non-expert 1 (slice %)	86	93	96	11	3	31
Evaluator 2	Non-expert 2 (Slice%)	91	98	99	0	0	22
Evaluator 1	Non-expert 1 (Manual %)	10	30	80	0	0	1
Evaluator 2	Non-expert 2 (Manual %)	15	25	82	0	0	2

Table 3 Validation 3: Absolute errors (AE) calculation. ResNet CNN represents true values. AE slice represents estimated values for slice (%) classification. AE manual represents estimated values for manual rating (%). Evaluators consist of two experts and two non-experts.

Genotypes	ResNet CNN	AE Slice	AE Manual	Evaluators
V.thunbergii	60	-1.1	0	Expert 1
'Tigvoasa'	68.4	4.1	1.6	Expert 1
'Pinot Meunier'	89	6	3	Expert 1
'Riesling'	0	0	0	Expert 1
'Regent'	0.4	-0.4	-0.4	Expert 1
'Cabernet Sauvignon	2.2	-0.4	-2.2	Expert 1
V.thunbergii	60	1	-2	Expert 2
'Tigvoasa'	68.4	2.8	-3.4	Expert 2
'Pinot Meunier'	89	8	3	Expert 2
'Riesling'	0	0	0	Expert 2
'Regent'	0.4	-0.4	-0.4	Expert 2
'Cabernet Sauvignon'	2.2	-0.7	-2.2	Expert 2
V.thunbergii	60	26.7	-50	Non-expert 3
Tigvoasa	68.4	24.5	-38.4	Non-expert 3
'Pinot Meunier'	89	7.4	-9	Non-expert 3
'Riesling'	0	11	0	Non-expert 3
'Regent'	0.4	2.6	-0.4	Non-expert 3
Cabernet Sauvignon	2.2	29	-1.2	Non-expert 3

V.thunbergii	60	31.5	-45	Non-expert 4
Tigvoasa	68.4	29.3	-43.4	Non-expert 4
Pinot Meunier	89	9.5	-7	Non-expert 4
Riesling	0	0	0	Non-expert 4
Regent	0.4	-0.4	-0.4	Non-expert 4
Cabernet Sauvignon	2.2	19.8	-0.2	Non-expert 4

Table 4 Summary of audience manual rating of six genotypes. Non-hairy genotypes: Riesling, cabernet Sauvignon and Regent. Hairy genotype: Tigvoasa, Pinot Meunier and V. thunbergi.

	Riesling	**Pinot Meunier**	**Cabernet Sauvignon**	**Tigvoasa**	**Regent**	**V. thunbergii**
ResNet CNN %	0	89	2.2	68.4	0.4	60
Evaluator 1	0	80	2	15	0	20
Evaluator 2	0	100	10	80	0	50
Evaluator 3	1	70	0	20	0	10
Evaluator 4	0	70	5	25	0	15
Evaluator 5	20	80	30	50	15	70
Evaluator 6	0	100	0	30	0	10
Evaluator 7	20	100	20	0	20	50
Evaluator 8	0	96	0	63	0	52
Evaluator 9	0	75	0	5	0	2
Evaluator 10	0	80	7	20	5	27
Evaluator 11	0	80	10	20	0	40
Evaluator 12	0	90	5	40	0	20
Evaluator 13	10	90	25	50	20	35
Evaluator 14	0	80	0	40	20	30
Evaluator 15	0.5	98	5	25	3	30
Evaluator 16	0	98	0	50	0	30

Table 5 Absolute errors estimation of audience validation.

	Riesling	**Pinot Meunier**	**Cabernet Sauvignon**	**Tigvoasa**	**Regent**	**V. thunbergii**
Evaluator 1	0	-19	-0.2	-68.4	-0.4	-8
Evaluator 2	0	-19	-0.2	-63.4	-0.4	-10
Evaluator 3	0	-14	-0.2	-53.4	-0.4	-10
Evaluator 4	0	-9	-0.2	-48.4	-0.4	-20
Evaluator 5	0	-9	-0.2	-48.4	-0.4	-25
Evaluator 6	0	-9	-0.2	-48.4	-0.4	-30
Evaluator 7	0	-9	1.8	-43.4	-0.4	-30
Evaluator 8	0	-9	4.8	-43.4	-0.4	-30
Evaluator 9	0	1	4.8	-38.4	-0.4	-33
Evaluator 10	0	1	4.8	-28.4	-0.4	-40
Evaluator 11	0	7	6.8	-28.4	2.6	-40
Evaluator 12	0	9	9.8	-18.4	4.6	-45
Evaluator 13	1	9	9.8	-18.4	14.6	-50
Evaluator 14	10	11	19.8	-18.4	19.6	-50
Evaluator 15	20	11	24.8	-5.4	19.6	-58
Evaluator 16	20	11	29.8	11.6	19.6	10

|| जय श्री राम ||

Acknowledgments

- I must first express my gratitude to my research supervisors, Prof. Dr. Töpfer, Prof. Dr. Snowdon, and Dr. Hausmann, without whose support and diligent participation at each stage of the process, this research would not have been completed. I want to express my gratitude for your immense encouragement, guidance and patience over the past few years. Additionally, I want to express my sincere thanks to the examination committee.

- I would like to thank Prof. Dr. Zyprian, Dr. Schwander , Dr. Zendler and Dr. Röckel for your suggestions, comments and feedback offered throughout my research. I am grateful for your generosity.

- To complete my dissertation, I required more than just academic support, and I am grateful to Dr. Anna Kicherer for patiently listening to me and providing advice when I most needed it. Thank you for the cheerful and optimistic attitude.

- As we worked on the same project, I want to thank Dr. Anna Schwandner for helping me get my research off to a good start. I appreciate your contributions and suggestions, especially in the beginning of my PhD.

- Million thanks to Lenon (Dr. Modesto), Henri (the best intern) for wonderful memories and your help during the LDA season.

- Thank you Dr. Müllner for being a wonderful colleague and a researcher. Thank you for the endless scientific discussions, suggestions during microscopic studies and proof reading.

- Special thanks to Barbara Brechter, Carina Mook & Claudia Vogel for your exceptional support in lab. I am thankful to Patricia for your patience and advice in microscopy.

- I gratefully appreciate the German Federal Ministry of Food and Agriculture for funding the project VITIFIT within the research program BÖLN (grant no 2818OE033).

|| जय श्री राम ||

- My deepest gratitude goes to my wife, Nina Malagol for her wholehearted encouragement, love and unwavering support during three years of arduous journey of conducting research and writing this thesis. Although it is a cliche, indeed, my thesis would not have existed without your motivational backing and inspiration. I would like to thank my son, without you I would have graduated one year earlier (Papa loves you!)

- To Bhimrao and Rajeshree Malagol, ನನ್ನನ್ನು ಬೆಂಬಲಿಸಿದ ಮತ್ತು ಪ್ರೋತ್ಸಾಹಿಸಿದ ತಾಯಿ ಮತ್ತು ತಂದೆಗೆ ಧನ್ಯವಾದಗಳು. ಇಂದು ನಾನು ಡಾಕ್ಟರ್ ಮಲಗೋಲ್ ಆಗಿದ್ದರೆ ಅದಕ್ಕೆ ನೀನೇ ಕಾರಣ. ನಿಮ್ಮ ಶ್ರಮ ಮತ್ತು ತ್ಯಾಗದ ಫಲ ಇಲ್ಲಿದೆ. ಈಗ ನೀವು ನನ್ನನ್ನು ಡಾ.ನಾಗರ್ಜುನ್ ಎಂದು ಹೆಮ್ಮೆಯಿಂದ ಕರೆಯಬಹುದು

- To Ute and Bernd Seel for your love and never-ending support.

- To my best friends, Shreyas Kulkarni, Suraj Bagewadi, and Prashant Kivati, who have always been there for me and pushed me to reach my current level of success.

- Vielen Dank Kirsten Schmeling, dass du mir während meines Masterstudiums einen Teilzeitjob gegeben und mich ermutigt hast, zu promovieren. Danke, dass du mir immer wieder gesagt hast: „Du sollst den Dr.-Titel bekommen, weil du ihn verdienst.“

- I am thankful to my horse Kissy D‘oroux for keeping my mind diverted from 24x7 research thoughts.

- In closing, I want to thank myself for having faith in me and persevering.


JKI
Julius Kühn-Institut
Bundesforschungsinstitut für Kulturpflanzen